I.I.S.N.

U.C.L.-Louvain-la-Neuve

CYCLONE

Rapport d'activité 2002

INSTITUT INTERUNIVERSITAIRE DES SCIENCES NUCLEAIRES

UNIVERSITE CATHOLIQUE DE LOUVAIN

RAPPORT SCIENTIFIQUE DE L'UTILISATION DU CYCLOTRON ET DES ACTIVITES DE L'UNITE DE PHYSIQUE NUCLEAIRE

2002

Institut de Physique Nucléaire
et Centre de Recherches du Cyclotron
Chemin du Cyclotron, 2
B-1348 Louvain-la-Neuve
Belgique
Tél. 010/47.32.73 - 47.29.98
Téléfax : 010/45.21.83

Table des Matières

I. RECHERCHES AUPRÈS DES ACCÉLÉRATEURS DE LOUVAIN-LA-NEUVE

1. ASTROPHYSIQUE NUCLÉAIRE

1.1. Experimental determination of the $\ell = 0$ ^{7}Be + p scattering lengths

C. Angulo, M. Cogneau, M. Couder, M Gaelens, P. Leleux, M. Loiselet, G. Ryckewaert, G. Tabacaru, F. Vanderbist (Centre de Recherches du Cyclotron et Institut de Physique Nucléaire, Université catholique de Louvain, Louvain-la-Neuve, Belgium); M. Azzouz, D. Baye, P. Descouvemont, (ULB, Brussels, Belgium); T. Davinson (University of Edinburgh, UK); A. Di Pietro, P. Figuera, R.G. Pizzone (LNS, INFN-Catania, Italy); F. de Oliveira Santos (GANIL, Caen, France); N. de Séréville (CSNSM Orsay, France)

Résumé : *La section efficace élastique ^{7}Be + p a été mesurée auprès du cyclotron CYCLONE110 aux énergies centre de masse entre 0.3 et 0. 75 MeV avec un faisceau radioactif de ^{7}Be (intensité ~ 3 × 10^6 pps dans la cible). Les protons de recul on été détectés avec le système LEDA aux angles c.m. $\theta_{c.m.}$= 120.2° - 170.2°. Les données ont été analysées avec la méthode de la matrice R. Nous avons déterminé les longueurs de diffusion pour $\ell = 0$, a_{01} = 25 ± 9 fm (spin I = 1) et a_{02} = -7 ± 3 fm (spin I =2) et nous les comparons aux valeurs attendues à partir des propriétés de symétrie de charge. Nous avons également obtenu l'énergie E_R et la largueur Γ_R de la résonance 1^+ (E_x = 0.77 MeV). Nous discutons les implications des résultats sur le facteur S à basse énergie de la réaction ^{7}Be(p,γ)^{8}B, une réaction clé dans le problème des neutrinos solaires.*

The ^{7}Be+p scattering lengths affect the extrapolation [1] of the astrophysical *S*-factor of the ^{7}Be(p,γ)^{8}B capture reaction at solar energies, a key reaction for the solar-neutrino problem [2]. Although the ^{7}Be(p,γ)^{8}B cross section has been measured many times during the last decades using different methods (see, for example, ref. [3]), an accurate measurement of the ^{7}Be(p,γ)^{8}B cross section down to the solar energies (about 20 keV) seems so far an extremely difficult experimental challenge. Presently, the experimental studies of the ^{7}Be(p,γ)^{8}B reaction have reached the 100 keV energy range but uncertainties remain for the extrapolation of the *S*-factor to determine *S(0)*. The reason is that this extrapolation is based on theoretical models that require the knowledge of quantities such as the Asymptotic Normalization Constant (ANC) *C* [4] and the ℓ=0 scattering lengths a_{0I} [5] (I is the channel spin). Here, we will be interested in the scattering lengths only. The relationship between *S(0)* and C^2, often used in indirect methods to derive the ^{7}Be(p,γ)^{8}B S-factor [6], is affected by the scattering lengths, but usually its dependence is neglected by taking a_{0I} = 0. Although existing models [5] suggest that the a_{0I} value is not large enough to lead to important corrections, there has not been any experimental confirmation yet. Due to the importance of the ^{7}Be(p,γ)^{8}B reaction for the solar-neutrino physics [2], small corrections on *S(0)* may lead to non-negligible consequences for the solar-neutrino problem.

A second field of interest of the ^{7}Be + p scattering length is related to charge-symmetry properties in mirror systems. From the comparison of scattering lengths for the ^{7}Be + p and ^{7}Li + n interactions one can extract some information on charge-symmetry. Existing literature data on the ^{7}Li + n scattering lengths are used here for comparison.

1.1.1. Experiment

The ^{7}Be+p elastic scattering cross section has been measured at the CRC-RIB facility at c.m. energies $E_{c.m.}$ = 0.3-0.75 MeV, i.e. in the vicinity the $J^\pi = 1^+$ (ℓ=1) state at E_x = 0.77 MeV in ^{8}B [7]. The main purpose of the experiment is to obtain the $\ell = 0$ ^{7}Be+p scattering lengths. Details of the experiment and the data analysis can be found in Ref. [8]. We have used the reverse elastic scattering technique by bombarding a 0.27 mg/cm^2 polyethylene target with a $^7Be^{1+}$ radioactive beam at three laboratory energies E_{lab} = 4.4, 5.7 and 6.3 MeV. The averaged ^{7}Be beam intensity on target was of the order of 3 × 10^6 pps. The recoil protons were detected in two LEDA [*L*ouvain-la-Neuve *E*dinburgh *D*etector *A*rrray] multi-strip systems [9] covering the angles θ_{lab} = 4.9º-11.7º and θ_{lab} = 22.6º - 29.9º. A Mylar foil was positioned in front of all LEDA sectors to stop the high energy scattered ^{7}Be and the recoiled ^{12}C particles. For each LEDA strip, the energy and the time-of-flight (TOF) of the particles with respect to the cyclotron RF were recorded. The recoil protons were well separated from the

uncorrelated background for all spectra in the entire angular range. Data obtained in the overlapping energy region near the 1^+ resonance were in good agreement. Figure 1 shows a typical summed TOF spectra at θ_{lab} = 4.9º obtained with a ^{7}Be beam energy of (a) 5.7 and (c) 6.3 MeV. The recoil proton signal, marked by a selection on the figure, are displayed on (b) and (d) as a function of the proton laboratory energy. The proton spectra are slightly degraded by the opening angle of the detectors, the energy straggling of the protons in the target and in the Mylar foil, and the electronic noise. These effects are taken into account in the data analysis. Two PIPS (Passivated Implanted Planar Silicon) detectors located at 60º with respect to the beam axis were used for normalization by detecting the scattered ^{7}Be particles on a very thin Au coating, evaporated on the target upstream face.

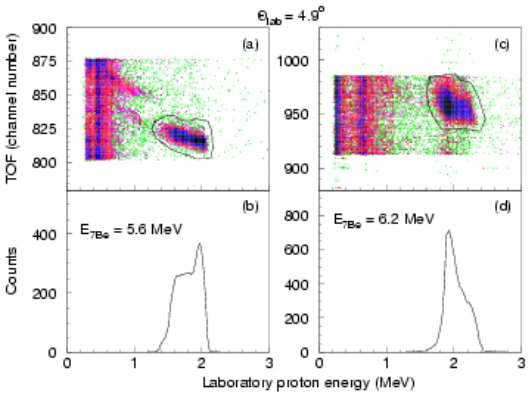

Figure 1 : Summed TOF spectra at θ_{lab} = 4.9º obtained with ^{7}Be beams at laboratory energies (a) 5.7 and (c) 6.3 MeV. The recoil proton signal (selection on the figure) are displayed on (b) and (d) as a function of the proton laboratory energy.

1.1.2. Data analysis

The resulting ^{7}Be+p cross sections are presented in Figure 2 for four typical c.m. angles $\theta_{c.m.}$ = 120.2º, 131.1º, 156.6º and 170.2º versus the c.m. energy. The error bars are statistical errors only. The dotted curves are the Rutherford cross sections. The cross section data have been analysed using the *R*-matrix method [10] (solid curves in Figure 2). The 1^+ resonance, which is expected to play a dominant role in the scattering cross section in the energy range covered here, is characterized by $J^\pi = 1^+$and $\ell = 1$, but the channel spin I is not determined. Here, both I = 1 and I = 2 values will be considered, but the mixing is neglected. The 1^+ phase shift is parameterized in the *R*-matrix formalism [10], which involves the resonance energy E_R and the resonance width Γ_R. In addition to the 1^+ resonance, the $\ell = 0$ contribution is expected to play a significant role. The $\ell = 0$ phase shifts have been parameterized by using the effective-range expansion [11], valid at low energies,

$$2k\eta\left[\frac{\pi}{(e^{2\pi\eta}-1)\tan\delta_{0I}^{I-}}+h(\eta)-\ell n\ \eta\right]=-\frac{1}{a_{0I}}+\frac{1}{2r_I^e k^2}+\ldots,$$

where a_{0I} and r^e_I are the scattering lengths and the effective ranges for channel spin I, respectively, k is the wave number, and h(η) is a function of the Sommerfeld parameter η. We have tested the sensitivity of the *R*-matrix fits with respect to the following parameters: (i) the *R*-matrix channel radius *a*, which has been set to *a* = 4, 5 and 6 fm; (ii) the effective range r^e_I, taken as r^e_I = 1, 2, 3, 4 and 5 fm, and (iii) the energy correction ΔE, more specifically the effect of the variation of the energy straggling. The results are given in Table 1. The errors include the uncertainties with respect to all the parameters (experimental errors and theoretical uncertainties). The best fit (χ^2/N = 0.66) is found for *a* = 5 fm, r^e_I = 2 fm and for a channel spin I=1 for the 1^+ resonance.

Parameter	Present	Literature
a_{01} [fm]	25 ± 9	-
a_{02} [fm]	-7 ± 3	-
E_R [keV]	634 ± 5	632 ± 10(*)
Γ_R [keV]	31 ± 4	37 ± 7(*)

(*) From Ref.[7]

Table 1 : Parameters of the 1^+ resonance and ^{7}Be+p scattering lengths.

1.1.3. Discussion of the $^7Be(p,\gamma)^8B$ *S*-factor

Owing to the very low binding energy of ^8B (137 keV with respect to ^7Be+p threshold), the low energy astrophysical S-factor is determined by properties of the Coulomb functions and by the Asymptotic Normalization Constant (ANC) of the ground state. Taking into account the *s* and *d* contributions, the $^7Be(p,\gamma)^8B$ S-factor at low energies is given by [1]

$$S(E) \approx S(0)\,(1 + s_1 E).$$

On the other hand, the S-factor at zero energy S(0) and the slope of the curve s_1 are related to the ANC and to the scattering length by [1]

$$S(0) \approx 38.0\, C^2\, (1 - 0.0013\, a_0)\ \text{eV-b},$$

$$s_1 \approx -1.81\, (1 + 0.0087\, a_0)\ \text{MeV}^{-1},$$

where C is expressed in $fm^{-1/2}$, a_0 in fm, S(0) in eV-b and s_1 in MeV^{-1}. Notice that quantities C^2 and a_0 represent averaged values involving I = 1 and I = 2 channel spins of the ^8B ground state: C_1 and C_2 for the ANC, a_{02} and a_{01} for the scattering length a_0.

As indicated above, the relationship between *S(0)* and C^2, often used in indirect methods to derive the $^7Be(p,\gamma)^8B$ *S*-factor [6] is affected by the scattering lengths. Determining a_0 with a good precision is not possible without the spectroscopic factors and the ANC values of the ^8B ground state in both the I=1 and the I=2 channels. Here, we have made used of the results of a microscopic calculation [12] which suggests that the dominant component for the ^8B ground state is I = 2, and that therefore the scattering length is mainly sensitive to a_{02}. Using the present experimental value $a_{02} = -7 \pm 3$ fm, one finds that $S(0)/C^2$ increases by about 1 % and the slope s_1 decreases by about 6 %. Even if the absolute effect of the scattering lengths is weak, it is not negligible and have to be taken into account to constrain theoretical models employed for the extrapolation of the $^7Be(p,\gamma)^8B$ S-factor at zero energy.

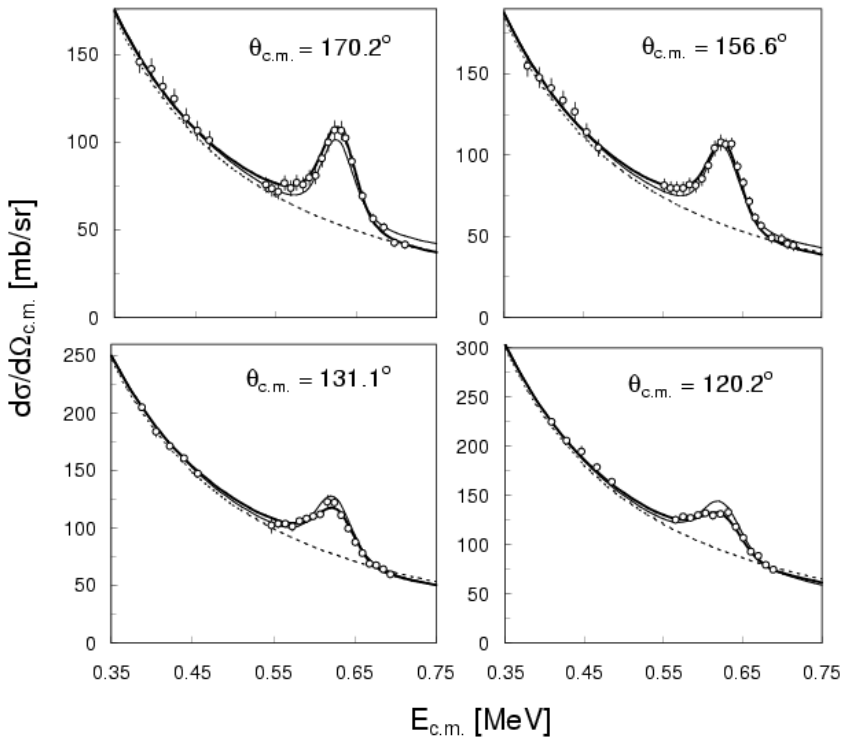

Figure 2 : Elastic cross section versus c.m. energies for the system ^7Be+p for c.m. angles 120.2º, 131.1º, 156.6º, and 170.2º. The thicker solid curves are the best R-matrix fits assuming I=1 for the 1^+ resonance with parameters of Table 1. The thinner curves are the fits for I=2. The dotted curves are the Rutherford cross sections.

1.1.4. Charge-symmetry between ^{7}Li + n and ^{7}Be + p scattering lengths

The experimental determination of the ^{7}Be+p scattering lengths addresses the question of charge-symmetry with respect to the ^{7}Li + n system. Experimental data for the mirror system ^{7}Li + n provide the following scattering lengths [13] : a_{01} = (0.87 ± 0.07) fm and a_{02} = (-3.63 ± 0.05) fm.

According to the a_0 experimental values for the ^{7}Li+n system, the charge-symmetry approximation would provide for ^{7}Be + p: a_{01} ~ 2 to 3 fm and a_{02} ~ -7 to -11 fm, to be compared with the results given in Table 1. While the a_{02} value obtained from charge-symmetry arguments is in good agreement with the experimental one, a_{01} is smaller than the one obtained from the ^{7}Be+p elastic scattering measurement. The present results can be used to constraint theoretical models.

1.1.5. Conclusions

This work presents the first experimental determination of the ^{7}Be + p scattering lengths. The large a_{01} value does not significantly affect the ^{7}Be + p phase shifts since large scattering lengths provide a weak contribution to the phase-shift expansion. The uncertainties on the properties of the 1^+ resonance (energy and proton width) have been reduced; reasonable fits of the data also require a dominant I=1 resonance channel spin component. This is supported by a microscopic cluster model [12] which gives 3.5 as the ratio between I = 1 and I = 2 component for the 1^+ state. Astrophysical consequences for the ^{7}Be(p,γ)^{8}B low-energy *S*-factor are weak, but not negligible if one considers the precision needed in solar models. The present scattering length, a_0 = -7 ± 3 fm, essentially affects the slope of the ^{7}Be(p,γ)^{8}B S-factor near zero energy by about 6 %.

[1] D. Baye, Phys. Rev. C62 (2000) 065803.
[2] J.N. Bahcall et al., Phys. Lett. B433 (1998) 1.
[3] C. Angulo et al., .Nucl. Phys. A656 (1999) 1.
[4] See for example, J.C. Fernandes et al., Phys. Rev. C61 (2000) 064616.
[5] F.C. Barker, Aust. J. Phys. 33 (1980) 177.
[6] A.M. Mukhamedzhanov et al., Phys. Rev. C51 (1995) 3472.
[7] F. Ajzenberg-Selove, Nucl. Phys. A490 (1988) 1.
[8] C. Angulo et al, Nucl. Phys. A716 (2003) 211-229.
[9] T. Davinson et al., Nucl. Instr. Meth. A454 (2000) 350.
[10] A.M. Lane and R.G. Thomas, Rev. Mod. Phys. 30 (1958) 257.
[11] M.A. Preston and R.K. Badhuri, Structure of the Nucleus, Addison-Wesley, NY, 1975.
[12] P. Descouvemont and D. Baye, Nucl. Phys. A567 (1994) 341.
[13] L. Koester et al., Z. Phys. A312 (1983) 81.

1.2. Performance of the recoil separator ARES for (p,γ) reaction measurements

M. Couder, C. Angulo, P. Leleux, G. Tabacaru, F. Vanderbist (Institut de Physique Nucléaire, Université catholique de Louvain, Louvain-la-Neuve, Belgium)

Résumé : *Les performances du séparateur de recul ARES pour la mesure de la section efficace de la réaction ^{19}F(p,γ)^{20}Ne (E_r = 635 keV) sont présentées ainsi qu'une brève description des mesures préliminaires à cette mesure.*

The aim of ARES (Astrophysics REcoil Separator) is to measure (p,γ) and (α,γ) cross section induced by radioactive beam by detecting the product ions. The inverse kinematics (heavy ion beam on light target ion) implies that product and beam ions have the same momentum behind the target. A velocity selection with a Wien filter allows us to reject the beam ions. A charge selection is realized before this Wien filter with a dipole magnet. An additional rejection is provided by a ΔE-E detector. ARES has been intensively tested with a (p,γ) reaction induced by a stable beam : ^{19}F(p,γ)^{20}Ne (E_R = 635 keV, ωγ = 1.6 eV, Γ = 6.3 keV) in which ^{20}Ne ions are produced with a half-aperture of 20 mrad and a total energy width of 1 MeV.

1.2.1. Beam related measurements

The recoil proton spectra from $^{19}F(p,p)$ elastic scattering has allowed to check that the resonance was well located in the CH_2 target. The usual pattern from Coulomb-resonant interference is an obvious proof. The beam energy resolution has been measured by sending the ^{19}F beam at 13.2 MeV on an Au(5 μg/cm^2) + C(10 μg/cm^2) target, from the scattered ^{19}F on Au a beam energy resolution of 170 keV (1.3 %) was deduced. An energy resolution of 300 keV after a 80 μg/cm^2 CH_2 target was obtained, mainly due to target inhomogeneity. The stopping power of ^{19}F and ^{20}Ne at 13 MeV had been measured by sending beams of attenuated intensity in a silicon detector with and without CH_2 target: the stopping power : 17.1 ± 0.4 keV/μg/cm^2 for ^{19}F and 19.4 ± 0.4 keV/μg/cm^2 for ^{20}Ne. These values are 15 % higher than the SRIM tables [1] and 10 % lower than the Northcliffe and Schillings tables[2]. Finally the charge states distribution of ^{20}Ne behind CH_2 target has been measured and compared to the Shima et al [3] calculation. A good agreement with Ref. [3] is obtained for the most abundant charge state 7^+ (37 %), while discrepancies exit for adjacent charge states.

1.2.2. Characterization of ARES

The measurements in section 1.2.1. were needed prior to the characterization of ARES. First of all the transmission efficiency of the ^{19}F beam was measured. ARES was optimised to transmit the ^{19}F beam having crossed a 80 μg/cm^2 CH_2 target. A 70 % efficiency was obtained. The rejection of the beam was the next step, we have adapted the magnetic field in the dipole magnet and in the Wien filter to select the ^{20}Ne momentum and velocity respectively. There remained about 200 counts per second in the ΔE-E detector for 10^9 pps on target which means a beam rejection factor of 2×10^{-7}. Finally the ability of ARES to transmit a broad energy distribution has been tested by sending a ^{20}Ne beam on a CH_2 target tilted by 30° while ARES was optimised for the transport of the $^{20}Ne^{7+}$ component beyond the target. The target angle was changed, from 0° to 60° in small steps, and the transported beam was recorded at each step in the final Faraday cup. The FWHM of the transported distribution is 500 keV. The width of the energy distribution of the ^{20}Ne produced in the $^{19}F(p,\gamma)$ reaction being 705 keV due to the kinematics, this means that significant loss of product ions will occur.

1.2.3. Results and simulations

ARES being tuned for $^{20}Ne^{7+}$ as described in the previous section, a ^{19}F beam of 6×10^8 pps has been sent on a CH_2 target for 20 hours. The resulting ΔE vs ΔE + E spectra is shown on figure 1a, the locus of the ^{20}Ne being encircled. Knowing the resonance strength and the integrated ^{19}F beam, the global efficiency of ARES for transporting ^{20}Ne ions produced in the reaction can be deduced: the data in figure 1a yield an efficiency of 4.0 %, which represents a transmission of 11.5 % for the $^{20}Ne^{7+}$ ions. Let us remark that this "low" transmission is obtained for a beam intensity up to 10^9 pps; for much lower beam intensities, poorer rejection factors could be tolerated, the slits opening at the dipole exit and the Wien filter exit could be increased and the transmission would be larger. Moreover the high Q-value of the $^{19}F(p,\gamma)$ reaction implies a large half aperture and a large energy distribution of the produced ^{20}Ne. Most of the reaction induced by radioactive beams has a smaller Q-value which will increase the transmission efficiency.

In all cases where ωγ is unknown, the transmission of ARES will be obtained from a simulation code (GEANT 3.2.1.). The ability of this code to reproduce the measured transmission in the present case was checked as follows: The first step consisted in reproducing the ^{19}F beam transmission beyond the CH_2 target with the beam aperture as the only free parameter. The second step consisted in the simulation of $^{20}Ne^{7+}$ ions produced in the target, at depths distributed according to a Lorentzian resonance of c.m. energy $E_r = 635$ keV and width $\Gamma = 6$ keV. Figure 1b shows a simulated spectrum, normalised to the same integrated ^{19}F beam on target as the measured spectrum. The good agreement between the data and the simulation is an important issue as mentioned above. A detailed report on the present measurements has been published [4].

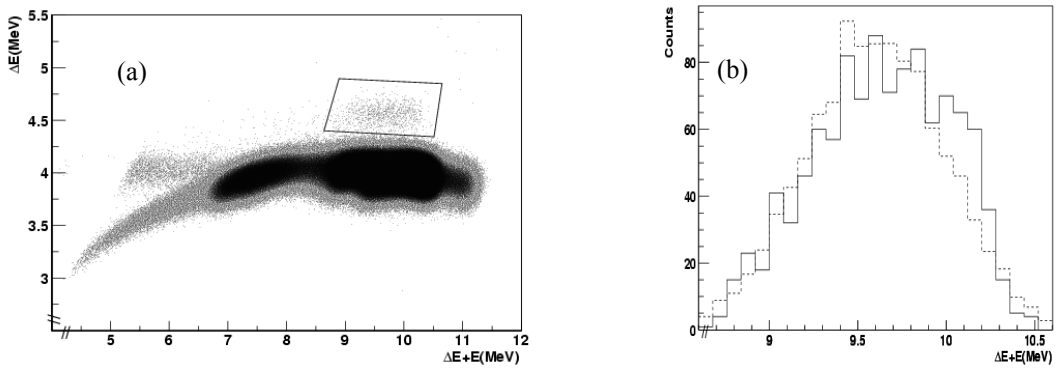

Figure 1 : (a) Two dimensional ΔE vs ΔE+E spectrum obtained in the measurement of the $^{19}F(p,\gamma)^{20}Ne$ reaction. The bright area consists in ^{19}F beam ions not suppressed before reaching the telescope. The framed area contains ^{20}Ne events. (b) Total energy (ΔE+E) spectrum of the ^{20}Ne events in the encircled region of fig. 1a (solid histogram). The dotted histogram is the simulated spectrum, obtained for the same integrated ^{19}F beam as the experimental spectrum.

[1] J.F. Ziegler and J.P. Biersack, SRIM program version 40 (unpublished), (see also http://www.srim.org).
[2] L.C. Northcliffe and R.F. Schillings, Nucl. Data Tables A7 (1970) 233.
[3] K. Shima, T. Ishihara, T. Miyoshi, T. Momoi and T. Mikumo, Phys. Rev. A29 (1984) 1763.
[4] M. Couder et al, Nucl. Instr. Meth. Phys. Res. A506 (2003) 26-34.

1.3. Study of ^{12}N states by ^{11}C + p elastic scattering

I.A. Roberts, T. Davinson, M. Aliotta, A. Murphy, A. Robinson, A. Murphy, A. Robinson, Ph. Woods (University of Edinburgh, United Kingdom); C. Angulo, M. Couder, M. Gaelens, P. Leleux, , G. Tabacaru, F. Vanderbist (Centre de Recherches du Cyclotron et Institut de Physique Nucléaire, Université catholique de Louvain, Louvain-la-Neuve); P. Descouvemont (PNTPM, ULB, Brussels); A. Di Pietro, P. Figuera (LNS, INFN-Catania, Italy)

Résumé : La section efficace élastique ^{11}C+ p a été mesurée auprès du cyclotron CYCLONE110 aux énergies laboratoires 6.2 et 9.6 MeV avec un faisceau radioactif de ^{11}C. Les protons de recul ont été détectés avec le système LEDA aux angles c.m. $\theta_{c.m.}$= 120.2° - 170.2°. Le but de l'expérience est de trouver les paramètres des états d'intérêt astrophysique du ^{12}N.

In certain astrophysical conditions, when the stellar temperatures rises higher than $T_9 = 0.2$ ($T_9 = T/10^9$ K), some proton (or alpha) capture reactions on radioactive nuclei may be faster than the β decay of these nuclei[1]. This is the case for explosive hydrogen burning, including hot CNO cycle [2] and the hot pp chain [3,4], and it is expected to occur in peculiar astrophysical sites, such as the core of super massive stars. In such scenarios, the temperature and the density are high enough to favour proton (or alpha) capture with respect to β decay. If a capture reaction is faster than the competing β decay, the cross section is usually enhanced by a low-energy resonance. This is the case of the reaction $^{11}C(p,\gamma)^{12}N$, which is part of the hot pp chain; this reaction is believed to be completely determined by the properties of the 2^- (E_x = 1.19 MeV, E_{cm} = 0.598 MeV) resonance in ^{12}N [6]. This resonance has an angular momentum $\ell = 0$ which enhances the tail contribution to the reaction rate. Below the resonance energy, this tail contribution depends on the product of the proton width and the gamma width, $\Gamma_p \times \Gamma_\gamma$ [7], and the total resonance width is essentially given by the proton width, $\Gamma_{tot.} = \Gamma_p$. A lower 2^+ state (E_{cm} = 0.36 MeV) is a p-wave resonance and decays to the ground state by E2 or M1 transitions. It is therefore strongly suppressed with respect to the 2^- resonance. The total width of the 1.19 MeV state is presently known with a large uncertainty [8]. The gamma width of the state is still open to discussion (see, for example, Ref. [5]), and its measurement is planned in the near future using the ARES recoil separator [9].

Figure 1 shows the astrophysical S-factor of the $^{11}C(p,\gamma)^{12}N$ reaction calculated in the Breit-Wigner approximation for the two extreme values of Γ_p, 140 and 80 keV, respectively [7]. The gamma width value used in this calculation is $\Gamma_\gamma = 45$ meV from Ref. [5] (a Coulomb break up experiment obtains $\Gamma_\gamma = 6^{+7}_{-3.5}$ meV [10]). At the temperatures of interest for astrophysics, $T_9 > 0.2$, the difference between the two S-factor curves is about a factor of 2. The reaction rate of $^{11}C(p,\gamma)^{12}N$ is affected by the same uncertainty.

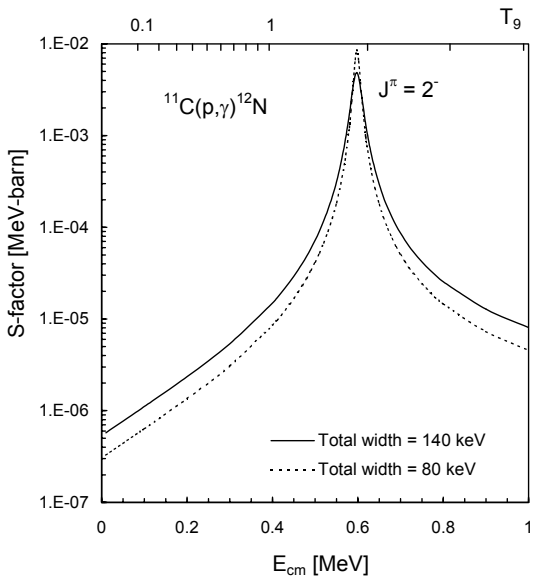

Figure 1 : Astrophysical S-factor of the reaction $^{11}C(p,\gamma)^{12}N$ versus the centre-of-mass energy. The curves are calculated for 2 different values of the total resonance width, Γ_p = 140 keV (full curve) and Γ_p = 80 keV (dotted curve). The value adopted for the partial gamma width is Γ_γ = 45 meV [5]. The temperature is also shown in units of T_9 ($T_9 = 1\times10^9$ K).

We have recently measured the elastic scattering cross section of the system ^{11}C+p in order to obtain a more precise value of the total resonance width, Γ_p. We have used the reverse elastic scattering technique by bombarding a polyethylene target with a $^{11}C^{1+}$ radioactive beam at laboratory energies E_{lab} = 6.2 and 9.6 MeV. The recoil protons were detected in two LEDA [Louvain-la-Neuve Edinburgh Detector Arrray] multi-strip systems [11] covering the angles θ_{lab} = 4.9°- 11.7º and θ_{lab} = 22.6º - 29.9º. For each LEDA strip, the energy and the time-of-flight (TOF) of the particles with respect to the cyclotron RF were recorded. The recoil protons were well separated from the uncorrelated background for all spectra in the entire angular range. Data obtained in the overlapping energy region were in good agreement. Figure 2 shows preliminary (normalized to each other) data in relative units at θ_{lab} = 4.9º. We will use the R-matrix method to derive the parameters of the 1.19 MeV ^{12}N state. Data are under analysis.

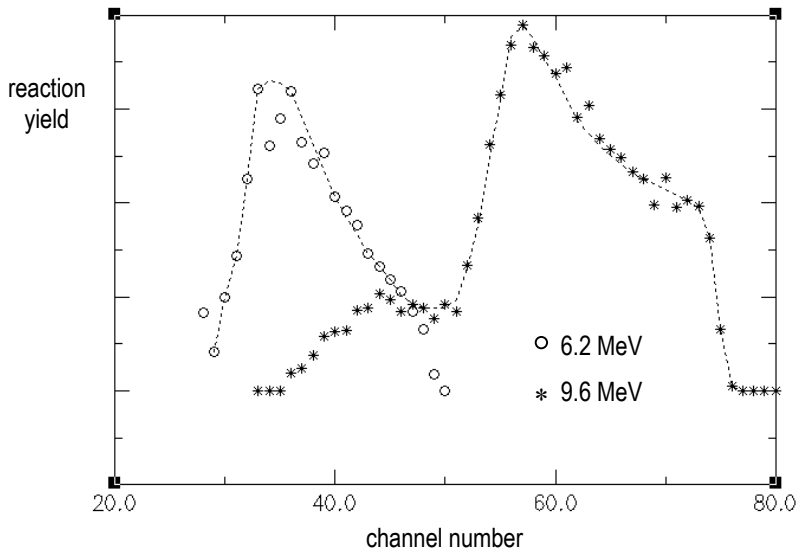

Figure 2 : Preliminary results showing the combined (normalised to each other) yield (in relative units) for beam energies 6.2 MeV and 9.6 MeV.

[1] R.H. Wallace and S.E. Woosley, Astrophys. J. Suppl. 45 (1981) 389.
[2] G.J. Mathews and F.S. Dietrich, Astrophys. J. 287 (1984) 969.
[3] M. Wiescher et al., Astrophys. J. 343 (1989) 352.
[4] A. Jorissen and M. Arnould, Astron. Astrophys. 221 (1989) 161.
[5] P. Descouvemont, Nucl. Phys. A646 (1999) 261.
[6] P. Descouvemont and I. Baraffe, Nucl. Phys. A514 (1990) 66.
[7] P. Descouvemont, Annales de Physique 26, No 3 (2001).
[8] F. Ajzenberg-Selove, Nucl. Phys. A506 (1990) 1.
[9] M. Couder et al., Nucl. Instr. Meth. Phys. Res. A506 (2003) 26-34.
[10] A. Lefebvre et al., Nucl. Phys. A592 (1995) 69.
[11] T. Davinson et al., Nucl. Instr. Meth. Phys Res. A454 (2000) 350.

1.4. Study of the ^{7}Li(d,p)^{8}Li reaction - a precursor for ^{7}Be(p,γ)^{8}B reaction

J.E. McDonald, G. Hamouri, C.M. Przybycien (University of Hartford, Connecticut, USA); J.A. Dooley, M. Gai (University of Connecticut, USA); R.H. France III (Georgia CSU, Milledgeville, Georgia, USA); Th. Delbar (Institut de Physique Nucléaire, Université catholique de Louvain, Louvain-la-Neuve, Belgium); Ch. Bordeanu and M. Hass (Weizmann Institute, Rehovot, Israël)

Résumé : Les mesures de la réaction ^{7}Li(d,p) ont été poursuivies, ainsi que l'étude détaillée de toutes les sources d'erreurs systématiques. Cette étude est spécialement importante car elle permet de simuler la réaction ^{7}Be(p,γ)^{8}B, les états finaux se désintégrant en 2α étant identiques.

A measurement of the ^{7}Li(d,p)^{8}Li reaction at E_{Li} = 2.5 - 3.5 MeV was performed at WNSL at Yale, which constituted and is in continuation of the Ph.D. thesis of Dr. James E. McDonald [1]. This measurement was performed on the new "UConn" beam line constructed by WNSL for use of the LNS and its international collaboration (see fig. 1). This cross section is critical in some cases for normalizing the cross section of the ^{7}Be(p, γ)^{8}B reaction (adopted as σ_{dp}= 146 ± 10 mb [2]). It also serves as a precursor for the ^{7}Be(p,γ)^{8}B measurement, our approved PH120 experiment at Louvain-la-Neuve .

We measured the two back to back alpha particles produced by ^{8}Li by means of a rotating collection wheel with three detector stations. The ^{7}Li beam first traverses a thin gold foil with the scattered ^{7}Li used to monitor the beam throughout the experiment. The beam then traverses a $(CD_2)_n$ target, where some of the ^{7}Li reacts with deuterium, forming ^{8}Li. An aluminum degrader is used to slow the byproduct ^{8}Li so that it is stopped in two thin (500 μg/cm^2) aluminum catcher foils mounted on the twin wheels. The catcher foil containing the ^{8}Li is quickly rotated (90° in approximately 98 ms) through a series of three counting stations, where the back-to-back alpha particles are measured in fast coincidence. A lifetime decay curve fit for ^{8}Li is used to extract the number of atoms collected on the collection foil, as can be seen in fig. 2 and fig. 3.

The beam-target luminosity was measured using a monitor detector placed at 0° to measure the recoil deuterons from elastic scattering. This allowed us to eliminate many systematic uncertainties that plagued previous experiments.

The absolute efficiency of the detector array was thoroughly investigated [3], as well as by measuring the yield of alpha-particles relative to a far away detector with well known efficiency placed at 45°. A special source holder was built to mount a ^{148}Gd in the exact location of the collection foil. This apparatus is also being used to measure the cross section of the ^{7}Be(p, γ)^{8}B reaction using the cyclotron CYCLONE at Louvain-la-Neuve.

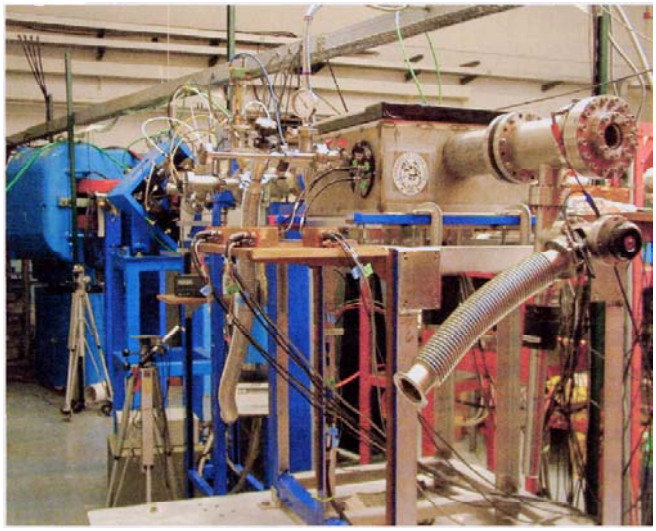

Figure 1 : The new UConn beam line constructed at WNSL at Yale.

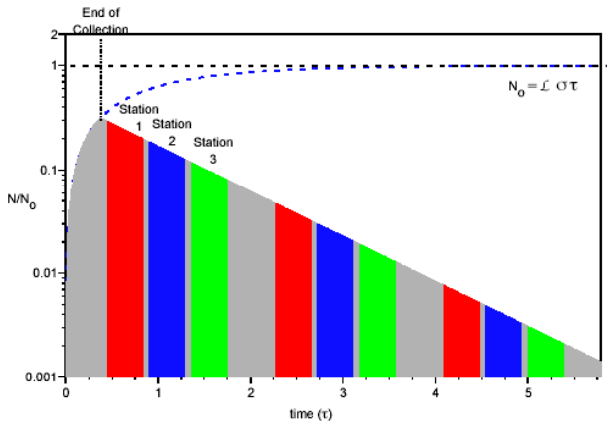

Figure 2 : The time evolution, collection and decay of ^{8}Li of the current experiment.
The shaded areas represent the activity detected at each counting station due to one collection period.

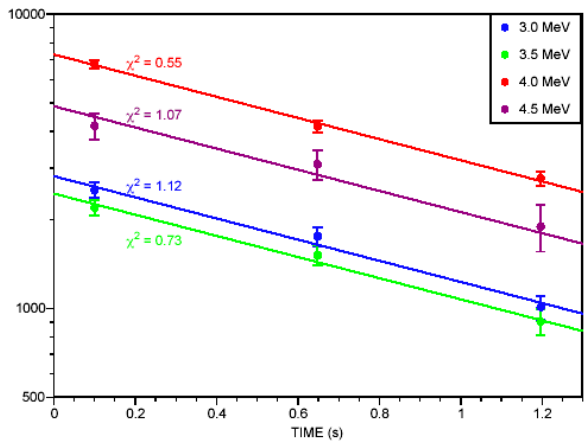

Figure 3 : A one parameter curve fit to the measured activity using the expression shown, from which we extracted the number of collected ^{8}Li atoms (N_m):

$$A(t) = N_m \cdot \frac{\left(1 - e^{-t_c/\tau}\right)}{\left(1 - e^{-4\Delta t/\tau}\right)} \cdot e^{-t/\tau}$$

[1] J.E. McDonald, R.H. France III, M. Gai, J.A. Dooley, Th. Delbar, and D. Visser, Bull. Amer. Phys. Soc. 45, 11 (2000).

[2] E.G. Adelberger, S.A. Austin, J.N. Bahcall, A.B. Balantekin, G. Bertsch, G. Bogaert, L. Buchmann, F.E. Cecil, A.E. Champagne, L de Braeckeleer, C.A. Duba, S.R. Elliott, SJ. Freedman, M. Gai, G. Goldring, C.R. Gould, A. Gruzinov, W.C. Haxton, K.M. Heeger, E. Henley, M. Kamionkowski, R.W. Kavanagh, S.E. Koonin, K. Kubodera, K. Langanke, T. Motobayashi, V. Pandharipande, P. Parker, R.G.H. Robertson, C. Rolfs, R. Sawyer, N. Shaviv, T.D. Shoppa, K. Snover, E. Swanson, R.E. Tribble, S. Turck-Chiez, J.F. Wilkerson, Rev. of Modern Phys. 70 (1998) 1265.

[3] J.A. Dooley, J.E. McDonald, R.H. France III, M. Gai, and D.W. Visser, Bull. Amer. Phys. Soc. 45, 11 (2000).

1.5. Destruction of ^{7}Li and ^{7}Be in cosmological and stellar environments

R.H. France III (Georgia CSU, Milledgeville, Georgia, USA) ; J.A. Dooley, M. Gai (University of Connecticut, USA) ; C.M. Przybycien, I.E. McDonald (University of Hartford, Connecticut, USA) ; L.T. Baby, M. Hass, C. Bordeanu (Weizmann Institute, Rehovot, Israël) ; Th. Delbar, A. Ninane (Institut de Physique Nucléaire, Université catholique de Louvain, Louvain-la-Neuve, Belgium)

Résumé : Profitant de l'existence d'une cible de ^{7}Be à l'Institut Weizmann (Israël), nous avons mesuré la section efficace de la réaction ^{7}Be(^{3}He,x)y. Cette réaction est une voie possible pour détruire le ^{7}Be dans un environnement stellaire. L'analyse finale est en cours.

The destruction of ^{7}Li and/or ^{7}Be in astrophysical environments is essential for understanding several stellar and cosmological processes. While most studies concentrate on the production of elements, the destruction of ^{7}Li and/or ^{7}Be is not well understood [1]. The destruction of ^{7}Li and/or ^{7}Be during the hot-pp cycle may alter our conclusions on the production of carbon in this process [1]. In particular in this case the reaction ^{7}Be(^{3}He,2α)2p competes with ^{7}Be(^{4}He,γ) ^{11}C and may reduce the production of carbon [1]. We also note that both during Big Bang Nucleosynthesis [2] and in the newly proposed Hypernova explosion ^{7}Li is also over-produced [3], thus underlying the need for studying the destruction of ^{7}Li and/or ^{7}Be. These stellar and cosmological environments involve high temperatures and thus effective burning energy (Gamow window) that are quite high, thus interactions of ^{3}He with ^{7}Li and/or ^{7}Be could play a role. In addition, experiments using ^{7}Be targets inevitably involve interactions with ^{7}Li as background due to the ^{7}Li available from the beta decay of ^{7}Be. And on the other hand, precision measurement of the cross section of the ^{7}Li(^{3}He,α_n) ^{6}Li involving a sharp alpha-particle line at approximately 7.0 MeV, (see fig. 1), can be used for absolute normalization of the interaction of ^{7}Be + ^{3}He with very little systematic uncertainty, provided the ratio of ^{7}Li/^{7}Be in the target is well known.

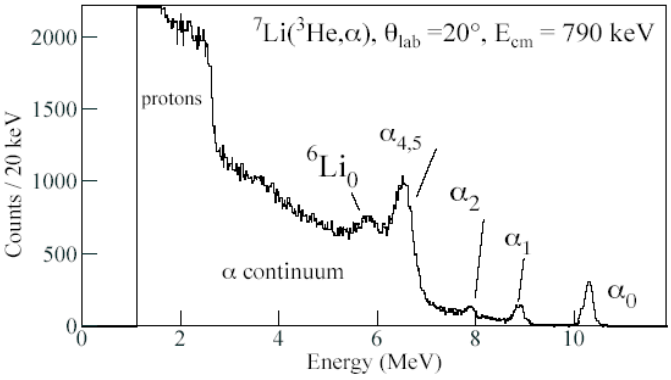

Figure 1 : Typical alpha-particle spectrum obtained using a projection of an E-ΔE telescope.

A ^{7}Be target was made available at the Weizmann Institute, after the completion of the measurement of the ^{7}Be(p,γ)^{8}B reaction, as approved by ISOLDE at CERN. The target represents a scientific opportunity and we are taking advantage of its existence at the Weizmann Institute. In preparation for the measurement of the interaction of ^{7}Be + ^{3}He as well as for studying the interaction of ^{7}Li + ^{3}He in itself, measurements were carried out at the Weizmann Institute 3 MV Van de Graaff Accelerator Facility. We used 344 - 700 keV ^{3}He beams with an average intensity of 400 nA, on a 2.9 kÅ ^{7}LiF (60 μg/cm^2), 100 keV thick target. A 2.2 mg/cm^2 nickel absorber foil was placed in front of the E-ΔE telescope to stop the intense scattered beam. A second measurement employed a 10 μg/cm^2 thin target and ^{3}He beam energies of 350 -1000 keV. Detector telescopes were placed at several backward angles (165°, 140° and 115°) and forward angles (20°, 45°) for measuring complete angular distributions. The beam current was measured using elastic scattering from a thin 5 mg/cm^2 gold foil detected in a monitor detector (without an absorber foil), as well as by using a beam current integrator with 300 volts suppression. In figure 1 we show sample data was from a projection of an E-ΔE telescope with a ^{3}He beam of 700 keV; the E-ΔE detector telescope used to obtain these data was composed of Si surface barrier detectors, 50 and 500 microns thick, and was placed at 125° [4]. One telescope was composed of two E (500 microns) detectors.

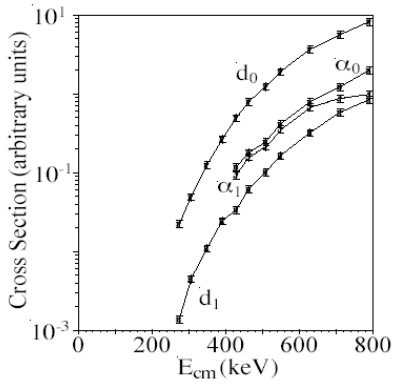

Figure 2 : Cross section for interaction of ^{7}Be + ^{3}He.

The cross section for ^{7}Be + ^{3}He interaction is shown in figure 2. Our measurements complement measurements of the ^{7}Be(^{3}He,$p_{0,2}$)^{9}Be [5,6].

[1] H.M.J. Boffin, G. Paulus, M. Arnould, and N. Mowlavi, Astron. Astrophys. 279 (1993) 173.

[2] D.N. Schramm, and R.V. Wagoner, Ann. Rev. Nucl. Part. Sci. 27 (1977) 37.
A. Merchant Boesgaard, and G. Steigman, Ann. Rev. Astron. Astrophys. 23 (1985) 319.

[3] B.D. Fields, F. Daigne, M. Casse, E.Vangioni-Flam, astro-ph/0107492.

[4] C.M. Przybycien, J.E. McDonald, M. Gai, R.H. France III, L.T. Baby, C. Bordeanu, M. Hass, Th. Delbar, Bull. Amer. Phys. Soc. 46 (2001) 105.

[5] D.P. Rath, R.N. Boyd, H.J. Hausman, M.S. Islam, and G. Kolnicki, Nucl. Phys. A515 (1990) 338.

[6] J. Yan, F.E. Cecil, U. Greife, C.C. Jewett, RJ. Peterson, and R.A. Ristenin, to be published.

2. NOYAUX EXOTIQUES

2.1. Spectroscopy of the proton drip line nucleus ^{19}Na by ^{1}H(^{18}Ne, ^{1}H)^{18}Ne elastic scattering

C. Angulo, M. Couder, M Gaelens, P. Leleux, G. Tabacaru, F. Vanderbist (Centre de Recherches du Cyclotron et Institut de Physique Nucléaire, Université catholique de Louvain, Louvain-la-Neuve, Belgium); P. Descouvemont, (PNTPM, ULB, Brussels, Belgium); T. Davinson, Ph.J. Woods (University of Edinburgh, UK), J.S. Schweitzer (University of Connecticut, Storrs, USA), N.L. Achouri, J.-C. Angelique (LPC, Caen, France), E. Berthoumieux (DAPNIA/SPhN, Gif sur Yvette, France), F. de Oliveira (GANIL, France); P. Himpe (KUL, Leuven, Belgium)

Résumé : *Nous avons étudié la diffusion élastique résonante ^{18}Ne+p en cinématique inverse avec un faisceau radioactif intense (4×10^6 pps) de ^{18}Ne au Centre de Recherches du Cyclotron. Nous avons utilisé le système de détection LEDA pour détecter les protons de recul. La section efficace élastique a été analysée en utilisant la méthode de la matrice R. Nous avons observé pour la première fois le deuxième état excité du noyau riche en protons ^{19}Na à l'énergie c.m. $E_{c.m.} = 1.066 \pm 0.003$ MeV avec un largeur proton $\Gamma_p = 10 \pm 3$ keV. Le shift de Coulomb entre les niveaux miroirs $1/2^+$ en ^{19}O et ^{19}Na est de 0.73 MeV, parmi les valeurs les plus grands observées dans les noyaux exotiques légers.*

The structure of nuclei near the drip lines is one of the major current interests in nuclear physics. Almost no spectroscopic information is available on the proton-rich nucleus ^{19}Na, which is proton unbound by 321±13 keV [1].Even though it is not far from stability, very little is known experimentally about its structure and level scheme: there are no spin assignments, and only the location of the ground state and of the first excited state have been determined by nuclear reactions involving stable beams [2,3] The aim of the present experiment[4] was to measure the energy and the width of the second excited state of ^{19}Na, which according to the mirror nucleus ^{19}O ($E_x = 1.4717 \pm 0.0004$ MeV) should have a spin $J^\pi = 1/2^+$ [1].

The experiment has been performed at the RIB facility at the Centre de Recherches du Cyclotron (CRC) at Louvain-la-Neuve, Belgium. Details of the experimental method and the data analysis can be found in Ref.[4]. Briefly, we have used the reverse elastic scattering technique, widely applied in the past for nuclear spectroscopy studies [5] by bombarding a proton-rich target with a ^{18}Ne beam at different laboratory energies E_{lab} = 21, 23.5 and 28 MeV. The average intensity of the ^{18}Ne beams on target was of the order of 4×10^6 pps, which was maintained for periods of several days. The target consisted of a 0.5 mg/cm^2 polyethylene $(CH_2)_n$ foil with a very thin Au coating evaporated on the upstream face of the target. The Au layer was used for normalization (see below).

The recoil protons were detected in two LEDA (**L**ouvain-la-Neuve **E**dinburg **D**etector **A**rray) systems[6] covering c.m. angles $\theta_{c.m.}$ = 170.2º- 156.6º and $\theta_{c.m.}$ = 131.1º- 120.2º. A 18 μm thick Mylar foil was situated in front of all LEDA sectors, except one, to stop the high energy scattered ^{18}Ne and most of the recoiled ^{12}C particles. The "uncovered" LEDA sector was used for monitoring the number of incoming beam particles by detecting the ^{18}Ne ions scattered on the thin Au layer, assuming a purely Rutherford elastic cross section for ^{197}Au(^{18}Ne,^{18}Ne)^{197}Au at the measured energies. The advantage of this method is that one obtains an intrinsic normalization simultaneously to the recoil proton measurement.

Time-of-flight spectra were obtained at all measured angles and at the three beam energies, covering laboratory proton energies from 2.1 to 5.5 MeV. Data obtained in overlapping energy regions are in excellent agreement. From the recoil proton spectra we have obtained differential cross sections for each angle and for c.m. energies in the range $E_{c.m.}$ = 0.7 to $E_{c.m.}$ = 1.5 MeV, by correcting the number of counts for the solid angle of the detectors, the number of protons in the target, and the total number of incident beam particles. Corrections for energy loss in the target and in the Mylar foil have also been applied[7] .Figure 1 shows the differential cross section versus c.m. energies for two typical c.m. angles (a) 170.2º and (b) 131.1º. The total error includes the statistical error and the uncertainties due to the normalization and the energy calibration. The dotted curve is the Rutherford cross section.

We have used the *R*-matrix formalism[8] to fit the differential cross sections in the entire angular and energy range. Details of the *R*-matrix analysis can be found in Ref.[4]. The fitted parameters are the pole parameters converted to the resonance energy E_R and the proton width Γ_p of the $1/2^+$ state in ^{19}Na. In order to account for the experimental energy broadening due to several effects such as energy straggling on target and on

the Mylar foil covering the detectors (ΔE_s), opening angle (ΔE_θ) and electronic energy broadening (ΔE_e), we have folded the calculations with a Gaussian distribution, with a full width at half maximum ΔE, which was set equal to the total energy broadening. Typical values of ΔE are 28 keV for an angle $\theta_{c.m.}$= 170.2º, 17 keV for $\theta_{c.m.}$= 156.6º, (ΔE_s is the most important contribution in both cases) and 90 keV for $\theta_{c.m.}$= 120.2º, (ΔE_θ is the most important contribution).

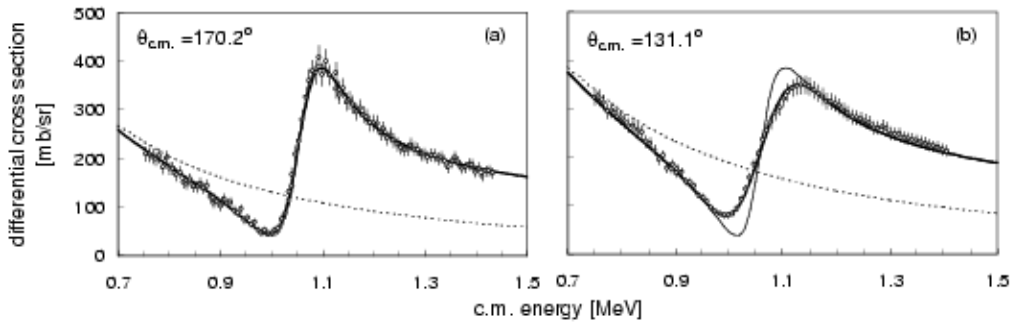

Figure 1 : ^{18}Ne+p elastic cross section versus c.m. energies for c.m. angles (a) 170.2° and (b) 131.1°. The thicker solid curves are the best R-matrix fit, including an energy correction ΔE. The thinner solid curve are the fits obtained without ΔE folding. The dotted curves are the Rutherford cross sections.

We have tested the sensitivity of the fit to the *R*-matrix channel radius *a* by performing global fits for three different values *a* = 4, 5 and 6 fm. The best fit (thicker solid curves in Figure 1) was found for *a* = 5 fm with a resonance energy and proton width:

$$E_R = 1.066 \pm 0.003 \text{ MeV},$$

$$\Gamma_p = 101 \pm 3 \text{ keV},$$

where the small errors are due to the strong sensitivity of χ^2 with respect to E_R and Γ_p. The thinner solid curve in Figure 1 (unresolved for (a)) are the fits obtained without ΔE folding. The corresponding dimensionless reduced width is θ_p^2 = 22.9%. This value is similar to or even larger than the reduced width of $\ell = 0$ states in other light nuclei such as ^{13}N (E_x = 2.37 MeV, θ_p^2 = 21.8 %) or ^{14}O (E_x = 5.17 MeV, θ_p^2 = 21.4 %). The large θ_p^2 value is also consistent with the important Coulomb shift. In ^{19}O, the excitation energy of the mirror state is E_x =1.472 MeV [1] whereas it is E_x =0.745±0.013 MeV for ^{19}Na. This Coulomb shift (≈ 0.73 MeV) is among the largest values observed in light nuclei. It is typical of single particle states, found in nuclei near the drip lines.

According to the mirror nucleus ^{19}O, several states should be present in the c.m. energy range 2 - 3 MeV. In order to obtain a global picture of the low-energy states of ^{19}Na, further investigations are planned in December 2003 at the CRC.

This work has been supported by the European Community-Access to Research Infrastructure action of the Improving Human Potential Program, contract Nº HPRI–CT–1999–00110 and the Belgian program P5/7 on interuniversity attraction poles of the Belgian-state Federal Services for Scientific, Technical and Cultural Affairs. M.G. acknowledges the support of the National Fund for Scientific Research (FNRS), Belgium. T.D. and P.J.W. acknowledge the support of the Engineering and Physical Sciences Research Council (EPSRC), UK.

[1] D.R. Tilley et al., Nucl. Phys. A595 (1995) 1.
[2] J. Cerny et al., Phys. Rev. Lett. 22 (1969) 612.
[3] W. Benenson et al., Phys. Lett. 58B (1975) 46.
[4] C. Angulo et al., Phys. Rev. C67, 014308 (2003).
[5] J.-S. Graulich et al., Eur. Phys. J. A13 (2002) 221, and references therein.
[6] T. Davinson et al., Nucl. Inst. Meth. A454 (2000) 350.
[7] SRIM2000 program, v.39, J.F. Ziegler and J.P. Biersack, 1998, 1999 IBM Co.
[8] A.M. Lane and R.G. Thomas, Rev. Mod. Phys. 30 (1958) 257.

3. RÉACTIONS NUCLÉAIRES

3.1. Study of fusion-fission and fusion-evaporation processes in the ^{20}Ne + ^{159}Tb interaction between 8 and 16 MeV/nucleon

J. Cabrera, Th. Keutgen, Y. El Masri, V. Roberfroid, I. Tilquin, Ch. Dufauquez, A. Ninane (Institut de Physique Nucléaire, Université catholique de Louvain, Louvain-la-Neuve, Belgium); R. Régimbart (LPC de Caen, France); R.J. Charity (Department of Chemistry, Washington University, St. Louis, Missouri, USA); D. Hinde (Department of Nuclear Physics, The Australian National University, Canberra, Australia); J.B. Natowitz, K. Hagel, R. Wada (Cyclotron Institute of Texas A & M University, USA)

Résumé : *Les études des temps de vie caractéristiques des processus de fission nucléaire par la technique dite de « l'horloge neutronique » sont généralement associées à des calculs théoriques basés sur des modèles statistiques et/ou dynamiques décrivant les mécanismes sous-jacents. C'est dans cette perspective que nous avons entrepris à Louvain-la-Neuve, l'étude des réactions de fission induite dans les collisions ^{20}Ne + ^{159}Tb entre 8 et 16 MeV/nucléon. Dans ce travail, nous avons réussi à déterminer :*

a) les sections efficaces de fusion-évaporation et fusion-fission de cette réaction à 8, 10, 13 et 16 MeV/nucléon ;

b) les distributions en énergie, en angle et les multiplicités de pré- et de post-scission des neutrons et des particules chargées légères (proton et alpha) émises lors de la désexcitation du noyau fissionnant ;

c) la balance énergétique totale du processus de fission tout en tenant compte des contributions des mécanismes de pré-équilibre et/ou de fusion incomplète.

Les comparaisons de ces résultats expérimentaux avec les prédictions du code statistique GEMINI et du code dynamique HICOL nous ont permis de déterminer certains domaines de temps de vie associé à la fission ainsi que les contributions du processus de fission rapide et ce en fonction des énergies d'excitation du noyau composite initial.

3.1.1. Introduction

Major fission lifetime studies were performed using the "Neutron clock" technique [1] which comprises measurements of the neutron multiplicities emitted before (pre-) and after (post-) fission has occurred. Such experimental multiplicities are usually coupled with statistical and dynamical model calculations evaluating the characteristic fission lifetimes. Statistical-model simulations need inputs such as: the initial excitation energy (E*) of the fissile nucleus (CN), its mass and initial intrinsic angular-momentum distribution. In case of the occurrence of an incomplete fusion or pre-equilibrium emissions, the CN characteristics may be substantially different from the case of the complete fusion between the projectile and the target nuclei. Moreover, the presence of fast fission at high angular momentum $\ell_{Bf=0} \leq \ell \leq \ell_{crit}$ will produce CN with significant deformed shapes which must be taken into account in the decay description. So, initial conditions (IN) of any simulations are related to evaporation residues and fission cross-section ratios and have to take into account the pre-equilibrium emission and the eventual presence of the fast fission process.

3.1.2. Experimental set-up

In these experiments, ^{20}Ne beams extracted from CYCLONE, the Louvain-la-Neuve cyclotron, were used to bombard a self-supporting 250 ± 8 μg/cm^2 thickness ^{159}Tb foil at energies of 8, 10, 13 and 16 MeV/nucleon. The evaporation residues (ER) and single fission fragments (F) were detected with two "micro-channel plate-Silicon diode" assemblies (GJ1,2). Coincident fission fragments were detected by two 20×20 cm^2, X and Y position sensitive, Multi-Wire Proportional gas Counters. Six silicon (Si) triple-telescopes, positioned only at backward angles, were used to detect light charged particles (p,α) in coincidence with the fission fragments. Neutron spectra and angular distributions have been obtained using the 96 NE213 liquid-scintillation DEMON counters, mounted in a 4π geometry around the reaction chamber with a distance-of-flight of 185 cm.

3.1.3. Evaporation Residues and Fission cross-sections

Figure 1.a displays an example of the fit to the ^{20}Ne (13 MeV/u) + ^{159}Tb evaporation-residue data using the Morgenstern et al. formalism[2,3]. Black dots represent the experimental ER velocity distribution in the laboratory frame and the full line corresponds to the result of the fit. Vertical lines correspond to the upper and

lower limits of the data considered in the fit. V_{CN}^{CF} is the expected mean velocity in case of a complete fusion interaction, while V_{CN} is the fitted mean velocity (or the distribution centroid). Figure 1.b displays the centre-of-mass (c.m.) experimental and fitted (full curve $\propto K/\sin(\theta_{cm})$) angular distributions of the fission fragments detected in the GJ1,2. Fits were performed for all ER detection angles and for all beam energies leading to the determination of the ER and Fission excitation functions.

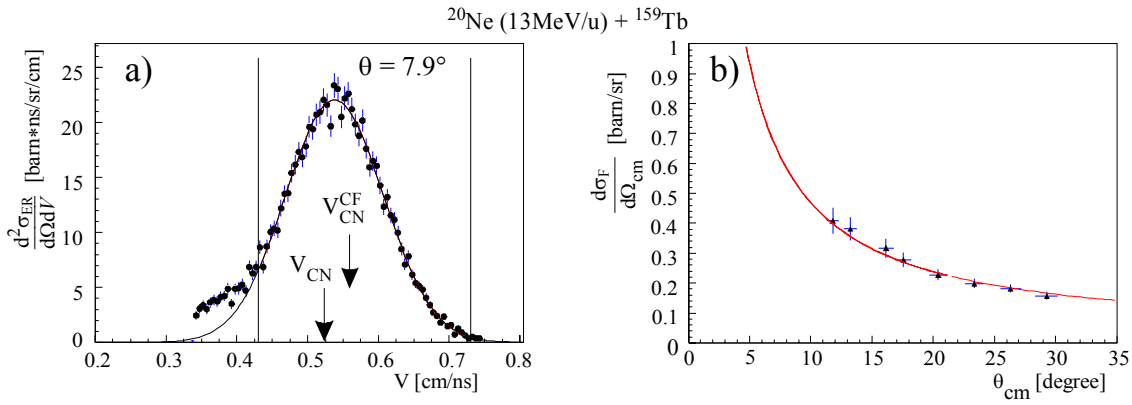

Figure 1.

The cross-sections evolution, as a function of the maximum CN excitation energy E* (assuming a complete fusion process), is shown in figure 2a. This figure also shows the sum of $\sigma_{ER} + \sigma_F$ giving the total fusion σ_{FU} cross-section. Error bars include statistical and data normalisation uncertainties. The corresponding critical angular momentum ℓ_{crit}^{CF} , calculated assuming the sharp cut-off approximation i. e. $\sigma_{FU} = \pi\lambda\!\!\!^{-2}(\ell_{crit}^{CF} + 1)^2$, is displayed in figure 2b.

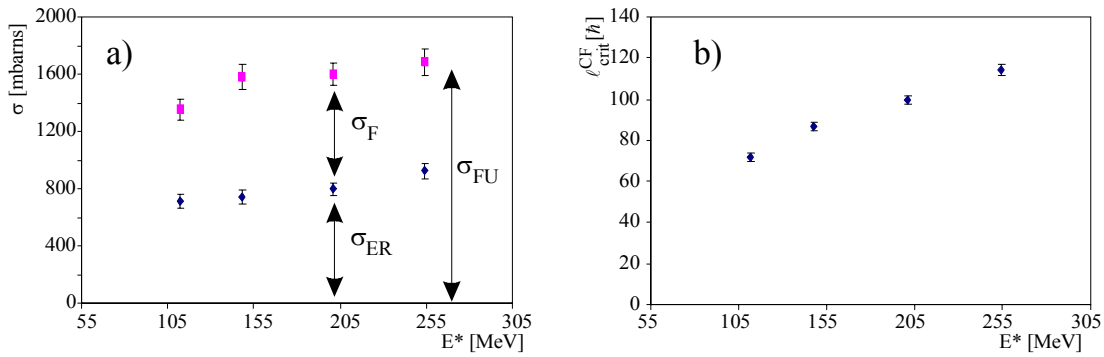

Figure 2.

A velocity shift between the expected CN mean velocity V_{CN}^{CF} in case of CF and the experimental mean velocity V_{CN} has been observed in the data of the three highest beam energies (see an example in Figure 1a). This shift clearly suggests the occurrence of pre-equilibrium emission (PE) inducing an incomplete fusion process (IF). Our experimental set-up was not adapted for the measurement of all types of mass losses by PE emission. We have used a 2nd-order polynomial interpolation of PE multiplicities extracted from systematics of light particles compiled from references[4-8]. Table 1 lists the light-particle PE multiplicities interpolated from these systematics. Total mass and charge losses by PE emission, were then calculated. The resulting PE neutron multiplicities are compared to the experimental ones extracted from the moving multi-source fit of DEMON data (see next section). Notice the excellent agreement observed between the estimated values and the experimental ones.

	Systematic					Exp.		
ε_p [MeV/u]	ν_n^{PE}	ν_p^{PE}	ν_d^{PE}	ν_t^{PE}	ν_α^{PE}	ν_n^{PE}	Δm [u]	M_{IN}^{PE} [u]
8	0.23±0.15	0.00±0.03	0.00±0.02	0.00±0.01	0.11±0.02	—	0.67±0.32	178±0.3
10	0.32±0.19	0.00±0.02	0.00±0.02	0.00±0.01	0.18±0.02	0.34±0.03	1.06±0.20	178±0.2
13	0.58±0.23	0.19±0.01	0.07±0.01	0.04±0.01	0.28±0.01	0.49±0.04	2.06±0.14	177±0.1
16	0.98±0.25	0.40±0.01	0.17±0.01	0.12±0.01	0.35±0.01	0.88±0.07	3.38±0.17	176±0.2

Table 1.

In the intrinsic angular-momentum distribution of CN assuming sharp cut-off approximation, the maximum angular momentum J_{crit}^{PE}, taking into account the angular momentum carried away by PE emission $\Delta\ell$, was extracted from the experimental ℓ_{crit} values. Using the Cerruti et al. formalism[9] and detailed balance calculations, the new CN excitation energy after PE emission E_{IN}^{*PE} was estimated. Its evolution, as a function of E*, is displayed in figure 3. J_{crit}^{PE} and E_{IN}^{*PE} will be used as inputs in the following theoretical simulations.

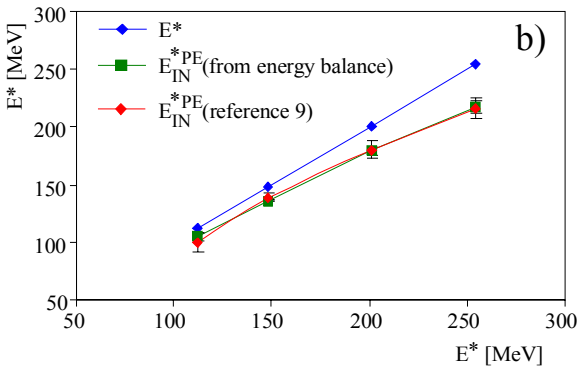

Figure 3.

3.1.4. Light particle multiplicities

The neutron multiplicities of pre-equilibrium ν_n^{PE} (Table 1), pre-scission ν_n^{pre}, post-scission ν_n^{post} and the related pre- and post-scission nuclear temperatures of corresponding emission sources T_n^{pre}, T_n^{post}, have been obtained through a moving multi-source fit of the neutron energy spectra and their angular distribution in a 4π space geometry using Watt (volume type emission) and Maxwell (surface type emission) type distributions. Figure 4 displays an example of fits to neutron energy spectra assuming four moving-source contributions: CN, FF1, FF2 and PE, at different angle θ_n and ϕ_n of DEMON detectors; the fitted neutron angular distribution in the reaction plane (ϕ_n = 0° and 180°) at 13 MeV/u is also displayed assuming the same contributing sources. The black curves correspond to the sum of all the contributions. Open circles display the experimental values with the corresponding total uncertainties.

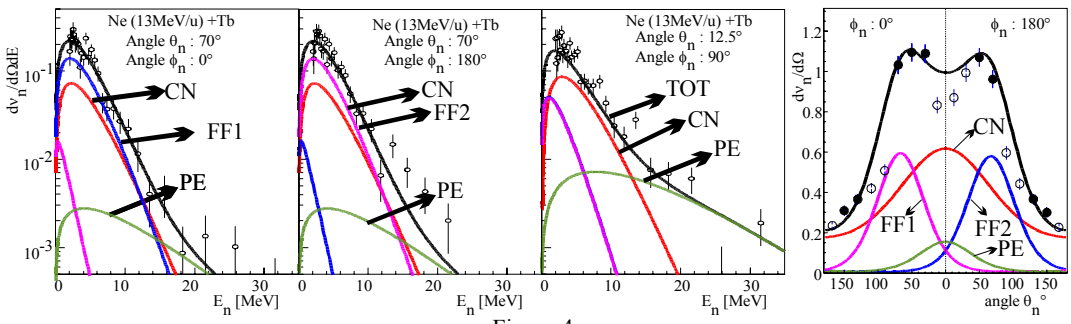

Figure 4.

Similarly the alpha and proton pre- and post-scission multiplicities were extracted from fits to their energy spectra assuming, in these cases, three Maxwellian emitting sources with the related effective barriers of emission: one for the CN emission and two for the fission fragments. As PE could not be experimentally

determined because the Si triple-telescopes were only positioned at backward angles with respect to the beam axis their multiplicities were taken from table 1.

3.1.5. Total energy balance of fission process

Using the extracted light-particle PE multiplicities, the calculation of the energy balance for the fission process was undertaken as shown in table 2. $E_{\nu\gamma}$, the residual excitation energy carried out by the gamma-ray emission, is in excellent agreement with the systematic of Back et al. [10].

ε_p [MeV/u]	E^{*PE}_{IN} [MeV]	E^{pre} [MeV]	Q_1 [MeV]	E^{*}_{af} [MeV]	$\overline{TKE}_F$ [MeV]	E^{post} [MeV]	Q_2 [MeV]	E^{*}_{res} [MeV]	$E_{\nu\gamma}$ [MeV]
8	101±8	12.2	-29.0±0.8	58.4±2.4	128±0.1	8.9	88±4	10.4±7.8	10.4
10	139 ±4	23.8	-40.4±0.4	74.7±1.5	140±0.1	8.3	85±1	11.5±3.5	11.5
13	180±8	40.3	-49.8±1.9	90.4±4.2	136±0.1	12.8	71±3	12.8±8.0	12.8
16	216±9	53.8	-59.5±1.0	103.1±4.4	134±0.1	16.1	61±2	13.9±9.2	13.9

Table 2.

3.1.6. Simulations

Decays of CN have been simulated with the recently modified statistical-model code GEMINI[11]. Initial CN parameters such as mass, charge and excitation energy were taken from the previous discussions and tables. Initial CN intrinsic angular-momentum distributions were divided in two regions at each beam energy. For $0 < J_{IN} \leq J^{Sierk}_{Bf=0} = 78\hbar$ (region (1)) where conventional fission or slow fission process is supposed to occur and no additional shape modification of CN was assumed apart from the normal evolution following the RLDM[12]. For $J^{Sierk}_{Bf=0} < J_{IN} \leq J^{PE}_{crit}$ (region (2)) GEMINI simulations were performed assuming a prolate shape deformation corresponding to a ratio of the symmetry to off-symmetry axis equal to 1.5 as predicted for our reactions by the dynamical simulations of HICOL code[13]. In the GEMINI code, such CN deformation was maintained only during the fission delay time τ_d where fission is supposed to be hindered. The Yrast lines and the light-particles transmission coefficients were modified to account for this deformation during this fission delay time.

As fast fission was not present at 8 MeV/u reaction, the simulations for this energy were used to extract and fix the parameters a_0 and a_f/a_n from the adjustment of pre- and post-scission light particle multiplicities and the corresponding σ_{ER}/σ_F ratio. The constant level-density parameter a_0 was found to be equal A/9 MeV^{-1} and the ratio of the level density at the saddle point to its value at the equilibrium point (a_f/a_n) was found to be 1.05. For this projectile energy, the fission delay time was found to be $\tau_d = \tau_d^{(1)}$ = 45 zs. For 10, 13 and 16 MeV/u, the simulations were divided in two steps. In a first-order approximation, we have consider that there was no ER formed in the CN decay in region (2) (i.e. $\sigma^{(2)}_{RE}$ = 0). This enables us to calculate $\sigma^{(1)}_{RE}/\sigma^{(1)}_{FF}$ ratios from the experimental σ_{RE}/σ_F ratios based on a weighted procedure using the corresponding $\sigma^{(1)}_i$ and $\sigma^{(2)}_i$ cross sections (i = RE or FF) associated with region (1) and (2) i. e.:

$$\frac{\sigma_{RE}}{\sigma_F} = \frac{\left(\sigma^{(1)}_{RE}/\sigma^{(1)}_{FF}\right)\sigma^{(1)} + \left(\sigma^{(2)}_{RE}/\sigma^{(2)}_{FF}\right)\sigma^{(2)}}{\sigma^{(1)} + \sigma^{(2)}} \quad \text{leading to:} \quad \frac{\sigma^{(1)}_{RE}}{\sigma^{(1)}_F} = \frac{\left(\sigma^{(1)} + \sigma^{(2)}\right)\left(\sigma_{RE}/\sigma_F\right)}{\sigma^{(1)}}.$$

Fission delay times $\tau^{(1)}_d$ for this region, were adjusted to correctly simulate these ratios $\sigma^{(1)}_{RE}/\sigma^{(1)}_F$. The corresponding $\nu^{(1)}_n$ multiplicity was used to calculate a weighted mean values for pre- and post-scission multiplicities which could be compared to the experimental values i.e.:

$$\nu_i = \frac{\nu^{(1)}_i \times \sigma^{(1)} + \nu^{(2)}_i \times \sigma^{(2)}}{\sigma^{(1)} + \sigma^{(2)}} \quad \text{with} \quad i = n, p, \alpha .$$

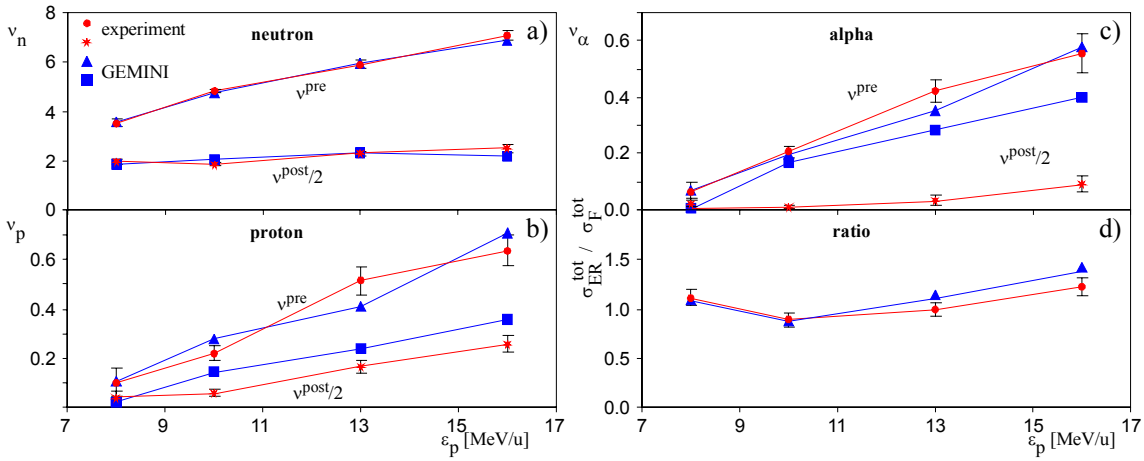

Figure 5.

In this way we could adjust from GEMINI simulations the fission delay time $\tau_d^{(2)}$ for the second region. The results of all these simulations (squares and triangles), assuming symmetric-fission partition, are presented in figure 5 and compared to the experimental values (circles and starts). Circles correspond to the experimental pre-scission multiplicities or cross-section ratios. The fission-fragment multiplicities ($\nu^{post}/2$ for symmetric fission partition), are represented by starts. The simulated results are represented by triangles and squares, respectively. The best resulting fission delay times for 10, 13, and 16 MeV/u extracted from these simulations were, in that order, 40, 15, 15 zs for region (1) and 0, 20, 15 zs for region (2) as shown in figure 6.c.

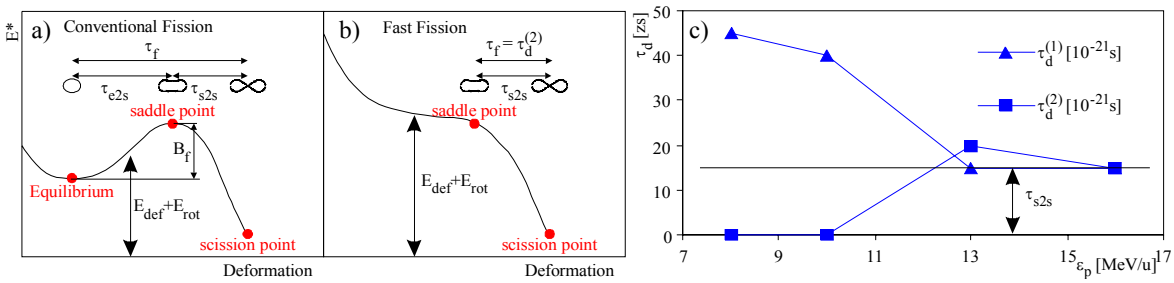

Figure 6.

3.1.7. Conclusions : characteristic fission times

In principle, the dynamic fission times τ_f can be divided in two contributions (figure 6.a): A time to proceed from the nucleus equilibrium point to its saddle point (τ_{e2s}) and a time to move from the saddle point to the scission point (τ_{s2s}). The dynamic fission delay time τ_d corresponds to the lower limit of the time of fission. This time takes into account the minimal time necessary for the nucleus to first deform and reach the saddle point and then the scission point. The decay properties of CN, simulated in the region (2) of the angular momentum distribution, give rise exclusively to fast fission. For those CN, the delay time $\tau_d^{(2)}$ coincides with the time of fission for these nuclei. If we consider that, these highly deformed nuclei are at the saddle point such as in figure 6.b, then $\tau_d^{(2)}$ would be the time necessary to proceed from the saddle point to the scission point in a normal situation. For energies of 13 and 16 MeV/u, the region (2) is significant and thus the statistics enabled us to highlight this concept and to extract this value. Moreover for these energies, where fast fission contribution is important, we obtain for the data of region (1) a comparable value with (~15 zs). This makes us assume that $\tau_d^{(1)} \approx \tau_d^{(2)} \approx 15 \pm 5$ zs $= \tau_{s2s}$ (figure 6.c), suggesting that in this case τ_f is dominated by τ_{s2s} with negligible τ_{e2s}. As region (2) for 8 and 10 MeV/u was null or negligible, $\tau_d^{(2)}$ did not give any information about τ_{s2s} and thus τ_f in these cases remains with substantial contributions from τ_{e2s}. Finding that τ_{s2s} appears constant for the two highest beam energies we have concluded that the τ_{s2s} time is constant and must remain such with increasing excitation energy. This assumption is confirmed by the dynamical code HICOL[13] predicting for our reactions a constant time of 45 zs.

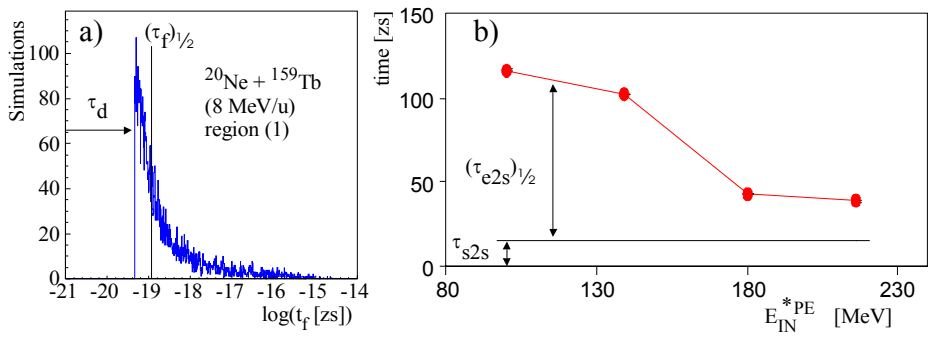

Figure 7.

Looking at the statistical-fission lifetime distribution from the simulations of region (1) (figure 7a), we can calculate the mean half-lifetime associated to the conventional fission $(\tau_f)_{1/2}$. As we can see, the fission-time distribution has a long tail which can cover up to 5 orders of magnitude. These long lifetimes have been observed in "crystal blocking" [14, 15] and "KX-ray detection" [16] techniques. The equilibrium to scission time $(\tau_{e2s})_{1/2}$ associated to the half-lifetime can be calculated by the difference $(\tau_{e2s})_{1/2} = (\tau_f)_{1/2} - \tau_{s2s}$. The calculated values are 101.44 ± 5.31 zs, 87.21 ± 5.27 zs, 27.58 ± 5.12 zs, 23.53 ± 5.10 zs for the beam energies of 8, 10, 13 and 16 MeV/u respectively and are plotted in figure 7b.

[1] D. Hilcher et al., Ann. Phys. Fr. 17 (1992) 471 and references therein.
[2] H. Morgenstern et al., Phys. Lett. B113 (1982) 463.
[3] J. Gomez del Campo et al., Phys. Rev C19 (1979) 2170.
[4] H. K. Leegte et al., Phys. Rev. C46 (1992) 991.
[5] T. C. Awes et al., Phys. Rev. C24 (1981) 89.
[6] E.Holub et al., Phys. Rev. C28 (1983) 252.
[7] D. J. Hinde et al., Phys. Rev. C45 (1992) 1229.
[8] D. Prindle et al., Phys. Rev C48 (1993) 291.
[9] C. Cerruti et al., Nucl. Phys. A453 (1986) 175.
[10] B. B. Back et al., Phys. Rev. C41 (1990) 1495.
[11] R. J. Charity et al., Nucl. Phys. A483 (1988) 371.
[12] A. J. Sierk, Phys. Rev. C33 (1986) 2039.
[13] H. Feldmeier, Rep. Prog. Phys. 50 (1987) 915.
[14] J. S. Foster et al., Nucl. Phys. A464 (1987) 497.
[15] F. Goldenbaum et al., Phys. Rev. Lett. 82 (1999) 5012.
[16] J. D. Molitoris et al., Phys. Rev. Lett. 70 (1993) 537.

3.2. Neutron-skin effects in the mirror reactions $^{58}Ni + ^{122}Sn$ and $^{64}Ni + ^{116}Sn$ between 6 and 7 MeV/nucleon

V.Roberfroid, L.Lebreton, J.Cabrera, Th.Keutgen, I.Tilquin, A.Ninane, C. Dufauquez, C. Ghisalberti, J. Lehmann, Y. El Masri (Institut de Physique Nucléaire, Université catholique de Louvain, Louvain-la-Neuve, Belgium); R.Regimbart (LPC of Caen, France); J.B. Natowitz, K. Hagel and R. Wada (Cyclotron Institute of Texas A & M University, USA)

Résumé : L'utilisation des noyaux magiques en protons, tant pour le projectile (Z=28) que pour la cible (Z=50), permet d'isoler un éventuel effet de peau de neutrons dans les réactions $^{58}Ni + ^{122}Sn$ et $^{64}Ni + ^{116}Sn$. L'objectif est l'étude, à l'aide de ces réactions, de l'éventuel effet de ces neutrons sur : la section efficace de fusion, la compétition entre la fusion-évaporation et la fusion-fission, les collisions très inélastiques et les multiplicités de particules légères associées, neutres ou chargées.

Following our previous report [1], ν_n^{pre} and ν_n^{post}, the pre- and post-scission neutron multiplicities emitted in a fusion-fission process, were determined for the three following reactions :

- ^{58}Ni+^{122}Sn at 375.5 MeV (b375),
- ^{58}Ni+^{122}Sn at 354 MeV (b354),
- ^{64}Ni+^{116}Sn at 382.5 MeV (b382).

This year, we have extracted ν_{α}^{pre}, ν_{α}^{post}, ν_{p}^{pre} and ν_{p}^{post}, the pre- and post-scission multiplicities of α and proton particles respectively from the analysis of the data associated to the six Si triple-telescopes. The results are reported in the table 1.

	ν_{n}^{pre}	ν_{p}^{pre}	ν_{α}^{pre}	ν_{n}^{post}	ν_{p}^{post}	ν_{α}^{post}
(b375)	3.2±0.16	0.26±0.03	0.16±0.02	2.3±0.2	0.26±0.03	0.19±0.02
(b354)	3.0±0.15	0.16±0.02	0.1±0.01	2.0±0.2	0.17±0.02	0.06±0.01
(b382)	3.0±0.12	0.16±0.02	0.11±0.01	1.9±0.2	0.23±0.02	0.1±0.01

Table 1 : Pre- and post-scission neutron, proton and α multiplicities in the three studied reactions. Uncertainties are only statistical.

One can observe that there is no clear evidence of any neutron skin effects (within the uncertainties) on the de-excitation of the ^{180}Pt compound nucleus. The precision on the light charged particles (LCP) multiplicities is quite bad as a consequence of the weak statistic.

To complete the data analysis, an energy balance can be done, assuming negligeable the emission of all other light particles (d, t and ^{3}He). The equations of energy conservation are written below for a complete scheme of fusion-fission process :

<u>Compound nucleus formation</u> : $K_p + M_p c^2 + M_t c^2 = K_{cn} + M_{cn} c^2 + E_{cn}^*$

Where K_p and M_p are the kinetic energy and the mass of the projectile, K_{cn} and M_{cn} are the kinetic energy and the mass of the compound nucleus, M_t is the mass of the target and E_{cn}^* the initial compound nucleus excitation energy.

<u>Compound nucleus de-excitation</u> : $M_{cn} c^2 + E_{cn}^* = E_{cn}^{*bf} + M_{cn}^{bf} c^2 + \sum_{i=n,p,\alpha} \nu_i^{pre} (\overline{K_i^{pre}} + m_i c^2)$

Where E_{cn}^{*bf} and M_{cn}^{bf} are the residual excitation energy and the mass of the compound nucleus after evaporation and just before fission (*bf*). $\overline{K_i^{pre}}$ and m_i are respectively the mean kinetic energy, calculated using the experimentally extacted nuclear temperature of the emitting compound nucleus, and the mass of the light particle *i* emitted.

<u>Fission of the compound nucleus</u> : $E_{cn}^{*bf} + M_{cn}^{bf} c^2 = 2E_{ff}^{*be} + 2M_{ff}^{be} c^2 + TKE$

Where E_{ff}^{*be} and M_{ff}^{be} are the excitation energy and the mass before evaporation (*be*) of the fission fragments assuming, in this case, a symmetric mass partition. *TKE* is the experimentally extracted total kinetic energy in the center-of-mass of the two fission fragments.

<u>De-excitation of the fission fragments</u> : $2E_{ff}^{*be} + 2M_{ff}^{bf} c^2 = 2E_{ff}^{*ae} + 2M_{ff}^{ae} c^2 + \sum_{i=n,p,\alpha} \nu_i^{post} (\overline{K_i^{post}} + m_i c^2)$

Where E_{ff}^{*ae} and M_{ff}^{ae} are the excitation energy and the mass after evaporation (*ae*) of the fission fragments in a symmetric partition and $\overline{K_i^{post}}$ the mean kinetic energy of the light particle *i* emitted by these fragments.

The results of these calculations are displayed in table 2.

Reaction	E^*_{cn} (MeV)	E^{*bf}_{cn} (MeV)	E^{*be}_{ff} (MeV)	E^{*ae}_{ff} (MeV)
(b375)	139	93	47	16
(b354)	124	81	45	17
(b382)	122	82	43	18

Table 2 : Initial and just before fission excitation energies E^*_{cn} and E^{*bf}_{cn} of the compound nucleus source of pre-scission particle emission. Initial and after evaporation excitation energies E^{*be}_{ff} and E^{*ae}_{ff} of the fission fragments in a symmetric fission sources of post-scission particle evaporation.

The residual excitation energy E^{*ae}_{ff} is expected to be released through γ-ray emission. In fact, following Back and al. systematics [2], one can predict, for our reactions, up to 16 total γ-ray multiplicity. Assuming a mean energy (per emitted γ) ranging between 1 and 1.5 MeV (to be expected in the fission fragment mass region), one can easily account for almost 16 to 24 MeV to be compared to the calculated residual excitation energy ($2.E^{*ae}_{ff} = 32\ MeV$). The resulting energy excess can be explained by an underestimation of the experimental light charged particle multiplicities. Indeed, the GEMINI code [3] predicts higher multiplicities for the α and protons emitted by the compound nucleus. To prove this assertion, an experiment was carried out in 2001 at the Legnaro laboratory (Italy) to study more specifically the properties of the associated light charged particle emissions in the b375 reaction. The analysis of the collected data is still in progress.

[1] Annual report of CYCLONE 2001.
[2] B. B. Back and al., Phys. Rev. C 41 (1990) 1495.
[3] R.J. Charity, Phys. Rev. C 53 (1996) 201.

3.3. Production of neutral and light charged particles in the alpha induced reactions on ^{nat}Si between 20 and 65 MeV

Ch. Dufauquez, Th. Keutgen, J. Cabrera, V. Roberfroid, A. Ninane, J. Van Mol, Y. El Masri (Inst. Physique Nucléaire, Université catholique de Louvain, Louvain-la-Neuve, Belgium) ; R. Régimbart (LPC, CAEN, France)

Résumé : *Des mesures ont été effectuées afin de déterminer les sections efficaces « inclusives » ($\frac{d^2\sigma}{dEd\Omega}$, $\frac{d\sigma}{dE}$, $\frac{d\sigma}{d\Omega}$ et $\sigma_{tot.}$) de production de particules légères chargées et neutre (n, p, d, t, ^{3}He et α) induites par des faisceaux alpha de 25.4, 45.5 et 57.8 MeV sur une cible de silicium naturel. Ci-dessous sont rapportés les résultats préliminaires obtenus à 25.4 MeV.*

In this experiment, detection of light charged particles was achieved by using, in the reaction chamber (see annual report 2000): i) seven Si triple-telescopes assemblies (85-705-705 µm thick) positioned at the backward angles with respect to the beam direction and ii) eight Si-Si-CsI telescopes assemblies (40-700 µm Si and 33 mm thick CsI) set at the forward angles. Neutron detection was provided by the 96 DEMON, NE213 liquid scintillator counters surrounding the reaction chamber at two meters distance-of-flight from the ^{nat}Si self-supporting target (215 µg/cm^2 thick).

The first step of our analysis was the establishment of sorting techniques allowing the creation of unambiguous regions of interest for each type of detected charged particles in the bidimentional plots ΔE_1-ΔE_2 and ΔE_2-ΔE_{CsI} derived from the Si-Si-CsI telescopes. (The analysis at the backward angles detection was already achieved last year (annual report 2001)). The second step of the analysis was to obtain the deriving particle energy spectra knowing their energy losses (ΔE_i) through the different members of these telescopes.

We are presently able to determine the complete lab. double–differential cross sections for all the light charged particles detected in this experiment. Fig. 1 displays these cross sections for the ^{nat}Si(α,α') reactions at

25.4 MeV incident alpha beam detected in the Si-Si-CsI telescopes (at 70°,60°,50°,40°, 30°, 25° and ± 10°) and in the Si triple-telescopes (at 105°, 120°, 125°, 140°, 145°, 160° and 165° with respect to the beam axis).

All the alpha energy spectra are divided into two regions, separated by the dotted line. The right side corresponds to the alpha selection, resulting from the particle discrimination in the bidimentional plot ΔE_1-ΔE_2 and the left side, at lower energies, to the alpha and ^{3}He which were stopped in the first Si stage (40 or 85 µm) of each type of telescope detector. In this left side region and principally at the backward angles, we can nevertheless make a distinction between pure alpha contribution and the mixing of alpha-^{3}He (↔) contribution. This limiting energy corresponds to the maximum energy of the ^{3}He produced in the ^{nat}Si(α,^{3}He) reaction. Thus the peak structure in this sub-region is mainly generated by ^{3}He contribution stopped in the 80 µm Si member of the triple-telescope while the continuum structure is due to α evaporation. This extension to lower energies allowed us to determine double differential cross sections for Si triple-telescope down to ~4.3 MeV and for Si-Si-CsI telescopes down to ~2.6 MeV .

The highest energy peaks (in the α spectra) were clearly identified as corresponding to the reported ground and excited energy levels of the residual ^{28}Si nucleus [1]. Fig. 1 they are indicated by red arrows and by the labels: g, 1, 2, … corresponding to the same indications reported on the level scheme of the nucleus.

However there are two points to underline:

1) Because of the ^{nat}Si target manufacturing procedure, the presence of some hydrogen contribution on the target surface was observed but without any consequences for the analysis. This is pointed out by the observation of two distinguished peaks in the two α energy spectra at ± 10°, mainly observed in the CsI detectors. All the other alpha spectra were not influenced as demonstrated by kinematics calculations. In fact the elastic scattering of the alpha particles in the H(α,α)p (Fig.1) reaction at 25.4 MeV incident energy is only allowed at laboratory angles less than 14.58° and at two specific alpha energies of 10.42 and 22.07 MeV.

2) In the near future an energy interpolation will be realized in order to resolve the energy dip in the built spectra for particles which have sufficient energy to punch through the first Si stage but not enough to be detected in the second Si telescope member due to the energy threshold of this latter. This is pointed on Fig. 1 by the dotted horizontal line mentioned above.

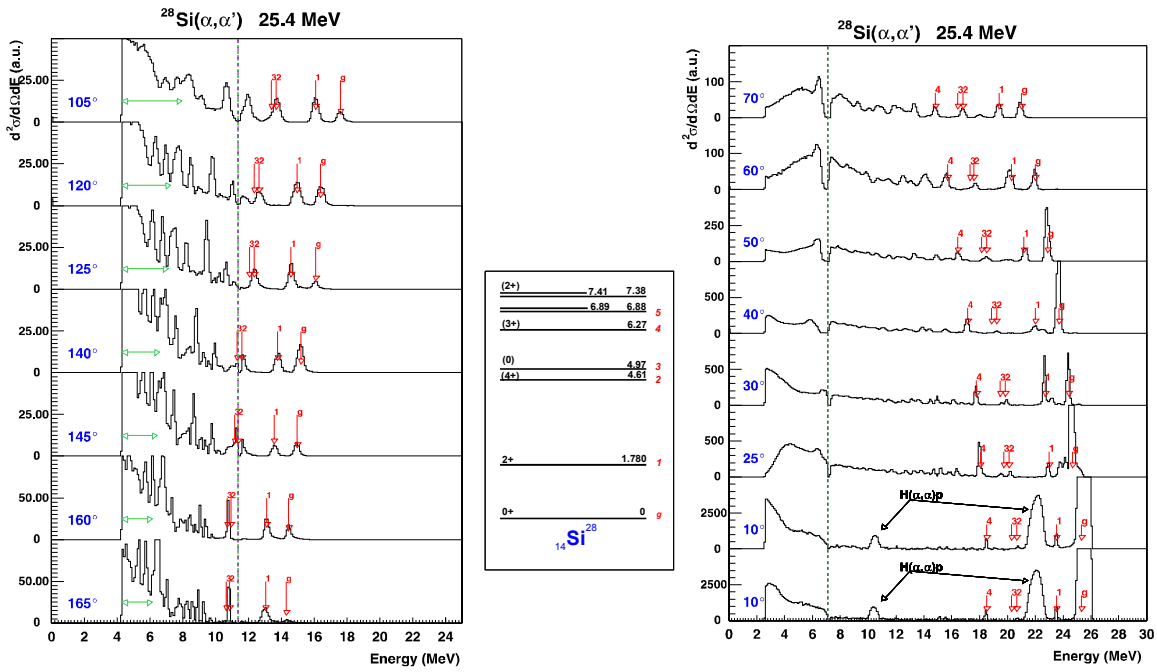

Figure 1 : Double-differential cross sections spectra in the laboratory frame of the alpha particles detected in the ^{nat}Si(α,α') reaction.

Similarly, Fig. 2 displays the double-differential cross sections for the $^{nat}Si(\alpha,d)^{30}P$ reaction also induced by the 25.4 MeV alpha incident projectiles. Again, one can observe the excellent energy resolution of the spectra. As indicated for the alpha spectra, one can easily follow, over a very large angular distribution, the evolution of the peaks corresponding exactly, in this case, to the ground and the excited level scheme of the residual ^{30}P nucleus.

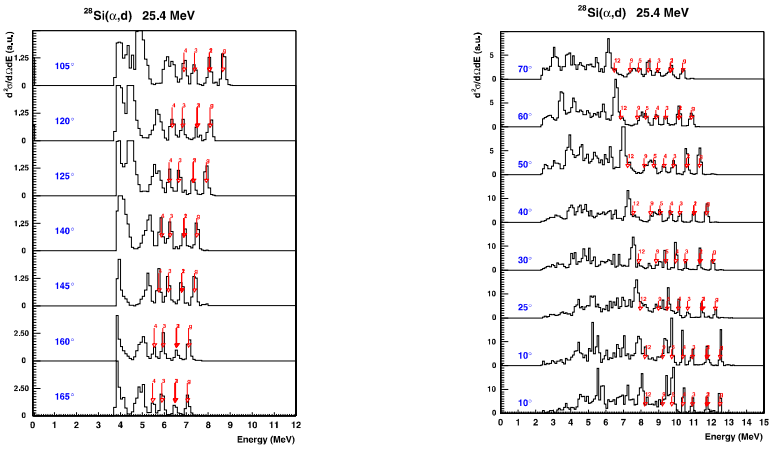

Figure 2 : Double-differential cross sections spectra of the deuteron particles detected in the $^{nat}Si(\alpha,d)^{30}P$ reaction.

Fig. 3 presents selected double-differential cross section spectra of (p, t and ^3He) secondary charged particles detected at some given laboratory angles. At this alpha incident energy (25.4 MeV), only p, d and α particles were clearly discriminated at the backward angles while p, d, t, ^3He and α were separated at the forward angles. Moreover, one can notice, as shown in the $^{nat}Si(\alpha,p)$ spectrum, the hydrogen presence in the Si target through the H(α,p)α peak. In this case, kinematics calculations give an energy of 12.23 MeV for this proton peak.

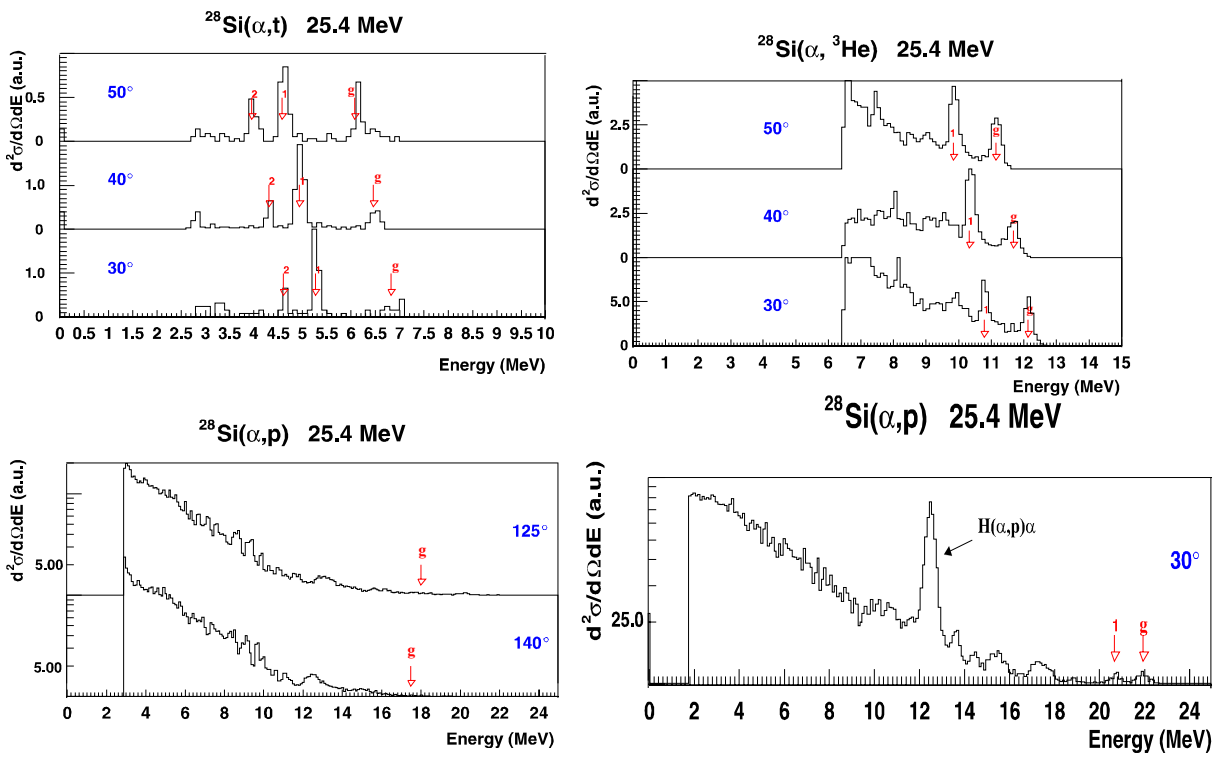

Figure 3 : Double-differential cross sections spectra of (p, t and ^3He) secondary charged particles detected at some given laboratory angles and produced with the 25.4 MeV alpha beam on ^{nat}Si target.

We are presently at the stage of achieving the data analysis of the 45.5 and 57.8 MeV alpha beams induced reactions. In the near future we are going to focus our analysis on the determination of the angular differential cross sections $\frac{d\sigma}{d\Omega}$ for all charged particles. The neutron data analysis will be the next step.

[1] C. Michael Lederer, Jack M. Hollander, I. Perlman, Table of isotopes, Sixth Edition, Wiley, Berkeley 1967.

3.4. First experiment using a new multidetector system based on monolithic telescopes

P. Figuera, F. Amorini, G. Cardella, A. Di Pietro, M. Papa, G. Pappalardo, M.G. Pellegriti, R.G. Pizzone, F. Rizzo, W. Tian, S. Tudisco (INFN: LNS and Sez. Catania, University of Catania); C. Angulo, S. Cherubini, A. Ninane (Centre de Recherches du Cyclotron et Institut de Physique Nucléaire, Université catholique de Louvain, Louvain la Neuve); R. Raabe, J.L. Sida (CEA Saclay)

Résumé : We recently developed a new multidetector based on monolithic silicon telescopes where the ΔE and residual energy stages are integrated on a single silicon chip. The first tests of the system have been performed in Louvain-la-Neuve using a ^{12}C beam and later the first real experiment has been performed using a ^{13}N beam. The observed characteristics of the multidetector will be discussed.

For those applications where compact detection systems with charged particle identification thresholds lower than 1 MeV/nucleon are requested, the conventional ΔE-E technique may be impossible to apply or may require the use of fragile and expensive detectors. To overcome these difficulties, in the last years we started to work on the development of some prototypes of monolithic telescopes where the ΔE and residual energy (ER) stages are integrated on the same silicon chip[1-3]. Such detectors have been built using ion implantation techniques, according to the scheme reported in figure 1. Basically a P^+ region has been obtained via B implantation on an N^- bulk. Such P^+ region acts as a common ground electrode both for the ΔE and ER stages. In this way a ΔE thickness of the order of 2 μm (including the dead layers) can easily be obtained, allowing for charge identification thresholds of the order of 300÷400 keV/nucleon in the mass region of Nitrogen[1]. After the development of some working prototypes having different geometries, we chose, as final device for our multidetector, a chip (15x4 mm^2) having 5 independent ΔE strips implanted on a common ER stage. Two of such devices, mounted on a common ceramic package, form a single detection module. The complete setup consists of up to 24 detection modules which can be arranged in different geometrical configurations according to the experimental needs. Signals from the detectors are fed into compact preamplifier boards working under vacuum. In the first real experiment performed in Louvain-la-Neuve 12 detection modules have been placed in plane covering the angular range $3^o \div 45^o$ on both sides of the beam to study the collision $^{13}N+^{9}Be$.

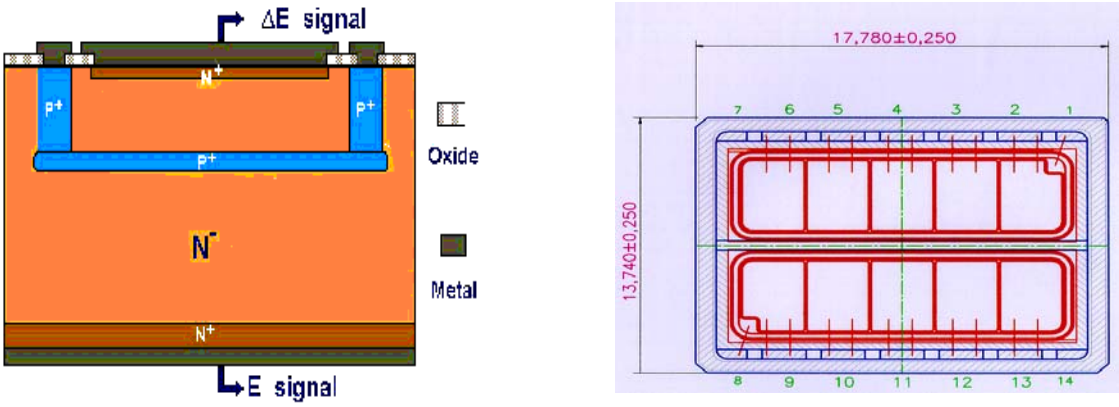

Figure 1 : a) Left Scheme of a monolithic telescope. b) Right Scheme of the front view of a single detection module. The two Si chips, having 5 ΔE stages each, are clearly visible in the figure.

A typical experimental problem in reactions induced by radioactive beams is the presence of an intense β background, which can be a real problem in those experiments aiming at the detection of low energy particles with conventional Si detectors. In figure 2 we show an on-line energy versus time spectrum collected in the collision $^{13}N+^{9}Be$ at 45 MeV, where the time reference has been given by the cyclotron HF. Here heavy ions,

protons and alphas are separated in time of flight, while the background due to the βs does not have any time correlation with the cyclotron HF.

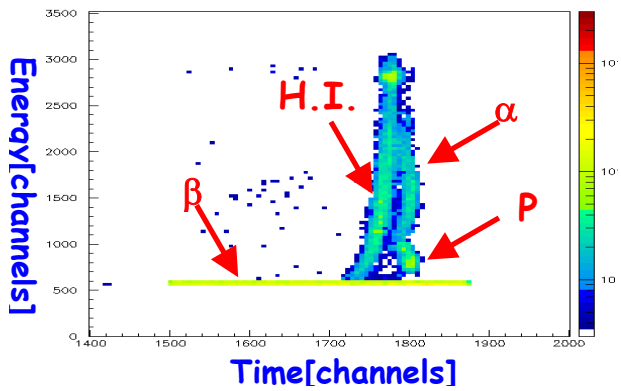

Figure 2 : Typical on-line energy versus time spectrum measured in the collision $^{13}N+^{9}Be$. The background due to βs, which is not correlated in time, is visible.

In figure 3, the same data of figure 2 are plotted in a ΔE versus residual energy spectrum which shows a good charge discrimination. Moreover, one can see that the β background is suppressed since the corresponding signals are going in the noise region of the ΔE, due to the extremely small thickness of this stage. The intense region at ΔE ≈ 0 is due to particles hitting different strips of the same detector and, if necessary, can be eliminated in the off line analysis.

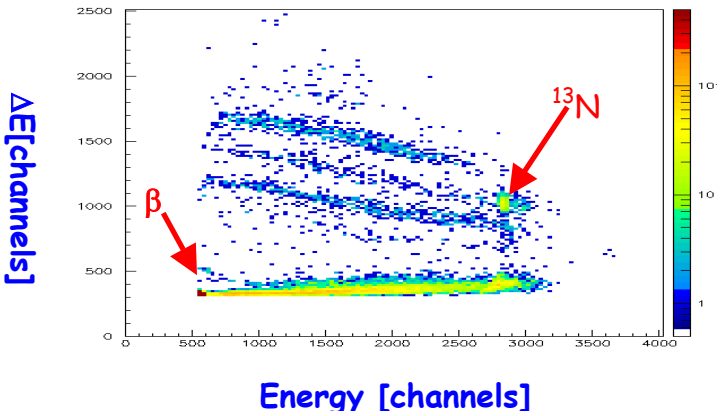

Figure 3 : On-line ΔE versus ER spectrum representing the same data plotted in figure 2.

Following the above discussion, we believe that the tests and the first data collected in Louvain-la-Neuve have shown that, using monolithic telescopes, we built a reliable multidetector with the following characteristics: very low identification thresholds (~ 300 ÷ 400 keV/nucleon in the mass region of Nitrogen); modular structure with the possibility to arrange it in very different configurations; high granularity; excellent β background suppression in reactions induced by radioactive beams.

[1] G. Cardella et al., Nucl. Instr. and Meth. A378 (1996) 262.
[2] S. Tudisco et al., Nucl. Instr. and Meth. A426 (1999) 436.
[3] A. Musumarra et al., Nucl. Instr. and Meth. A409 (1998) 414.

4. REACTIONS INDUITES PAR DES PROTONS

4.1. Study of proton-induced fission of actinide nuclei between 20 and 65 MeV bombarding energies

D. Belge, Ch. Dufauquez, Y. El Masri , T. Keutgen, A. Ninane, R. Prieels, V. Roberfoid and J. Van Mol (Institut de Physique Nucléaire, Université catholique de Louvain, Louvain-la-Neuve, Belgium)

Résumé : *Des mesures de sections efficaces de fission induite par protons sur les noyaux ^{238}U et ^{239}Pu ont été réalisées à 26.5 et 62.9 MeV. La masse des fragments de fission et leur distribution angulaire ont été mesurées en utilisant des chambres à gaz et à multifils X,Y (MWPC) ainsi que des ensembles jonction-galettes à microcanaux (GJ). Les distributions angulaires et énergétiques des neutrons, émis en coïncidence avec ces fragments, ont été enregistrées à l'aide du multidétecteur DEMON.*

4.1.1. Introduction

Neutron and proton-induced fission cross sections of heavy nuclei, at low and intermediate energies, are of great interest for fundamental physics and for applied nuclear research [1].

As a first step of a long range program, we have performed the measurements of the proton-induced fission cross sections on ^{238}U and ^{239}Pu nuclei at 26.5 and 62.9 MeV incident energies. The proton-induced fission cross-section for ^{238}U is to be considered as a standard which can be used to check our detection system, efficiency and data analysis methods. In coincidence with the fission fragments, the emitted neutron multiplicities, energy and angular distributions have been measured, for both targets, using the DEMON multidetector.

This report presents some preliminary results on the 62.9 MeV proton induced experiments.

4.1.2. Experimental set-up

In this experiment, we have used two different targets: ^{238}U and ^{239}Pu of 180 and 106 μgr/cm^2 thickness respectively. These targets were « sealed » between two ^{12}C layers, thick enough (50 μg/cm²) to stop the recoiling target nuclei and the evaporation residues (ER) of the reactions but not the fission fragments. Special care was taken to measure any possible contamination of the set-up equipment [1].

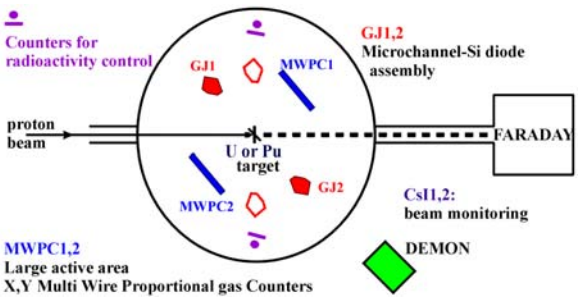

Figure 1 : Experimental set-up.

In the reaction chamber, three different types of detectors were used. Two microchannel plate-Si diode assemblies GJ1 and GJ2 measured, in single mode, at the laboratory angles of 135° and –45°, the time-of-flight and the energy, and thus, the mass of the fission fragments emitted by the targets. The resolutions of these detectors in energy and time are 40 keV (at 6 MeV alpha) and 700 psec respectively. Simultaneously, two X-Y Multi-Wire Proportional gas Counters (MPWC), positioned on both sides of the beam axis (45° and –135°), were dedicated to the coincident fission fragment detection (fission fragment correlation angle has been estimated close to 180°). Their angular (0.4°) and time (0.7 ns) resolutions lead to a good measurement of both fission fragment velocities and angular distributions. Thereafter an iterative calculation procedure is applied to extract the fission fragment mass partitions taking into account a) the energy losses in the target and the Carbon foils, b) the real mass of the fissionning nuclei (eventual pre-equilibrium contribution) and c) the linear momentum transfer in the reaction [2]. Around the reaction chamber, the 72 liquid scintillator cells allow the determination of the neutron energy and angular distributions associated to the fission process.

4.1.3. Preliminary results

Figure 2 displays the correlation between the detection angles of the fission fragments measured in coincidence in both MWPC. In this figure, the full line shows the expected correlation for a relative angle of 180°, in case of zero linear momentum transfer by the projectile. As the relative angles we observe are under this line, a partial linear momentum transfer should be accounted for.

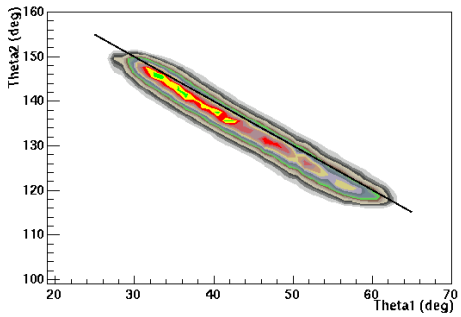

Figure 2 : Two-dimensional spectrum showing the measured angular correlation between both MWPC events (see text for more details).

The microchannel plate-Si detector assemblies GJi allow the direct measurement of the velocity and the energy of the fission fragments. Using these detectors, providing high efficient measurement of the fission fragments (close to 100 %), we can also determine the detection efficiency of the MWPC (expected to be lower than 100 %) and complete the angular distribution of the fission fragments measured at different angles by both MWPC and GJi.

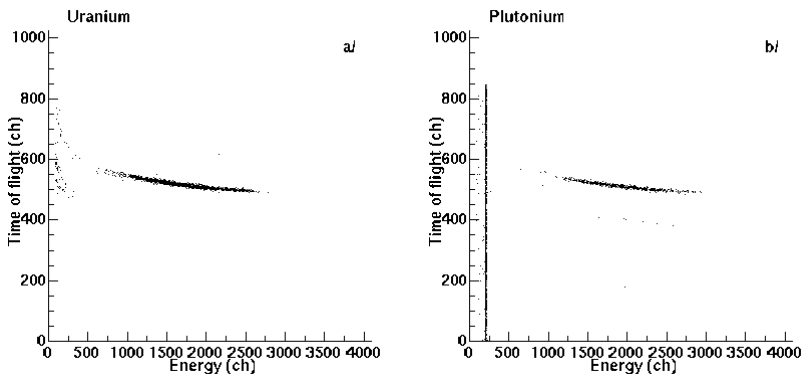

Figure 3 : Two-dimentional spectra showing time-of-flight and energy correlations measured events by GJi detectors for a/ Uranium and b/ Plutonium targets respectively.

Figure 3 presents the detected time-of-flight as a function of the energy measured by the GJi detectors for a/ the Uranium and b/ the Plutonium target respectively. In these figures, we observe the isolated fission fragments events (in the center). For the Plutonium target, we also observe a vertical line corresponding to low energy events beam time independent. These events correspond to the 5.3 MeV alpha activity emitted by the Plutonium target.

On November 8th, a mixed beam of 2.5 MeV/nucleon heavy ions was used to calibrate the 40 µm thick Si detectors associated to the GJi assemblies. Their elastic scattering on a ^{197}Au target allowed us to measure high energy ions (up to 200 MeV). These measurements will be used to establish the eventual pulse-height defect to be associated to these detectors [3].

In the present status, we are at the stage of extracting induced-fission cross sections, angular and mass distributions of the fission fragments. The neutron energy distributions will be extracted from the analysis of the DEMON detectors.

[1] CYCLONE, Rapport d'activité 2001, UCL-IISN.

[2] Th. Keutgen, Thèse de doctorat, 1999.

[3] S.B. Kaufman et al., Nuclear Instrument and Method 115 (1974) 47-55 ;
H.W. Schmitt et al., Phys. Rev. B137 (1965) 837.

5. REACTIONS INDUITES PAR DES NEUTRONS

5.1. Light charged particle production induced by fast neutrons (E_n = 25 – 65 MeV) on ^{59}Co and ^{nat}Fe

I. Slypen, N. Nica, S. Benck, E. Raeymackers, J-P. Meulders (Institut de Physique Nucléaire, Université catholique de Louvain, Louvain-la-Neuve, Belgium) ; V. Corcalciuc (Institute of Atomic Physics, Heavy Ion Department Bucharest, Romania)

Résumé : *Les sections efficaces doublement différentielles de production de protons, deutons, tritons et alpha induits par neutrons rapides (E_n compris entre 25 et 65 MeV) sur des cibles de ^{59}Co et ^{nat}Fe ont été mesurées à 9 angles entre 20° et 160°. Les résultats sur la cible de cobalt sont à présent publiés tandis que l'analyse concernant les données sur le fer se termine. Seules les sections de production des tritons sont incomplètes à ce jour.*

For several years, our group at the Louvain-la-Neuve cyclotron (CYCLONE) has performed several experiments dedicated to the measurement of light charged particle (proton, deuteron, triton and alpha-particle) production induced by fast neutrons on different targets. In recent years, the obtained set of experimental data was completed with two new targets, cobalt and iron. The reason for the choice of these two target elements is twofold. On one hand, they bridge the gap in our former measurements, providing the possibility to follow the evolution of the reaction mechanisms involved in such type of reactions, with target mass. On the other hand, the increased interest in accelerator driven systems (ADS) where these two elements are important constituents, requires a good knowledge of the different types of cross sections for their interaction with fast neutrons. The existing data are very scarce.

Experimental results concerning light charged particle production in proton induced reactions are available for iron and neighboring nuclei such as ^{60}Ni, ^{56}Fe and ^{54}Fe [1], at comparable incident proton energies (28.8, 38.8 and 61.7 MeV, depending on the target nucleus). Our data together with those of Ref. [1] provide complementary information on nucleon induced light charged particle emission in this mass region and offer a larger base for testing nuclear models.

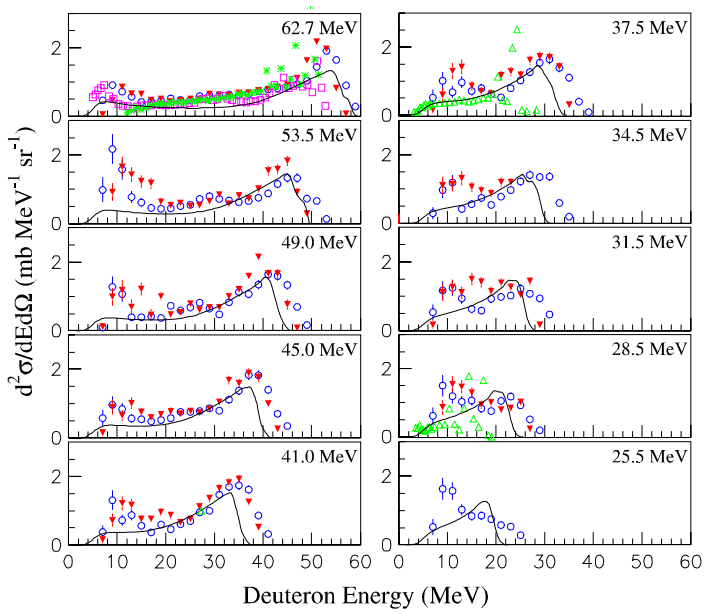

Figure 1 : Double-differential cross sections for respectively ^{59}Co(n,dx) reactions (open circles) and ^{nat}Fe(n,dx) (full triangles) at 20° lab. for the indicated incident neutrons energies. Corresponding data from proton induced reactions for ^{60}Ni (61.7 MeV, diamonds), ^{56}Fe (61.5 MeV, 20° lab., stars; 61.5 MeV, 22° lab., squares) and ^{54}Fe (38.8 and 28.8 MeV, at respectively 20° and 15°, open triangles). GNASH calculations [3] are presented as continuous lines. Some points of proton induced experiments have been cut because they were out of scale.

The data analysis on cobalt is at present entirely completed and the results have already been published in Ref [2]. Concerning the iron data, the analysis is well advanced since only the triton production spectra have not been extracted.

Double-differential cross sections (energy spectra) were measured at the nine laboratory angles (from 20 to 70° in steps of 10°, 110°, 140° and 160°) and at 10 incident neutron energies between 25 and 65 MeV. Fig. 1 shows the double-differential cross sections for the production of deuterons (20° lab.) for the indicated incident neutron energies. The results on iron and cobalt are in very good agreement as expected for close mass nuclei. The agreement between neutron and proton induced reaction results is good, especially in the pre-equilibrium region of the spectra. Differences in the high-energy region are due to a better resolution of the proton experiments and also to the fact that the proton induced reactions lead to other residual nuclei than neutron induced reactions, so that, direct processes dominating this region are different. The GNASH code calculations [3] have been performed for the cobalt and are in fair agreement with the deuteron data.

Figure 2 shows the energy-differential cross sections for the emission of the four particles at 62.7 MeV incident neutron energy. The results on cobalt and iron are in excellent agreement. They are also in very good agreement with data from proton induced reactions, except for tritons. Intranuclear cascade model calculations describe quite well the experimental data for the proton emission, especially in the pre-equilibrium region. The GNASH calculations describe well the data for all four particles. Nevertheless, for α-particles the GNASH code calculations agree with the data of Ref. 5 in the low energy part of the spectra.

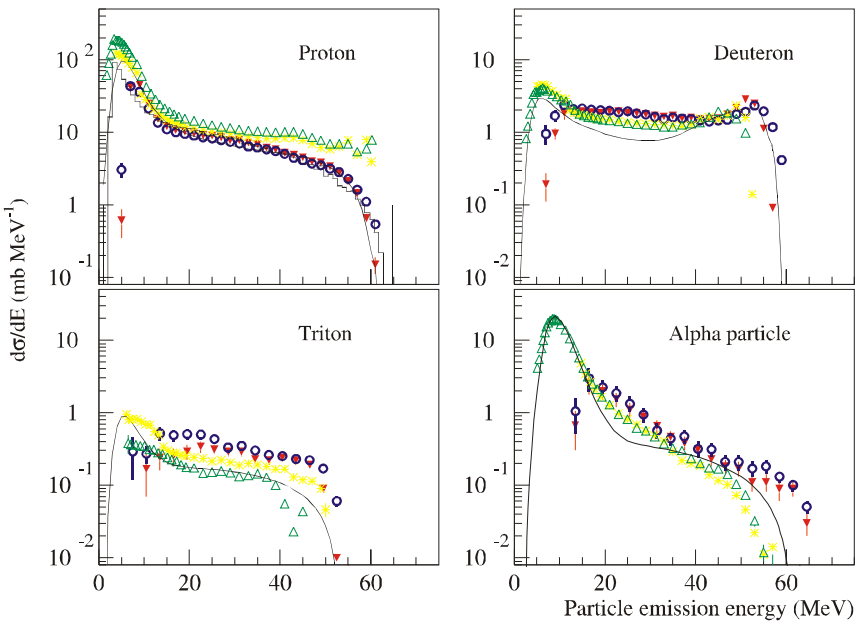

Figure 2 : Energy-differential cross sections for the four particles on ^{59}Co and on ^{nat}Fe at 62.7 MeV incident neutron energy. Symbols are those used in Fig. 1. Data for ^{59}Co(n,αx) [5] are indicated as open stars. Theoretical calculations from INCL3 [4] are shown as histograms.

In the future, analysis for the triton production on iron has to be finalized and calculations with theoretical models have to be performed on iron.

[1] F.E. Bertrand and R.W. Peelle, Phys. Rev. C8, 1045 (1973) and Oak Ridge Report ORNL-4799 (1973).
[2] N. Nica et al., J.Phys.G : Nucl. Part. Phys. 28 (2002) 2823–2842.
[3] P.G. Young, E.D. Arthur, M.B. Chadwick, LANL Report No. LA-12343-MS (1992), GNASH-FKk version gn9cp0, PSR-0125, program received from NEA Data Bank (1999).
[4] J. Cugnon, Nucl. Phys. A462, 751 (1987) and J. Cugnon et al., Nucl. Phys. A620, 475 (1997).
[5] S. M. Grimes et al., Nucl. Sci. Eng. 124, 27 (1996).

5.2. Measurement of microscopic cross sections in fast neutron induced reactions (E_n= 25 - 65 MeV) on bismuth and natural uranium

E. Raeymackers, S. Benck, I. Slypen, J.-P. Meulders, N. Nica (Institut de physique nucléaire, Université catholique de Louvain, Louvain-la-Neuve, Belgium); V. Corcalciuc (Institute of Atomic Physics, Heavy Ion Department, Bucharest, Romania)

Résumé : *L'analyse des données pour l'obtention des sections doublement différentielles de production de protons, deutons, tritons et alpha induite par neutrons rapides sur cibles de bismuth et d'uranium naturel a été finalisée pour toutes les énergies du spectre de neutrons incidents (pic principal et continu) et pour tous les angles mesurés. Après interpolation et extrapolation, ces sections ont été intégrées afin d'obtenir les sections différentielles en énergie et les sections totales de production.*

This year, the data analysis relative to the measurements of secondary light charged particle emission induced by neutrons on bismuth and natural uranium target has been finalised. Double-differential cross sections for proton, deuteron, triton and alpha particle production on bismuth and uranium have been extracted at the nine measured angles (from 20° to 70° in 10° steps; 110°, 140° and 160°) and for the following neutron energies : 62.7 ± 2 MeV, 53.5 ± 2.5 MeV, 49.0 ± 2.0 MeV, 45.0 ± 2.0 MeV, 41.0 ± 2.0 MeV, 37.5 ± 1.5 MeV, 34.5 ± 1.5 MeV, 31.5 ± 1.5 MeV, 28.5 ± 1.5 MeV and 25.5 ± 1.5 MeV.

Some results are presented in figure 1 for 2 incident neutron energies and for the hydrogen isotopes production. The laboratory detection angle is 20°. Data on bismuth and uranium are shown, respectively, as squares and filled circles. Results from proton induced reactions on bismuth of Bertrand and Peelle[1] are shown for comparisons.

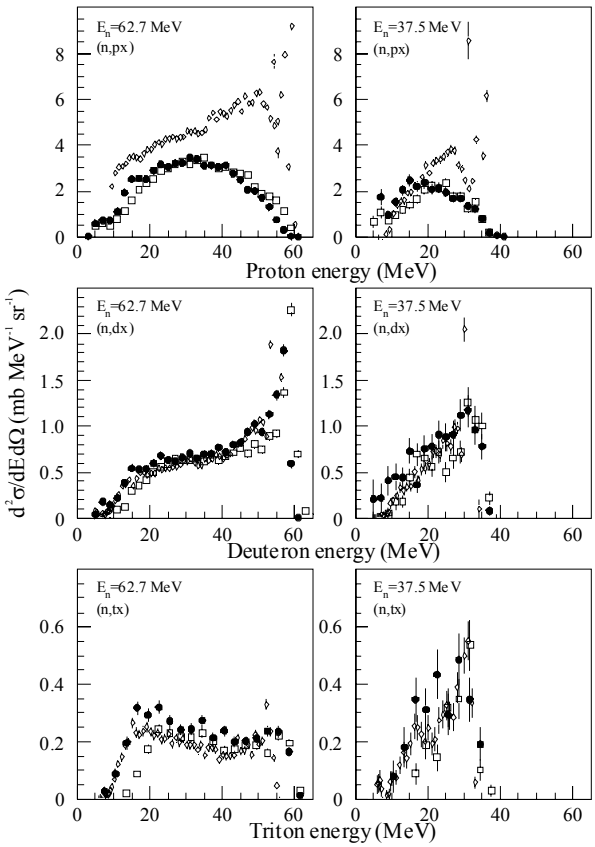

Figure 1 : Double-differential cross sections at 20° lab. for proton, deuteron and triton emission for bismuth (squares) and uranium (filled circles) for 62.7 MeV and 37.5 MeV incident neutron energy. Diamonds are the proton induced reaction results on bismuth of Bertrand and Peelle[1].

For deuterons and tritons, the agreement between neutron and proton induced reaction data is good. For protons, one notices a difference between neutron and proton induced reactions. This difference is expected and can be explained[2].

In order to obtain complete angular distributions, these cross sections have been interpolated and extrapolated with a formula *a.exp(b.cos θ)* proposed by the Kalbach systematics[3]. From the complete angular distribution, the energy and angle-differential cross sections are obtained by respectively angle or energy integration. A further integration gives the total production cross sections.

Figure 2 shows energy-differential cross sections at 41.0 MeV incident neutron energy, for both targets and for the four light charged particles. As already observed in figure 1, there is no large difference between the two sets of experimental results. The quite important experimental error bars in this figure are mainly due to a lower statistic in the continuum part of the incident neutron energy spectrum relative to the main peak. There are actually 10 times less neutrons per MeV in the continuum than in the main peak.

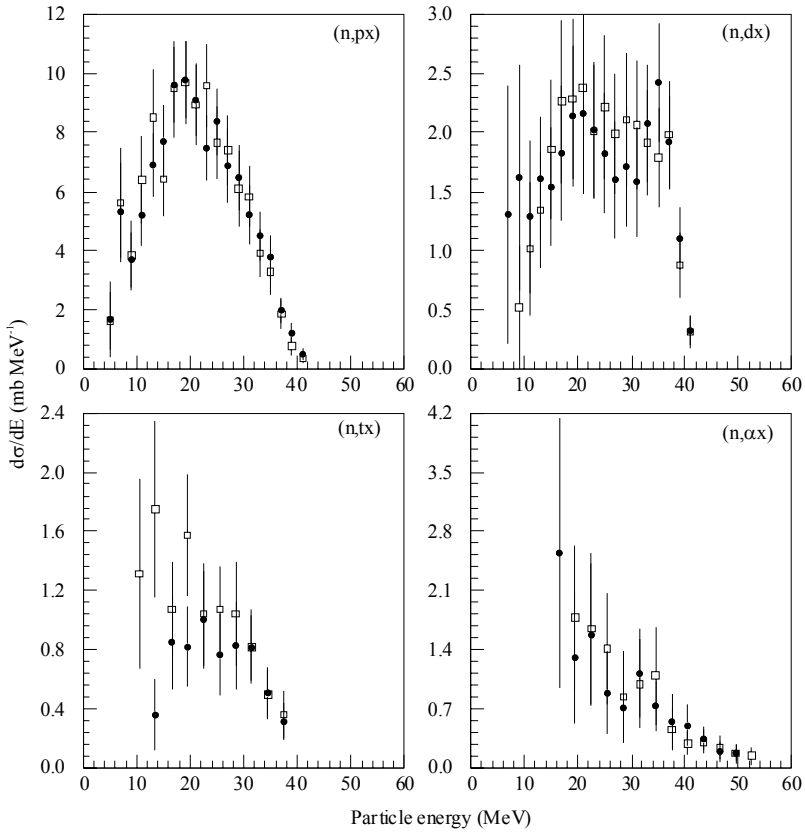

Figure 2 : Energy-differential cross sections for proton, deuteron, triton and alpha particle emission at 41.0 MeV incident neutron energy on bismuth target (filled circles) and natural uranium target (squares).

In the future, theoretical calculations based on different models (mainly the intra-nuclear cascade model and the exciton model) will be performed, for all detected light charged particles and for all the incident neutron energies, on both bismuth and uranium targets.

[1] F.E. Bertrand and R.W. Peelle, ORNL-4799, UC-34-Physics (1973).

[2] S. Benck, I. Slypen, J.P. Meulders, V. Corcalciuc, M. B. Chadwick, P. G. Young, A. J. Koning, Phys. Rev. C58 (1998) 1558.

[3] C. Kalbach, Phys. Rev. C37 (1988) 2350.

5.3. (n,xn) cross section measurements by in-beam γ-ray spectroscopy

P. Baumann, M. Kerveno, S. Lukic, G. Rudolf (IReS, Strasbourg) ; A. Pavlik (Universität Wien, Wien); E. Jericha (Technische Universität Wien, Wien); J.P. Meulders (Institut de physique nucléaire, Université catholique de Louvain, Louvain-la-Neuve, Belgium); S. Jokic (Vinca Institute, Belgrade)

Résumé : L'étude précise des réacteurs pilotés par accélérateur, dans le cadre des travaux menés sur la transmutation des déchets nucléaires, nécessite la connaissance précise des sections efficaces des réactions (n,xn). En utilisant la spectroscopie γ sous faisceau avec un détecteur HPGe, nous avons réalisé deux tests, l'un avec une cible de tungstène, l'autre avec une cible de thorium, pour montrer la faisabilité de ces mesures auprès du faisceau de neutrons du cyclotron CYCLONE de l'UCL.

In ADS, the (n,xn) reactions are more important than in conventional reactors because of the external neutron source (produced by spallation reaction) which covers a large energy range. As the (n,xn) reactions contribute to the neutron balance in the core and modify the neutron energy spectrum, it is necessary to have a more precise estimate of their cross sections. At present, due to the rare neutron beams and the difficulty of these measurements, only scarce experimental data exist and only for neutron energies below 20 MeV. So a real experimental effort has to be developed to measure the (n,xn) cross sections in order to provide new sets of experimental data which could supply directly the data bases or be used to test and improve the theoretical models of these reactions.

Taking inspiration from the pioneer work done at Los Alamos with the detector Geanie[1,2,3], we have proposed the in-beam γ-ray spectroscopy to determine (n,xn) cross sections at the neutron beam of the UCL cyclotron at Louvain-la-Neuve. To test this method we used a planar HPGe detector, 1.5 cm in depth, placed at about 3 m from the neutron source and at about 12 cm from the target. This system was shielded by up to 7 cm lead against γ rays coming from directions other than the target. Two tests have been performed, one (2 shifts in May) with a ^{nat}W target and another (3 shifts in October) with a ^{232}Th target at respectively 45 and 38 MeV incident neutron peak energy. The results of those experiments are shown in Figure 1 (for W target) and in Figure 2 (for Th target). As we can see several peaks coming from (n,xn) reactions with x=1,2,3,4,5 are well separated in the energy spectrum obtained with the ^{nat}W target and this is also true for the active target ^{232}Th.

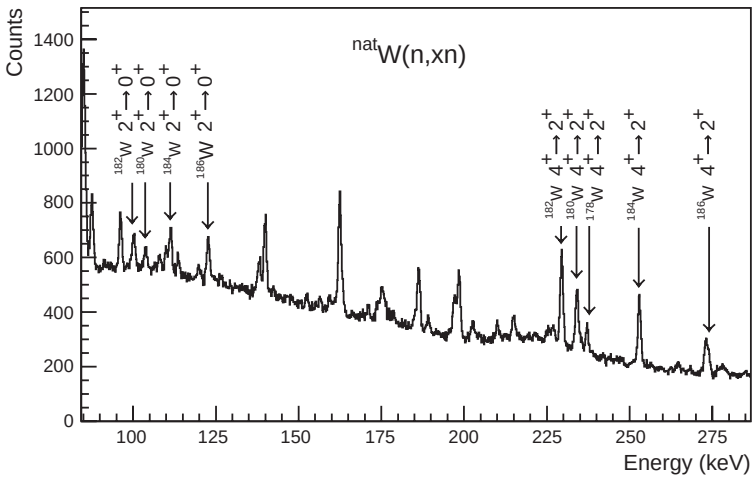

Figure 1 : Portion of prompt γ spectrum obtained in 75 minutes with a ^{nat}W target at 45 MeV incident neutron peak energy.

More precisely, with the ^{nat}W target (0.5 mm thick) and an acquisition time of about 75 minutes one sees (Figure 1) the lines corresponding to the $4^+ \rightarrow 2^+$ and the $2^+ \rightarrow 0^+$ transitions in :

- ^{182}W, fed by the ^{182}W(n,n'), ^{183}W(n,2n), ^{184}W(n,3n) and ^{186}W(n,5n) reactions
- ^{180}W, fed by the ^{182}(n,3n), ^{183}W(n,4n) and ^{184}W(n,5n) reactions
- ^{178}W, fed by the ^{182}W(n,5n) reaction only
- ^{184}W, fed by the ^{184}W(n,n') and ^{186}W(n,3n) reactions
- ^{186}W, fed by the ^{186}W(n,n') reaction only.

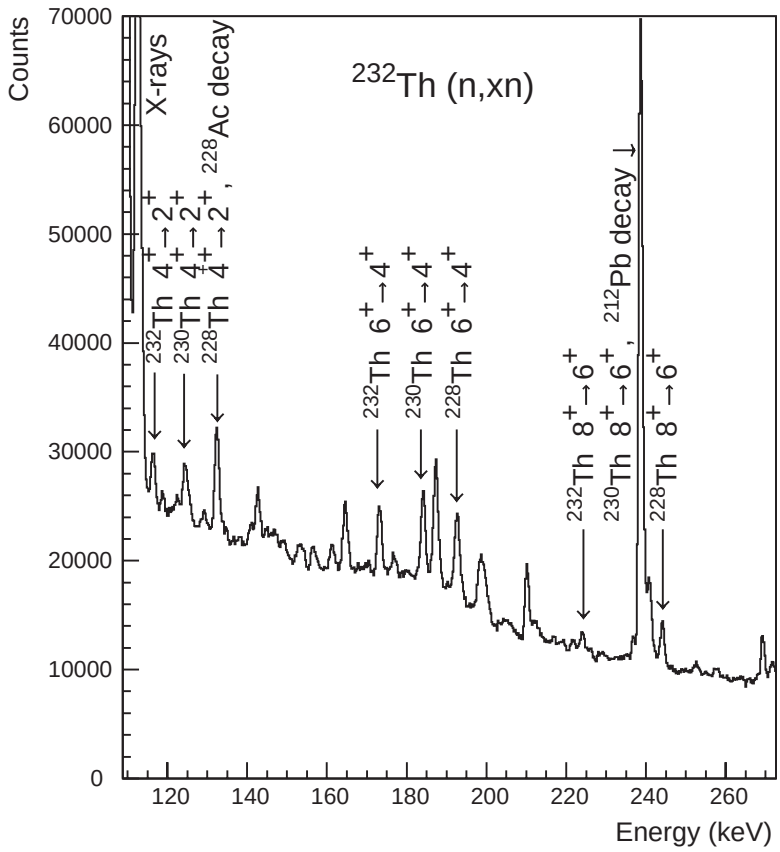

Figure 2 : Portion of prompt γ spectrum (after partial background subtraction) obtained in 17 hours with a ^{232}Th target at 38 MeV incident neutron peak energy.

With the ^{232}Th target (0.3 mm thick) and an acquisition time of about 17 hours one sees (Figure 2) the lines corresponding to the $4^+ \rightarrow 2^+$, $6^+ \rightarrow 4^+$ and $8^+ \rightarrow 6^+$ transitions in :

- ^{232}Th, fed by the ^{232}Th(n,n') reaction
- ^{230}Th, fed by the ^{232}Th(n,3n) reaction
- ^{228}Th , fed by the ^{232}Th(n,5n) reaction.

In addition we observe lines corresponding to the β-decay of fission products in particular ^{116}In. From this preliminary experiment we have checked that the ^{232}Th(n,5n) reaction cross section at E_n = 38 MeV is on the order of 1 barn as expected from theoretical calculations[4].

Following these promising tests we aim to perform a precise measurement of (n,xn) cross sections. For that, some improvements of the experimental techniques are necessary. In particular, it will be essential to integrate time of flight measurements in the acquisition system in order to select, during data analysis, the events coming from the neutron mono-energetic peak. A second important requirement is the neutron flux measurement. All these developments are in progress, to be completed by a new beam time proposal for the end of 2003.

[1] A. Pavlik et al., Phys. Rev. C57 (1998) 2416.
[2] L.A. Bernstein et al., Phys. Rev. C57 (1998) 2799.
[3] H. Vonach et al., Phys. Rev. C50 (1994) 1952.
[4] J.R. Beene, N.G. Nicolis, private communication.

5.4. Study of neutron-induced fission of nuclei in vicinity of ^{208}Pb

I.V. Ryzhov, A.G. Mitryukhin, V.C. Oplavin, G.A. Tutin (Khlopin Radium Institute, Saint-Petersburg, Russia); J.P. Meulders, Y. El Masri, T. Keutgen, R. Prieels (Institut de Physique Nucléaire, Université catholique de Louvain, Louvain-la-Neuve, Belgium); R. Nolte, H. Schuhmacher (Physikalisch-Technische Bundesanstalt, Braunschweig, Germany)

Résumé : L'étude de la fission induite par des faisceaux de neutrons de 32.8, 45.3 et 59.9 MeV sur des cibles de ^{205}Tl, $^{204,206\text{-}208}$Pb et ^{209}Bi a été effectuée auprès de l'accélérateur CYCLONE de Louvain-la-Neuve. Les faisceaux de neutrons ont été produits par la réaction ^{7}Li(p,n)^{7}Be sur une cible de lithium de 5 mm d'épaisseur. Cette étude nous a permis de mesurer, à ces trois énergies et pour chaque cible, les sections efficaces de fission ainsi que les distributions angulaires des fragments produits lors de cette réaction. L'obtention de ces distributions angulaires est toujours en cours d'analyse.

Neutron-induced fission cross sections of ^{205}Tl, $^{204,206\text{-}208}$Pb and ^{209}Bi as well as fission fragment angular distributions have been measured at the neutron beam facility of the Université catholique de Louvain (UCL). Quasi-monoenergetic neutron beams with peak energies 32.8, 45.3 and 59.9 MeV were produced by the ^{7}Li(p,n)^{7}Be reaction using a 5 mm thick lithium target. In order to maximize the statistics the proton beam current on the lithium target has been maintained at a level of about 10 μA throughout a prolonged experimental week (21 shifts).

Fission fragments have been detected with a multi-section Frisch-gridded ionization chamber (MFGIC) placed in "Appendix Q". The MFGIC (see Figure 1) consists of a stack of twin ionization chambers with Frisch grids and makes it possible to measure a variety of the fission process characteristics for seven different targets. The detector was loaded with sub-actinide targets under study plus natural uranium target as a reference one. The fissile materials were deposited (by vacuum evaporation) on each side of 0.05 mm thick duralumin foils (the chamber cathodes) stretched between the supporting rings. The total fissile mass of the reference target (deposited in the form of $^{nat}UF_4$) was measured by alfa-counting, while the masses sub-actinide targets (pure metals) were determined by weighting. Diameter of each target was 80 mm.

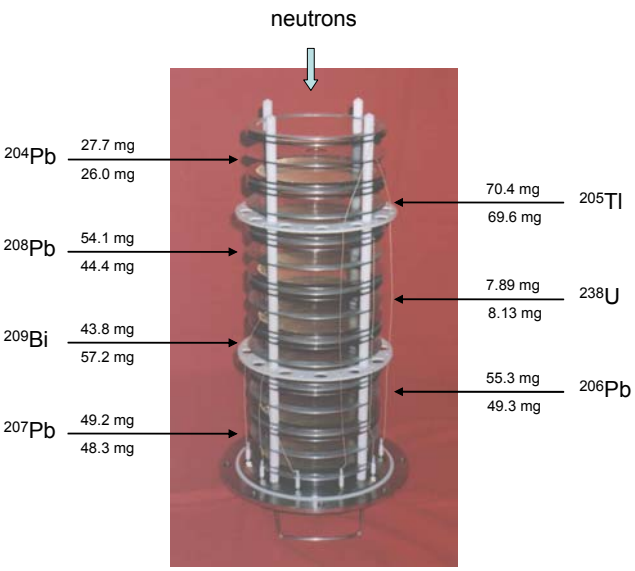

Figure 1 : A multi-section Frisch-gridded ionization chamber loaded with the fissile targets (in the back-to-back geometry). Relative uncertainty of the fissile masses indicated for the forward and the backward-facing targets is about 1 %.

The detector was so positioned that the reference target was at a distance of 10.2 m from the neutron production target. At this position the beam diameter (FWHM) was about 10 cm with the average fluence rate of "peak neutrons" of about $2\cdot10^{4}$ cm^{-2} s^{-1}.

Using the method described in detail in Ref. [1] the distributions of fission events over the neutron time-of-flight (TOF) have been obtained for each target as well as the fission fragment energy and angular distributions. In order to derive the fluence of "peak neutrons", a decomposition of the reference TOF-spectra has been done using the relative spectral neutron fluences measured at the UCL [2] and the recommended cross sections for ^{238}U(n,f) [3]. The neutron fluence monitoring procedure has been tested by the cross measurements in which the fluence of 59.9 MeV neutrons has been simultaneously determined with the MFGIC and a fission chamber monitor (FCM) calibrated relative to a proton recoil telescope [4]. The "peak fluence" determined with FCM (at a distance of 6 m from the Li-target) was related to the MFGIC position using the $1/r^2$ law and taking into account the neutron absorption in the air. The results of the intercomparison were found to be consistent within 3 %.

The fission cross sections were obtained from:

$$\sigma_f = \frac{k_w k_L}{2\Phi_0}\left(\frac{N_f^B}{N_A^B} + \frac{N_f^F}{N_A^F}\right)$$

where Φ_0 is the fluence of "peak neutrons" at the reference target position, k_w the correction for the isotope composition, k_L the fluence correction for a given target position, $N_A^{F(B)}$ the number of fissile nuclei, $N_f^{F(B)}$ the number of "peak fissions" corrected for the fission fragment absorption in the deposit and for the fission events lost below the pulse height threshold. The superscripts F and B in the above expression denote the forward- and the backward-facing targets, respectively.

Figure 2 shows the measured (n,f) cross sections as a function of the fissile parameter of the compound nucleus. Analysis of the fission fragment angular distributions is in progress as well as the theoretical model analysis of the data.

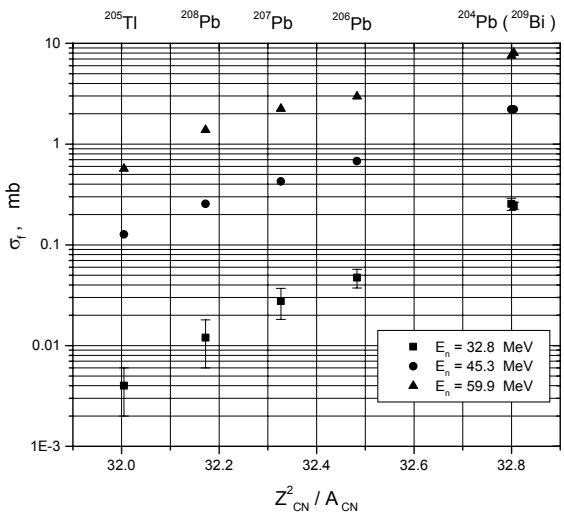

Figure 2 : Measured (n,f) cross sections along the fissile parameter of the compound nucleus. Missing uncertainties correspond to the symbol size. The target nuclei are indicated at the top.

[1] G.A. Tutin, I.V. Ryzhov, V.P. Eismont, A.V. Kireev, H. Condé, K. Elmgren, N. Olsson, P.-U. Renberg, Nucl. Instr. and Meth. A457 (2001) 646.

[2] R. Nolte, private communication.

[3] A.D. Carlson, S. Chiba, F.-J. Hambsch, A.N. Smirnov, INDC (NDC)-368, IAEA, (1997).

[4] H. Schuhmacher, H.J. Brede, V. Dangendorf, M. Kuhfuss, J.P. Meulders, W.D. Newhauser, R. Nolte, Nucl. Instr. and Meth. A421 (1999) 284.

6. PHYSIQUE DES NANOSTRUCTURES

6.1. Nanoscopic Superconducting Slab in Static Electric and Magnetic Fields

D. Bertrand, J. Govaerts, G. Stenuit (Institut de Physique Nucléaire, Université catholique de Louvain, Louvain-la-Neuve); V. Bayot, A. Crahay (FSA/TELE/DICE and CERMIN, UCL)

Résumé : Utilisant une configuration géométrique spécifique de champs électrique et magnétique appliqués à une tranche supraconductrice d'épaisseur nanoscopique, des mesures ont été réalisées afin d'établir expérimentalement la pertinence de l'extension covariante de Lorentz des équations phénoménologiques de Ginzburg-Landau de la supraconductivité. Ces mesures n'ont toutefois permis jusqu'ici de tirer aucune conclusion à ce sujet, et appellent à présent à une meilleure connaissance du potentiel électrostatique auquel est soumis l'échantillon en présence des champs électrique et magnétique.

As discussed in previous annual reports[1,2], a series of measurements have been performed in order to discriminate experimentally between the Lorentz-covariant extension and the usual Ginzburg-Landau (GL) theory of superconductivity[3]. These experiments have been carried out with a mesoscopic Al slab submitted to a normal electric field as well as a tangential magnetic field. In a first part of the experimental protocol, the electric field was fixed at given values while the magnetic field was ramped upwards across its critical value, allowing the monitoring of the change in the phase transition point (fig.1). In a second stage of the procedure, the electric and magnetic fields were both kept at successive fixed values, while the temperature was swept up and down around the critical temperature (fig. 2).

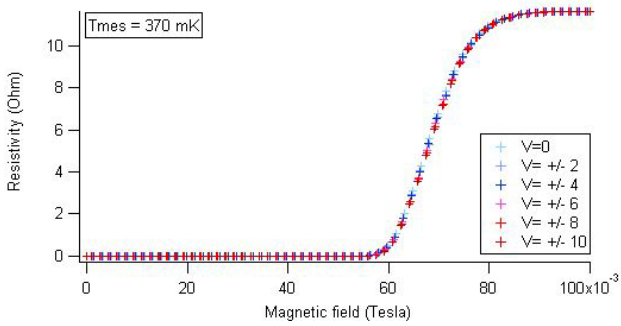

Figure 1 : Transition between superconducting and normal phases of the sample observed in sweeping magnetic field, for fixed values of the electric field induced by applying a voltage V (in volts) on the plates of a capacitor; a voltage of 2V corresponds to approximatively 2 MV/m for the electric field.

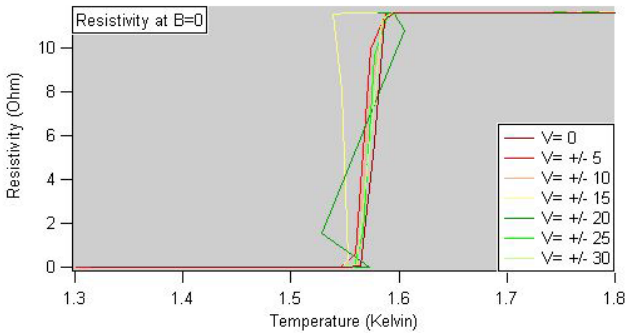

Figure 2 : Transition between superconducting and normal phases of the sample, observed in temperature sweeps, for fixed values of electric and magnetic fields (this picture is restricted to one value of the magnetic field); the differences between the curves are due to thermal fluctuations.

As displayed on both graphs, no apparent dependence on the electric field arises for any critical parameter, suggesting therefore that an external electric field does not affect significantly the superconducting state. This conclusion seems in total opposition not only with the covariant theory, but also with the usual GL framework. A thorough understanding of this intriguing feature is thus required before considering further any comparison between both formalisms.

Presumably, progress on this front should follow from a better knowledge of the electrostatic potential inside and outside the device. According to Lipavský *et al.*[4], an electrostatic potential of the Bernoulli type could combine with the thermodynamic potential in the superconductor, resulting in an effective potential acting on the condensate of Cooper pairs. The main consequence would be the appearance of surface charge that screens the external electric field and prevents the sample from "seeing" it. The advantage of Lipavský's expression for the potential is that the resulting relations remain valid even far from the critical temperature. Numerical simulations are now being performed and we hope to report for a better understanding of the experimental results in the next annual report.

[1] D. Bertrand *et al.*, Rapport Annuel CYCLONE 2000, p. 71.

[2] D. Bertrand *et al.*, Rapport Annuel CYCLONE 2001, p. 46.

[3] J. Govaerts, D. Bertrand and G. Stenuit, On Electric Fields in Low Temperature Superconductors, Supercond. Sci. Technol. 14 (2001) 463-470.

[4] P. Lipavský, J. Koláček, K. Morawetz and E.H. Brandt, Electrostatic Potential in a Superconductor, Phys. Rev. B 65 (2002) 144511 (18 pages).

6.2. Vortex Matter in Lead Nanowires

G. Stenuit, J. Govaerts and D. Bertrand (Institut de Physique Nucléaire, Université catholique de Louvain, Louvain-la-Neuve); S. Michotte and L. Piraux (Institut de Physico-Chimie et de Science des Matériaux, Université catholique de Louvain, Louvain-la-Neuve)

<u>Résumé</u> : *Une description théorique et expérimentale de la magnétisation de nanofils de plomb à une température bien inférieure à T_c est proposée. Expérimentalement, la réponse magnétique est obtenue à l'aide d'un magnétomètre SQUID. Le comportement d'hystérèse et les transitions de phase ont été examinés à différentes températures dans un champ magnétique externe croissant et décroissant. Les états de Meissner et d'Abrikosov ont également été observés dans ce supraconducteur de type-I. Ce constat met dès lors en évidence le comportement non trivial de la frontière κ_c ($= 1/\sqrt{2}$ dans un échantillon macroscopique) entre supraconducteurs de type-I et de type-II à l'échelle mésoscopique. En appliquant les équations de Ginzburg-Landau indépendantes du temps pour des configurations à symétrie cylindrique, nous sommes en mesure d'expliquer et de reproduire les magnétisations expérimentales endéans 10 % de marge d'erreur.*

6.2.1. Introduction

Recent developments in nanotechnologies and measurement techniques allow nowadays the experimental investigation of the magnetic and thermodynamic superconducting properties of mesoscopic samples far below the critical temperature T_c[1,2]. In order to compare the magnetization curves (magnetization versus external magnetic field at a given temperature T) of an array of lead nanowires to the theoretical predictions, some assumptions must be considered to simplify the model.

First of all, due to the small radius of the nanowires, only the one dimensional radial Ginzburg-Landau equations are used. Indeed, for such sizes, temperatures and κ values, the phase diagram (B_{ext},Energy) exhibits only those states whose vorticity L is strictly less than 2 since Giant Vortex states are too large compared to the radius.

In addition, the magnetization presents a weak diamagnetic (in the L=0 state) and paramagnetic (in the L=1 state) response in the mesoscopic limit. The mutual magnetic interactions between nanowires may thus be neglected in our model. Therefore, considering a Gaussian distribution for the radii of nanowires making up the array, the total magnetization may be expressed as the sum of the magnetization of each type of nanowire multiplied by their statistical weight.

6.2.2. Analysis of the Experimental Results

The analysis, whose details are available elsewhere[3], involves a comparison between experimental and theoretical magnetization curves of lead nanowires (T_c=7.2K), with a mean radius of 116 nm and a variance of 11 nm. These values being fixed, the free parameters of the model are λ (the penetration length) and ξ (the coherence length). Finally, in order to study the hysteretic behaviour of the sample, it is worth mentioning here that the experimental magnetization curves have been obtained when the external magnetic field (parallel to the z-axis of the nanowires) is swept up and down after zero field cooling.

For example, Figure 1 shows experimental and theoretical results for T=5.75 K and T=5 K. Beyond the qualitative and quantitative agreement between the curves, it should be stressed that the experimental hysteretic behaviour was predicted by the model. Indeed, as shown in Figure 2, the Meissner state (L=0) exhibits a bistable region close to the transition with a jump in the magnetization and hysteresis between normal and superconducting states.

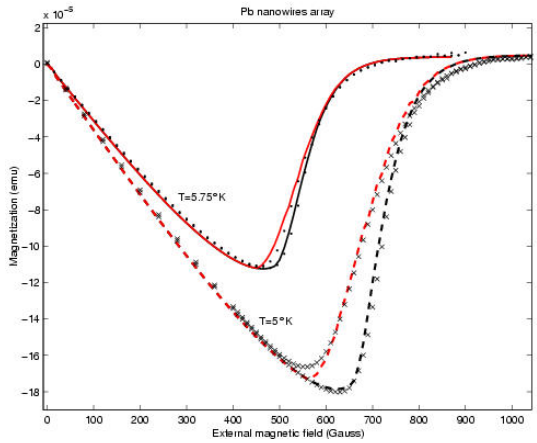

Figure 1 : Comparison between the experimental (markers) and theoretical (solid and dotted lines) total magnetization with L=0. From top to bottom, curves at T=5.75 K and T=5K. The adjusted values for λ and ξ are (58,139) and (51,113) nm, respectively.

For lower temperatures, the Abrikosov state (L=1) extends the (B_{ext},Energy) phase diagram, as shown in Figure 2. Due to the Bean-Livingston barrier[4], the hysteretic behaviour is enhanced in such cases. In contradistinction, for temperatures close to T_c, only the Meissner state (L=0) without hysteretic behaviour contributes to the magnetization of the sample (see Figure 2).

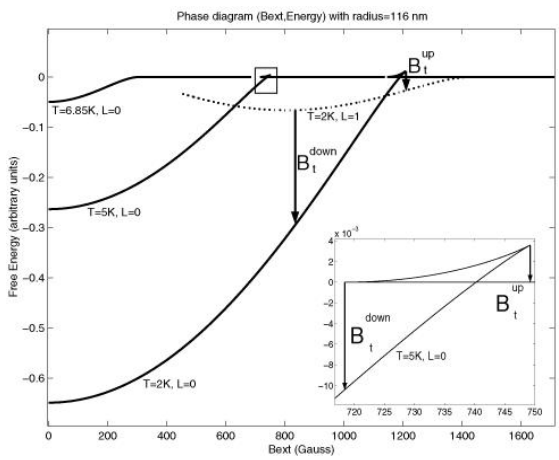

Figure 2 : The normalized free energy as a function of the external magnetic field for R=116 nm and T=6.85, 5 and 2 K. The inset is a zooming of the boxed area which exhibits the hysteretic behaviour of the free energy close to the critical magnetic field at T=5K.

6.2.3. Comments and Conclusions

In order to explain and reproduce within 10 % of precision the magnetic properties of the considered lead nanowire array, only cylindrically symmetric solutions suffice. In particular, the Meissner state (L=0) and, for the lowest temperatures, the Abrikosov state (L=1) were experimentally observed in these apparently type-I superconductors. However, the presence of an Abrikosov state is not surprising since the distinction between type-I and II looses its relevance at mesoscopic scales[5].

By changing the temperature of the sample in the SQUID magnetometer, we were able to modify and to check the three characteristic regions already observed by Geim *et al.*[1]: the type-II behaviour for small radius, the type-I phase transition in the Meissner state, and the vortex state with type-II phase transition from the superconducting to normal state. Finally, it should also be stressed that the absence of jumps in state transitions is explained by the spread in values for the radius of all nanowires within the sample.

[1] A.K. Geim, I.V. Grigorieva, S.V. Dubonos, J.G.S. Lok, J.C. Maan, A.E. Filippov and F.M. Peeters, Nature 390 (1997) 259.

[2] S. Michotte, L. Piraux, S. Dubois, F. Pailloux, G. Stenuit, J. Govaerts, Physica C377 (2002) 267-276.

[3] G. Stenuit, S. Michotte, J. Govaerts, L. Piraux and D. Bertrand, Vortex Configurations in Mesoscopic Superconducting Nanowires, to appear in Mod. Phys. Lett. B, 10 pages.

[4] C.P. Bean and J.B. Livingston, Phys. Rev. Lett. 12 (1964) 14.

[5] G.F. Zharkov, Phys. Rev. B63 (2001) 224513.

6.3. Track etching in polymers

R. Legras, S. Demoustier-Champagne, F. Dehaye, L. Dauginet-de Pra, E. Ferain* (Université catholique de Louvain, Unité de physique et de chimie des hauts polymères)

Résumé : *L'unité de physique et de chimie des hauts polymères (POLY) est engagée dans une activité de recherches portant sur l'interaction entre les ions lourds énergétiques et les polymères depuis 20 années environ; durant toute cette période, la collaboration avec le Centre de Recherches du Cyclotron a permis à de nombreux chercheurs d'avoir accès à un équipement permettant une irradiation contrôlée et reproductible de films polymères au moyen de faisceaux d'ions lourds tels que Ar 220 Mev et Xe 574 MeV.*

Dans ce cadre, une étude a porté sur le développement d'un procédé de "track etching" permettant la réalisation de membranes microporeuses par attaque chimique sélective d'un film polymère préalablement irradié par des ions lourds énergétiques. Cette étude a conduit à la définition d'une technologie brevetée et actuellement utilisée par la société Whatman sa pour la production de membranes en polycarbonate et polyéthylène téréphtalate.

Plus récemment, ces membranes de type "track etched" ont été utilisées pour la synthèse de micro- et nanomatériaux aux propriétés inattendues et intéressantes, et pouvant servir de matériaux de base à la mise au point de dispositifs dédiés à des applications spécifiques. La méthode de synthèse utilisée consiste au remplissage des pores de la membrane par le matériau requis et conduit à la formation de micro- ou nanomatériaux polymères ou métalliques sous la forme de tubes ou de filaments.

Quelque soit la propriété de ces tubes ou de ces filaments considérée, leur morphologie, et par conséquent la taille et la forme des pores dans lesquels ils sont synthétisés, doit être parfaitement contrôlée. Une étude significative a donc porté sur une nouvelle optimisation du procédé de "track etching", avec pour but principal la réalisation de membranes dont les pores ont un diamètre compris entre 10 et 100 nm, et aussi afin de fournir à nos partenaires de recherches des membranes aux caractéristiques parfaitement connues et contrôlées.

Les principaux résultats de cette étape d'optimisation, obtenus dans le cadre de projets de recherches financés par la Communauté Européenne et par la Région Wallonne, sont décrits dans ce rapport. La

* *ferain@poly.ucl.ac.be, tel 0 10 47 35 60, fax 0 10 45 15 93*

synthèse des tubules et des filaments, et leurs principales propriétés, sont également brièvement présentées en fin de rapport avec référence aux plus récentes publications scientifiques.

6.3.1. Introduction

For about the last 20 years, the interaction between energetic heavy ions and polymers is a major research activity at the "unité de physique et de chimie des hauts polymers". The facilities provided by the "Centre de Recherches du Cyclotron" to irradiate polymer films in a controlled and reproducible way with heavy ions from Ar (220 Mev) to Xe (574 MeV), have enabled researchers to significantly improve their knowledge in this research area.

The track etching process, consisting in an irradiation of a polymeric material by energetic heavy ions creating linear damage tracks and followed by a chemical etching of these tracks to pores [1], has been intensely studied. First studies carried out on this process in polymer films have led to the development of a patented technology actually used by Whatman s.a. to regularly manufacture microporous particle track etch membranes (PTM). These kind of microfilters with well defined pore densities, from 10^5 to 10^9 cm^{-2}, and pore sizes in the range 0.1 µm to 12 µm are now requested from customers around the world for applications such as haemodialysis modules, biosensors, diagnostics and virus removal equipment.

More recently, these PTM have been used for the synthesis of micro- or nanomaterials having interesting fundamental properties and becoming an integral part of devices for specific applications. The synthesis method, called template-base method [2], consists in the filling of the pores of the PTM with one or many desired materials allowing the synthesis of polymeric or metallic micro-or nanomaterials in wires or tubules shape (Fig. 1) [3,4].

The use of track etch templates gives the opportunity to synthesis wires or tubules [3,5-7] with a well-controlled size and shape and displaying a small roughness and a large aspect ratio. All these wires or tubules can be removed from their host polymer using an appropriate solvent or etchant, when their morphological characterisation or when the properties of an isolated nanowire or nanotubule is considered. Nevertheless, all these wires or tubules are often kept in their host material to investigate their properties or to develop specific devices; sometimes, when the properties of an array of magnetic nanowires embedded in the host polymer layer are considered, the opportunity given by the track etching process to very simply monitor the mean distance separating these nanomaterials becomes essential. Moreover, the orientation of the pores and thus of the nanowires in relation to the polymer layer surface (all perpendicular, all uniformly tilted or randomly tilted) can be also easily monitored during the heavy ion irradiation step.

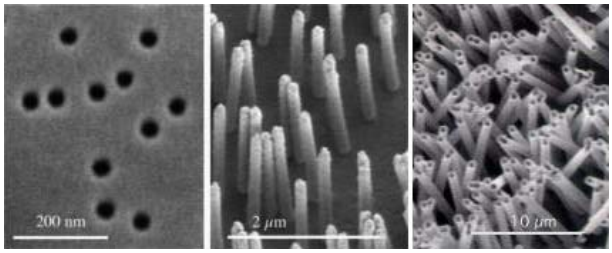

Figure 1 : Surface of a polycarbonate track etch membrane with 40 nm pore (left); these membranes, with pore size in the range 10 nm to 10 µm can be used as template for the synthesis of e.g. cobalt nanowires (middle) or gold nanotubes (left).

Whatever the considered nanomaterial properties or applications, there is a real need to be able to perfectly monitor their morphology; on this subject, commercially available track etch membranes made of polycarbonate or polyester membranes do not offer numerous possibilities of pore size in the range 10 nm to 100 nm where most interesting nanomaterial properties are expected. Moreover, some studies [8,9] have shown that the pore shape in these membranes is not cylindrical but rather toothpick shaped and control and understanding of the nanomaterials properties synthesised into these pores are therefore complex. Consequently, a major effort has been spent in our research group to develop a track etching process to produce reliable track etch nanotemplates in a controlled and reproducible way [10] and to supply on request research partners and other interested people with well-characterised templates.

All these developments have been mostly completed and are still running in the frame of the following research projects :

1. "nanoporous particle track etched membrane (PTM) and their use as templates for electrodeposited multilayers for giant magnetoresistance (GMR) applications"

   - funded by the European Community under the Industrial & Material Technologies Programme (01/1996 - 12/1999)

- partners : UCL-POLY (R. Legras (coordinator), E. Ferain), UCL-PCPM (L. Piraux), Whatman sa (H. Hanot), Thomson (F. Nguyen Van Dau), University of Paris Sud (A. Fert), Industry Microelectronics Center (P. Leisner) and University Louis Pasteur (K. Ounadjela, U. Ebels)

- 40 scientific papers, 4 patents, 20 PhD students and post-docs

2. "conductive nanowires for applications in microwave, magnetic and chemical sensing devices based on polymer track etched templates"

   - funded by the European Community under the Competitive and Sustainable Growth Programme (02/2000 - 2/2003)

   - partners involved : UCL-POLY (R. Legras (coordinator), S. Demoustier-Champagne, E. Ferain), UCL-PCPM (L. Piraux), CEA Grenoble (U. Ebels), CNRS Orsay (J.-M. George), Thalès (F. Nguyen Van Dau), Epigem (T. Ryan, T. Harvey), IFPD Dresden (M. Stamm)

3. "conception et réalisation de supports nanoporeux et de nanomatériaux - application à la réalisation de dispositifs haute fréquence"

   - funded by the Walloon Region (09/1999 - 02/2003)

   - partners : UCL-POLY (R. Legras, S. Demoustier-Champagne, E. Ferain), UCL-PCPM (L. Piraux), UCL-EMIC (I. Huynen)

In this first contribution to the Cyclone annual report about the work performed at UCL-POLY on the track etching in polymers, some generalities will be first reported about the realisation of polycarbonate track etch templates. Afterwards, the most recent developments made in the lab about track etching process will be described. They mainly relate to the realisation of nanoporous polycarbonate-based templates, a polymer well-known for its ability to track etching and often considered in studies about irradiation effects on polymers [11-14] ; more precisely, the pore shape control in polycarbonate film by a pre-irradiation treatment, the realisation of supported track etch templates and the feasibility of template patterning will be presented. Finally, synthesis and properties of nanoscale materials synthesised into these track etch templates will be briefly reviewed with references to recent published papers.

6.3.2. Generalities on the realisation of polycarbonate track etch templates

The energetic heavy ion irradiation of polycarbonate film or layer deposited on a support is carried out at the Cyclotron Research Centre of Louvain-la-Neuve using 220 MeV Ar^{9+} ion beams and the Whatman irradiation facilities. It allows to continuously irradiate large quantities of polymer films as well as to statically irradiate small supported polymer samples with a 50 cm wide and a 5 cm high homogenous ion beam.

Etching process is performed in successive temperature regulated baths respectively filled with hydrogen peroxide, caustic soda and acetic acid aqueous solutions, and having a small volume allowing an easy modulation of etching conditions. By this way, homogeneous template samples from some to several tens of square centimetres can be reproducibly realised. A conductivity cell developed earlier [15] is still available and is frequently used for the measurement of the track etching rate, mainly as a function of the conditions of the UV irradiation performed just after the ion irradiation. This treatment with UV-A or UV-B sources remains a critical step of the process as it influences significantly the final pore size and pore shape in the templates.

Pore size and pore density are controlled using a digital scanning electron microscope (LEO 982) allowing the surface observation of the template at very low voltage (down to 200 eV) under conditions where no metallic coating is required and in which pores as small as 15 nm can be observed. Pore shape, as well as pore wall roughness, arise from the observation of nanowires or nanotubules chemically synthesised or electrodeposited in the pores of the templates and recovered by filtration through silver membrane after dissolution of the polymeric template [16].

6.3.3. Pore shape control in polycarbonate film

As already mentioned in the introduction, the pore shape in commercially available polycarbonate track etch membranes is rather far from the expected and commonly accepted cylindrical shape, at least for pore sizes smaller than 0.5 µm. This effect is clearly shown by a difference of around 20 to 30 nm between the pore size at the membrane surface and the diameter of the nanowire synthesised in the pores of this membrane; it is

explained by a narrowing of the nanowires, and thus of the pores, at their extremities as shown by scanning electron microscopy [8,9].

To confirm this observation, numerous samples of polycarbonate membrane have been prepared from different commercial polycarbonate films : Lexan (25 µm thick, General Electric), Makrofol KG (10 µm thick, Bayer) and Pokalon (20 µm thick, Lonza). They all lead to a similar effect whatever the concentration of caustic soda in the etching aqueous solution, all other parameters of the process being kept constant. As this effect becomes really non negligible for pores or nanowires and nanotubules with diameter below 100 nm, some experiments were thus considered to obtain cylindrical pores on all their length.

This expected result was obtained considering the presence of a "hard" thin layer on both side of polycarbonate films characterised by a higher chemical resistance to etching solutions. Indeed, if these hard layers are removed before the heavy ion irradiation by means of a chemical etching similar to the one use for the track etching [17], no more narrowing effect is observed on the nanowires and their diameter corresponds to the pore size measured at the membrane surface in which they have been synthesised (Fig. 2). Such a hard layer is probably created during the manufacture of polycarbonate films.

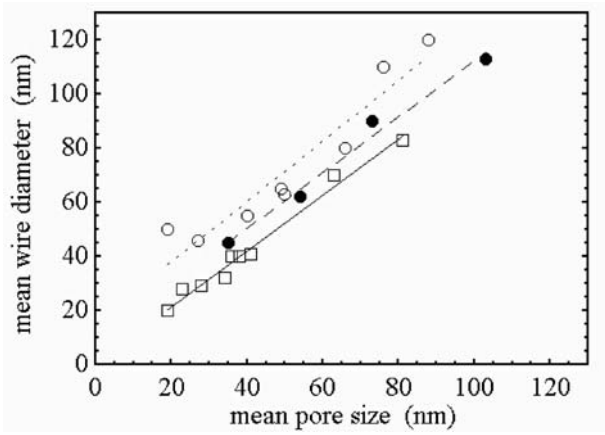

Figure 2 : Comparison between diameter of metallic wires and pore size measured at the surface of polycarbonate templates in which these wires have been electrolytically synthesised. Evolution from raw (○) to slightly (●) and highly (□) pre-etched polycarbonate film shows the beneficial effect of this etching prior to ion irradiation on the realisation of cylindrical pores and wires. All results have been equally obtained form Makrofol KG and Lexan polycarbonate films.

6.3.4. Realisation of supported track etch templates

The main limitation of track etch templates made of thick polymer films is the low pore filling rate in electrodeposition experiments when pore size becomes smaller than 30 nm. If typical values of pore filling rate are still higher than 90 % at 30 nm, they rapidly decrease below 1 % for pore size smaller than 15 to 20 nm, probably due to a low wetting of the pores by the electrolytic solution.

To overcome this effect and then to reach an efficient synthesis of nanoscale materials with very small pore size, we first tried to realise track etch templates from 2 and 5 µm thick polycarbonate films. Even if track etching process is efficient for these films, it rapidly appears that their handling in electrodeposition experiments is rather difficult. Therefore, the work has been focused on the realisation of supported track etch templates made of thin polycarbonate layer, with a thickness from 200 nm to several microns, spin-coated on indium-tin oxide coated glass or gold coated silicon wafers. UV irradiation as well as etching conditions have been adapted to these new kinds of devices to control pore size and pore shape. An effort has been also made to avoid the detachment of the polymer layer from its support during the etching, and a spin coating of a primer before the polycarbonate following by an annealing of the device prior to the ion irradiation are required [18].

Supported polycarbonate track etch templates with pore size from 10 to 100 nm are now regularly produced at lab-scale. They are mainly used for the synthesis of conducting polymer nanostructures and for the study of their electronic and conductive mechanisms. Devices dedicated to applications are also intensely developed in collaboration with industrial partners.

6.3.5. Patterning process in polycarbonate track etch template

Patterned track etch templates are here defined as templates where a known number of pores are confined in arranged areas. Their interest lies in the opportunity they consequently offer to locally synthesise a known number of nanowires or nanotubules and therefore to allow a more precise definition of the fundamental properties of these nanomaterials. Supported patterned templates are also very promising for the realisation of applied devices in which nanomaterials have to be only located above some areas of an electronic circuitry.

The patterning process, initially developed in our laboratory [19], is based on a clever combination of track fading and track sensitisation steps. After being irradiated with energetic heavy ions, the polycarbonate film or layer is heated around the glass transition temperature of the polymer for a well-defined time leading to a significant but not complete track fading. Afterwards, selected tracks only are re-sensitised using UV sources as in classical track etching process but for a longer time (Fig. 3). Consequently, only these re-sensitised tracks are converted in pores by the following etching while other faded tracks lead to short cone-shaped holes. The selective UV irradiation can be considered with UV sources illuminating through a UV mask or using a UV laser spot drawing the required pattern.

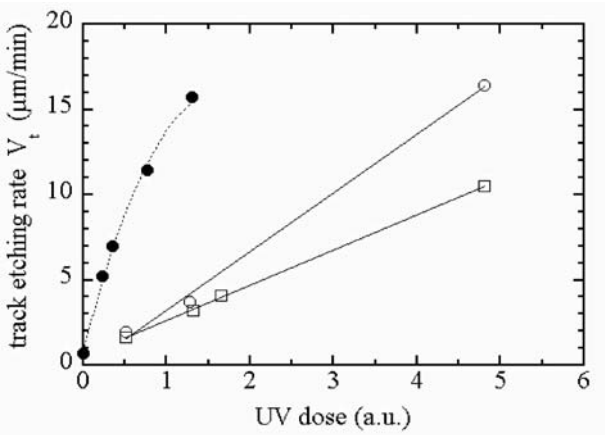

Figure 3 : UV irradiation effect on track etching rate in polycarbonate film : comparison between initial (●) and thermally faded tracks (○ : 15 min. @ 150 °C; □ : 60 min. @ 150 °C) is shown; after a thermal treatment, high track etching rate can be recovered with an appropriate UV irradiation dose.

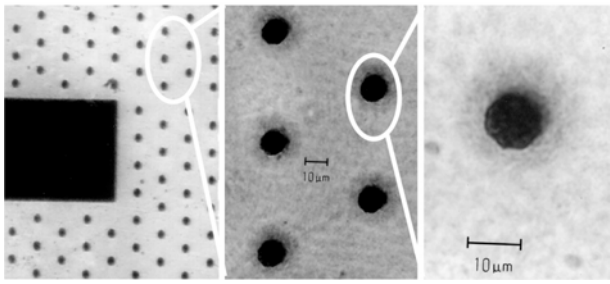

Figure 4 : Optical microscopic views of a patterned track etched membrane used as template for the chemical synthesis of polypyrrole nanotubules. Black zones correspond to areas where pores have been only etched and consecutively filled with polypyrrole. The pattern of these black spots corresponds very well to the pattern of the UV mask use for the track sensitisation.

An optimisation of this process has been experimentally carried out using a conductivity cell to determine track etching rates after fading and sensitisation tracks and to therefore assure a high enough contrast between non UV-irradiated and UV-irradiated zones. Pores sizes up to several hundreds of nanometers can be efficiently etched keeping the patterning defined during the UV treatment (Fig. 4). A study is now in progress in the frame of a PhD thesis to understand the fundamental process involved during the successive fading and sensitisation steps [20].

6.3.6. Polyimide templates

Even if a polymer such as polycarbonate offers numerous advantages for the realisation of track etch templates, its low chemical and thermal resistances can be a limit when nanomaterial synthesis requires the use of non aqueous electrolytic solutions.

A possible alternative is the use of polyimide film like Kapton irradiated with 574 MeV Xe ions, and its track etching feasibility has been demonstrated using e.g. a sodium hypochlorite aqueous solution [21-24]. For this polymer, the control of the pore shape seems also to be critical and an efficient process based on the monitoring of the pH of the etching solution has been already proposed to tailor the pore geometry from nearly cylindrical to funnel-shapes pores [24].

In the work on polyimide templates, we choose to focus our attention on different pre-etching treatments to obtain cylindrical pores. Rather unexpected pore shapes have been first obtained but recently we succeeded in the realisation of polyimide track etch templates, having homogeneous pores with a size around 40 nm and a nearly cylindrical shape (Fig. 5). The same pre-etching treatment has been also successfully applied to a 1 µm thick polyimide layer deposited on a silicon substrate. All these results are very promising for a lab-scale controlled production of polyimide templates.

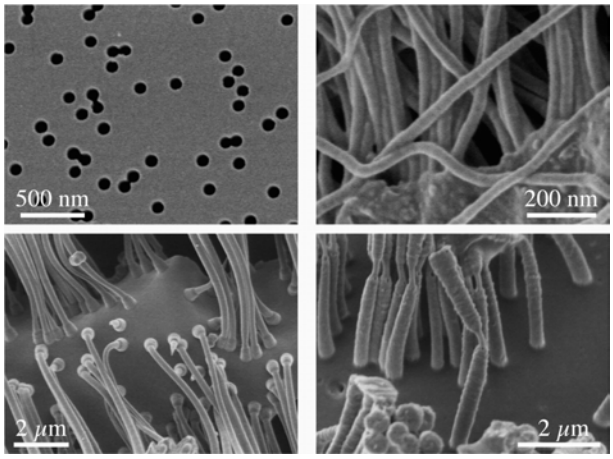

Figure 5 : Silicon supported polyimide track etch template with a homogeneous 40 nm pore size (upper left) and 40 nm size nearly cylindrical polypyrrole nanowires synthesised in polyimide template (upper right). With a specific treatment prior to etching, unexpected pore shape and consecutively wire shape can be also obtained (down left and right).

6.3.7. Nanomaterial synthesis, properties and applications

The use of track etch membrane as template for the synthesis of nanoscale materials is still actually considered as very attractive and useful by many research groups. About the developments described in this paper, they are mainly directed by the requirements of research partners in the frame of different research projects in which mainly three processes are considered for the synthesis of various combinations of polymers and/or metals : electrodeposition [5,6,18,25-30] where a metallic layer deposited on one side of the template, or the template support itself, is used as cathode for the electroplating; chemical polymerisation [6,26,29,31,32] where diffusion of a monomer and an initiator through the pores from both side of the template leads to a polymerisation reaction in these pores; and electroless plating [33] where a metal is deposited on the activated pore wall of the templates.

The micro- or nanomaterials so produced take the form of wires or tubes and are then considered as following [6]: metallic nanowires in array or isolated mode for their microstructure, magnetic properties [34-36] and microwave absorption [37]; multi-layerred nanowires for their giant magnetoresistance [34,38-40] properties; and conducting polymeric nanotubes for their morphology [25-27,31,32] and their electronic and conductive properties [28], as well as for their mechanical characteristics [41]. Potential applications in devices such as microwave filters for making shields for microwave ovens and mobile phones, or in chemical detectors and biosensors with conductive polymer nanotubes are also seriously considered.

6.3.8. Perspectives

In the future, we intend to push further the track etching technology mainly to produce templates more resistant to chemicals and useable under high temperature conditions, and also to extend possibilities offered by the patterning process. We intend also to extend the existing lab-scale technology to supply actual research partners as well as eventually new interested people with more free-standing or supported track etch templates.

[1] R.L. Fleischer, P.B. Price, R.M. Walker, in : Nuclear Tracks in Solids, University of California Press, Berkeley, Ca, 1975.

[2] G.A. Ozin, Adv. Mater. 4(10) (1992) 612-649.

[3] J.C. Hulteen, C.R. Martin, J. Mater. Chem. 7(7) (1997) 1075-1087 and references therein.

[4] S.K. Chakarvarti, J. Vetter, Radiat. Meas. 29(2) (1998) 149-159 and references therein.

[5] L. Piraux, S. Dubois, S. Demoustier-Champagne, Nucl. Instr. and Meth. B131(1-4) (1997) 357-363.

[6] L. Piraux, S. Dubois, J.-L. Duvail, A. Radulescu, S. Demoustier-Champagne, E. Ferain, R. Legras, J. Mater. Res. 14(7) (1999) 3042.-3050.

[7] M.E. Toimil Molares, J. Brotz, V. Buschmann,D. Dobrev, R. Neumann, R. Scholz, I.U. Schubert, C. Trautmann, J. Vetter, Nucl. Instr. and Meth. B185(1-4) (2001) 192-197.

[8] C. Schoenenberger, B.M.I. van der Zande, L.G.J. Fokkink, M. Henny, C. Schmid, M. Krueger, A. Bachtold, R. Huber, H. Birk, U. Staufer, J. Phys. Chem. B101(28) (1997) 5497-5505.

[9] E. Ferain, R. Legras, Nucl. Instr. and Meth. B131(1-4) (1997) 97-102.

[10] E. Ferain, R. Legras, Radiat. Meas. 34(1-6) (2001) 585-588.

[11] E. Ferain, R. Legras, Nucl. Instr. and Meth. B82(4) (1993) 539-548.

[12] T. Steckenreiter, E. Balanzat, H. Fuess, C. Trautmann, Nucl. Instr. and Meth. B151(1-4) (1999) 161-168.

[13] M.I. Chipara, J. Reyes-Romero, Nucl. Instr. and Meth. B185 (2001) 77-82.

[14] M.I. Chipara, V.V. Grecu, P.V. Nothingher, J. Reyes-Romero, M.D. Chipara, Nucl. Instr. and Meth. B88(4) (1994) 418-422.

[15] E. Ferain, R. Legras, Nucl. Instr. and Meth. B84(3) (1994) 331-336.

[16] E. Ferain, R. Legras, Nucl. Instr. and Meth. B131(1-4) (1997) 97-102.

[17] E. Ferain, R. Legras, H. Hanot, PCT Int. Appl. (2001) WO0149403.

[18] L. Dauginet-De Pra, E. Ferain, R. Legras, S. Demoustier-Champagne, Nucl. Instr. and Meth. B196(1-2) (2002) 81-88.

[19] E. Ferain, R. Legras, K. Ounadjela, PCT Int. Appl. (2001) WO0149402.

[20] F. Dehaye, E. Balanzat, E. Ferain, R. Legras, in: Proc. 5th Int. Symp. on Swift Heavy Ions in Matter, Taormina, Italy 2002.

[21] C. Trautmann, S. Bouffard, R. Spohr, Nucl. Instr. and Meth. B116(1-4) (1996) 429-433.

[22] S.K. Chakarvarti, S.K. Mahna, Nucl. Tracks Radiat. Meas. 20(4) (1992) 589-594.

[23] T. Zhu, R. Brandt, P. Vater, J. Vetter, Nucl. Tracks Radiat. Meas. 15(1-4) (1988) 771-774.

[24] C. Trautmann, W. Brüchle, R. Spohr, J. Vetter, N. Angert, Nucl. Instr. and Meth. B111(1,2) (1996) 70-74.

[25] S. Demoustier-Champagne, E. Ferain, C. Jérôme, R. Jérôme, R. Legras, Eur. Polym. J. 34(12) (1998) 1767-1774.

[26] S. Demoustier-Champagne, J. Duchet, R. Legras, Synthetic Met. 101 (1999) 20-21.

[27] C. Jérôme, S. Demoustier-Champagne, R. Legras, R. Jérôme, Chem. Eur. J. 6(17) (2000) 3089-3093.

[28] S. Demoustier-Champagne, P.-Y. Stavaux, Chem. Mater. 11(3) (1999) 829-834.

[29] M. Delvaux, J. Duchet, P.-Y. Stavaux, R. Legras, S. Demoustier-Champagne, Synthetic Met. 113 (2000) 275-280.

[30] S. Dubois, S. Micherl, J.P. Eymery, J.-L. Duvail L. Piraux, J. Mater. Res. 14(3) (1999) 665-671.

[31] J. Duchet, R. Legras, S. Demoustier-Champagne, Synthetic Met. 98 (1998) 113-122.

[32] J. Duchet, S. Demoustier-Champagne, Polymer 41 (2000) 1-8.

[33] S. Demoustier-Champagne, M. Delvaux, Mat. Sci. Eng. C15 (2001) 269-271.

[34] A. Fert, L. Piraux, J. Magn. Magn. Mater. 200(1-3) (1999) 338-358.

[35] S. Pignard, G. Goglio, A. Radulescu, L. Piraux, S. Dubois, A. Declemy, J.-L. Duvail, J. Appl. Phys. 87(2) (2000) 824-829.

[36] Y. Henry, K. Ounadjela, L. Piraux, S. Dubois, J.-M. George, J.-L. Duvail, Eur. Phys. J. B20(1) (2001) 35-54.

[37] G. Goglio, S. Pignard, A. Radulescu, L. Piraux, I. Huynen, D. Vanhoenacker, A. Vander Vorst, App. Phys. Lett. 75(12) (1999) 1769-1761.

[38] L. Piraux, J.M. George, J.F. Despres, C. Leroy, E. Ferain, R. Legras, K. Ounadjela, A. Fert, Appl. Phys. Lett. 65(19) (1994) 2484-2486.

[39] A. Radulescu, U. Ebels, Y. Henry, K. Ounadjela, J.-L. Duvail, L. Piraux, IEEE T. Magn. 36(5,1) (2000) 3062-3064.

[40] L. Vila, L. Piraux, J.M. George, G. Faini, Appl. Phys. Lett. 80(20) (2002) 3805-3807.

[41] S. Cuenot, S. Demoustier-Champagne, B. Nysten, Phys. Rev. Lett. 85(8) (2000) 1690-1693.

7. ACCÉLÉRATEUR VAN DE GRAAFF

7.1. Stoichiometric analysis of debased lead seals and authentication of Russian icons by proton RBS and PIXE techniques

M. Morelle, Y. El Masri, J. Van Mol (Institut de Physique Nucléaire, Université catholique de Louvain, Louvain-la-Neuve); J-C. Dran, J.Salomon, T. Calligaro and M. Dubus (C2RMF, Louvre, Paris)

Résumé : *Les analyses stœchiométriques effectuées auprès de l'accélérateur AGLAE du Musée du Louvre et auprès de la VdG de Louvain-la-Neuve se sont portées sur un lot d'icônes russes et des sceaux en plomb altérés. L'étude des icônes avait pour but leur authentification par l'analyse de leurs dorures. Une altération "anormale" observée en surface des sceaux en plomb, utilisés autrefois pour sceller des parchemins, a motivé la seconde étude. Notre objectif de départ était d'identifier ces types d'altérations pour en déduire les atmosphères nocives à la conservation de tels sceaux.*

7.1.1. Introduction

The stoichiometric studies initiated in this work [1] were aiming, on one hand, to authenticate some Russian icons through the analysis of their gilds and silver layers and, on the other hand, to identify the "abnormal" surface debasement of lead seals used in the past to seal official documents. Our first aim was to establish the different types of environmental alterations to infer the noxious environments for preserving these seals.

7.1.2. Experimental set-up

These studies were undertaken using the 2MeV AGLAE tandem accelerator of the Louvre Museum in Paris and the 4 MV Van de Graaff of the Louvain-la-Neuve research facility. Two nuclear techniques were used for the elemental analysis i.e. PIXE (Proton Induced X-ray Emission) [2] and RBS (Rutherford Backscattering Spectrometry) [3].

GUPIX [4] software was utilised to analyse and interpret PIXE associated data whereas SIMNRA [5] and XRUMP [6] computer programs were applied to sort data generated by the RBS technique.

Proton and alpha beams of 3 MeV were used in these experiments. With proton beam, many strong nuclear resonances occur on the light elements that constitute the target material and the experimental environment such as helium, carbon and specially oxygen with constructive and destructive interferences.

The Russian icon authentication experiments were performed using an "extracted" beam from AGLAE in continuously blown helium atmosphere.

7.1.3. Results

7.1.3.1. Icons

Figure 1 : Details of icons 122 and 47 (Private Coll.).

The gold braid parts of the icon pictures (see figure 1) were set perpendicular to the beam axis and simultaneously analysed by proton induced PIXE and RBS techniques. In general these icon gilds are composed of gold and silver plates or of alloys of these two metals. Figure 2 displays a PIXE spectrum showing clearly the characteristic X-ray peaks of gold (mainly LX-rays) and of silver (mainly KX-rays) plus those of other trace elements such as Fe, Ca and Pb which are basic components of pigments.

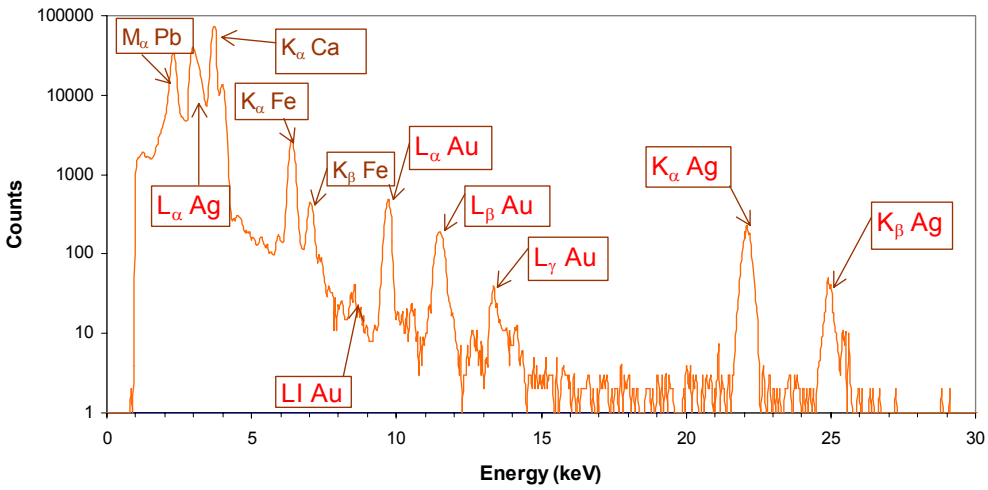

Figure 2 : Emitted X-rays spectrum after proton bombardment of icon 47 gild.

While figures 3 and 4 display two proton induced RBS spectra of icons containing Au and Ag elements, figure 5 shows the analysis of another icon where these two elements are completely lacking. In the latter figure the golden aspect is falsely generated by the presence of a 2 µm thick layer composed of an aluminium powder blended with alcohol-based shellac (as pointed out later by the electronic microscope scanner). In these spectra the helium peaks indicate the resonant RBS contribution of the proton-helium gas interaction. In figures 3 and 4 the RBS analysis clearly allows the discrimination between the gold-silver plated contribution (two distinct Au and Ag peaks) and the alloy contribution (unresolved peaks). One can also observe the presence of many trace elements such as C, O and heavier Si,Fe, Pb … present in the decoration pigments such as, for example, the red ochre (Fe_2O_3), the yellow iron-oxide, the $PbCrO_4$ chrome yellow or the white lead. All these spectra have been

analysed using SIMNRA computer code. These data analysis clearly shows the excellent and recommended complementary of both PIXE and RBS nuclear techniques in this field of applications.

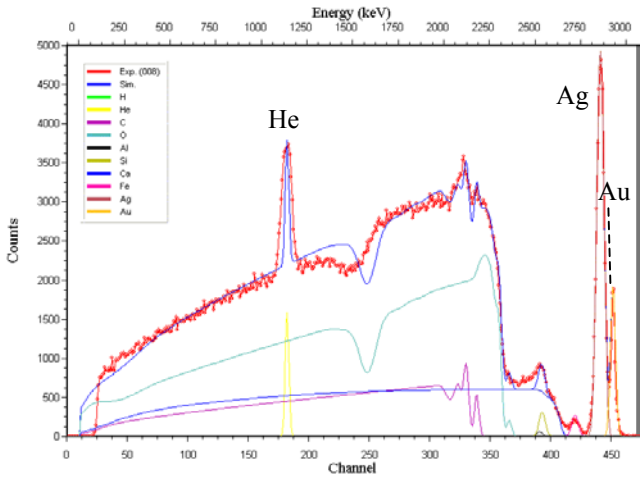

Figure 3 : Proton induced RBS spectrum on icon gild composed of gold-silver plates and analysed by SIMNRA code.

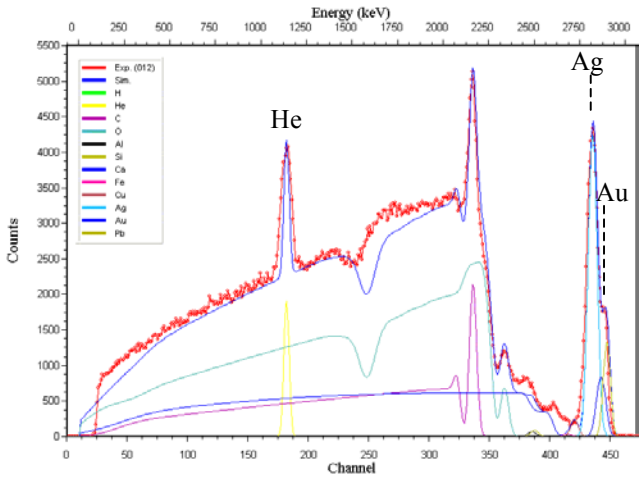

Figure 4 : Proton induced RBS spectrum of icon gild composed of gold-silver alloy and analysed by SIMNRA code.

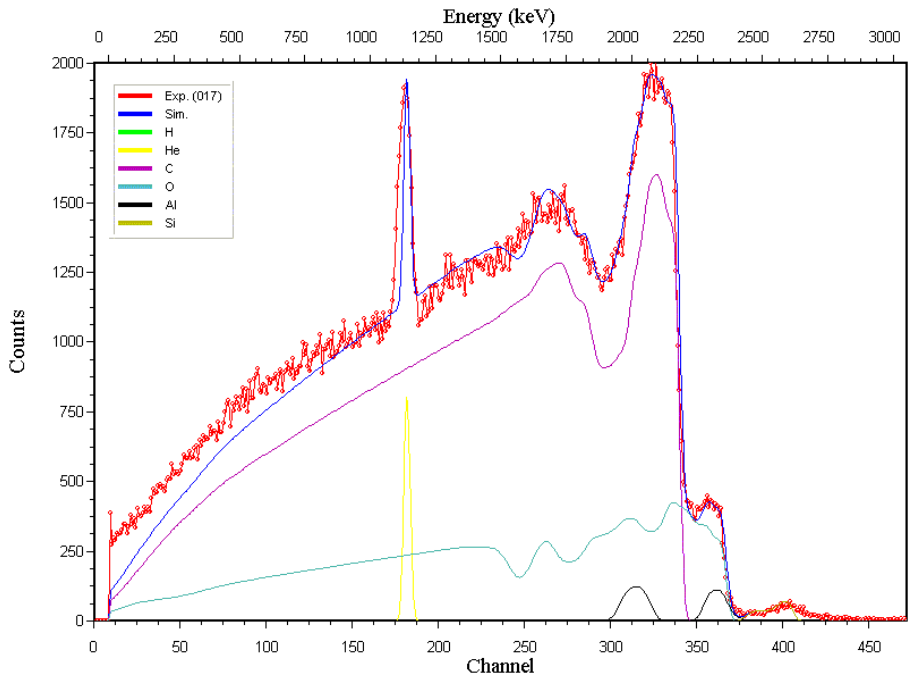

Figure 5 : Proton induced RBS spectrum on icon 122 gild, lacked of gold and silver. The histogram represents the experimental data, the blue line the sum of all element contributions depicted by different colours in SIMNRA code.

7.1.3.2. Lead seals

The surface debasement analysis has not been directly applied to original antique lead seals but on lead pieces kept during two years in the same conservation conditions (environment, atmosphere…) as the antique ones. We have also used, as references, some lead oxide targets of known composition in order to establish and test the sensitivity and the performances of RBS technique on these materials.

Figure 6a displays a proton induced RBS spectrum on a pure lead target successfully analysed by SIMNRA code imposing the “double diffusion” hypothesis of the incoming and the backscattered particles in the lead matrix. Figure 6b clearly shows the complete failure of a similar analysis with the computer code option of “single diffusion” especially in the low energy part of the spectrum. If the option of “double diffusion” is allowed by the SIMNRA code it, however, imposes the entire elemental analysis to be of pure Rutherford scattering type (i.e. Coulomb scattering). Thus, in such cases the SIMNRA code does not support any resonant type interaction such as the ones observed with proton beams on light elements like carbon, oxygen, sulphur, aluminium or silicon. In fact in these cases only “single diffusion” option is supported by the code. Therefore, until such improvements are brought to the widely used codes, the analysis of RBS spectra of any non-pure lead material such as lead oxides or lead carbonates matrixes or foils containing oxygen, carbon or sulphur elements is compromised. Our only way to determine the surface debasement types is to base on the height of lead signal compared to selected references.

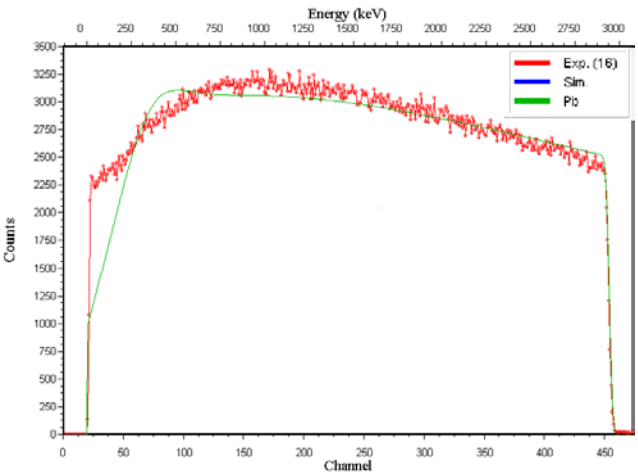

Figure 6a : Proton induced RBS spectrum on pure lead target analysed with SIMNRA code imposing “double diffusion" option.

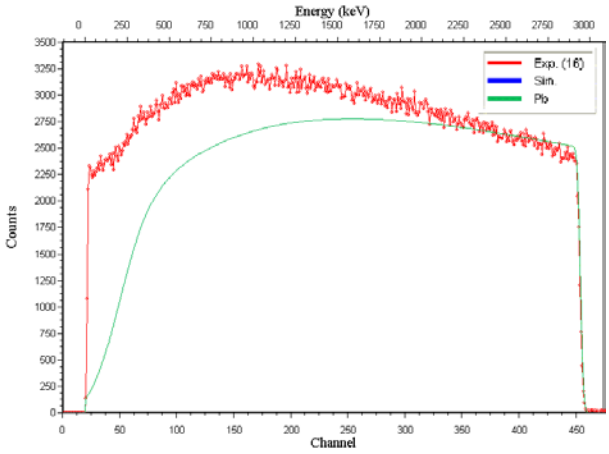

Figure 6b : Proton induced RBS spectrum on pure lead target analysed with SIMNRA code imposing “single diffusion” option.

By comparison, we were also successful in analysing with both SIMNRA and XRUMP codes the alpha induced RBS spectra on a $PbSO_4$ pastille as shown in figure 7. Nevertheless, the contributions of RBS interaction on oxygen and sulphur constituents are so weak compared to the lead signal that they are hardly discernible in the spectrum. This clearly limits the utility of such experiments.

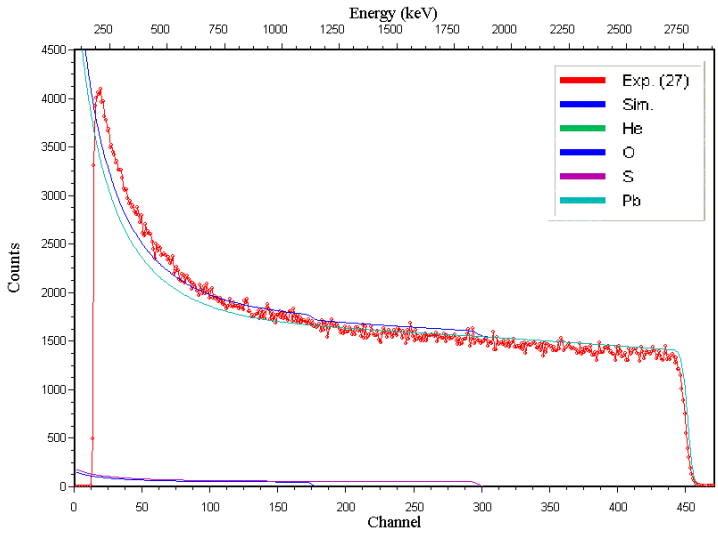

Figure 7 : Alpha induced RBS spectrum on Pb SO_4 and analysed by SIMNRA code.

7.1.4. Conclusion and future prospects

The simultaneous use of both RBS and PIXE techniques has shown very interesting results regarding the analysis of Russian icons and their authentication, whereas the analysis of lead seals required a different sorting approach of the RBS data. First, in order to detect the presence of light elements in lead samples, it appears important to take advantage of resonance phenomena, as induced by proton, deuteron and alpha beams at 3 MeV incident energy or higher. Secondly, the use of some complimentary techniques such as NRA, X-ray diffraction, electronic microscope scanner and perhaps others can be very helpful and even recommended. On the other hand, we have found, in many analyses, some lacuna in the software of the RBS data interpretation. Their main imperfection concerns their difficulties in simulating the particle double-diffusion in mixed resonant and non-resonant interactions

These experiments have also allowed us to test the potentiality of these elemental analyses based on nuclear techniques and their intrinsic limitations.

[1] M. Morelle, Analyse stœchiométrique de couches d'altération du plomb et authentification d'icônes russes par diffusion RBS de protons et la technique PIXE, Rapport de DEA (UCL Louvain-la-Neuve, 2002).

[2] S.A.E. Johansson, J.L. Campbell, A Novel Technique for Elemental Analysis, Wiley (Chichester, 1988).

[3] W.K. Chu, J.W. Mayer, M.A. Nicolet, Backscattering Spectrometry, Academic Press (New-York, 1978).

[4] Maxwell et al., Logiciel GUPIX (1995).

[5] M. Mayer, Logiciel SIMNRA, Max-Planck-Institut für Plasmaphysik (1998).

[6] J.W. Mayer et al., Logiciel RUMP, Cornell University.

II. RECHERCHES AUPRÈS D'AUTRES ACCÉLÉRATEURS

1. CHORUS: Production de particules charmées induites par des neutrinos ν_μ

Th. Delbar, D. Favart, Gh. Grégoire, S. Kalinin, I. Makhlioueva (Institut de Physique Nucléaire, Université catholique de Louvain, Louvain-la-Neuve) et collaboration CHORUS

L'année 2002 a été consacrée en majeure partie à mettre la dernière main au changement radical du logiciel d'analyse, en passant de la version "CHORAL" à la version "CHANT", comme annoncé l'an dernier. Ce changement était indispensable au vu des lacunes, inefficacités et lourdeurs de l'ancienne version. Le changement a été accompagné également d'une modification des bases de données. En parallèle, plusieurs études ont été finalisées en utilisant des données partielles, et ont déjà fait l'objet de publications indiquées ci-dessous.

Le groupe UCL a participé activement au changement de logiciel et à la constitution des nouvelles bases de données. En particulier, S. Kalinin a analysé des émulsions lors d'un séjour à Nagoya et a vérifié minutieusement la compatibilité entre les résultats produits par CHORAL et ceux fournis par CHANT. Nous nous attaquons désormais à l'analyse détaillée des erreurs systématiques des événements dimuons.

2. CMS

S. Assouak, E. Burton (FNRS), J. de Favereau (FRIA), G. de Hemptinne (FRIA), C. Delaere (FNRS), Th. Delbar, D. Favart, E. Forton, J. Govaerts, Gh. Grégoire, G. Leibenguth, V. Lemaître (FNRS-UCL), O.Militaru, K. Piotrzkowski, X. Rouby, O. van der Aa (FRIA) (Institut de Physique Nucléaire, Université catholique de Louvain, Louvain-la-Neuve)

2.1. Activités liées à la construction du tracker "avant"

Le groupe CMS-Louvain a été actif dans les domaines suivants :

1. Qualification des senseurs au silicium et sensibilité aux dégâts radiatifs
2. Conception des circuits de refroidissement des pétales
3. Construction de groupes froids
4. Tests de circuits hybrides
5. Tests ("burn-in") des modules et des pétales

Pendant l'année 2002, le groupe CMS-Louvain est entré dans la phase de production pour le point 1 ci-dessus. La conception d'un deuxième prototype de pétale est bien avancée et les essais sur le premier prototype sont terminés (point 2). Les dispositifs de tests des circuits hybrides ont été construits, réceptionnés et présentés aux entreprises chargées de la fabrication (point 4). La chaîne complète de tests des modules est opérationnelle (point 5). La boîte froide pour les essais de pétale est en cours d'assemblage (point 6). En outre nous avons entrepris d'explorer les possibilités d'observation de processus physiques inédits auprès du LHC.

2.1.1. Tests de tenue aux radiations des senseurs micropiste au Silicium pour CMS

S. Assouak, E. Forton, Gh. Grégoire (Institut de Physique Nucléaire, Université catholique de Louvain, Louvain-la-Neuve)

Abstract : *CMS microstrip sensor neutron qualification has been pursued this year. The sensor flow has been increasing accordingly with production and arrival of sensors. The flow will still increase until the end of the production phase. Hence, the need of an automated program able to control the probe station and its related electrical equipment became critical to sustain the testing rate. This automated system has been implemented and debugged this year. In parallel, we refined the irradiation setup. The improvements in both setups (measurement and irradiation) are presented, together with some irradiation results obtained on sensors and test structures.*

Le LHC, de par sa haute luminosité, entraîne inévitablement la production d'une multitude de particules secondaires, rendant l'environnement radiatif assez exigeant pour les détecteurs et les équipements. Ces derniers devront de surcroît y fonctionner pendant une dizaine d'années.

Par ailleurs, le trajectographe, placé au coeur de CMS, sera constitué de senseurs à micropistes en Silicium cristallin. L'envergure de l'expérience porte leur nombre à environ 25000, totalisant une surface de détection de plus de 200m^2. La production de ces senseurs est maintenant lancée et le nombre d'irradiations a augmenté en conséquence, nécessitant un système automatique pour réaliser les tests électriques sur les senseurs.

Cette année, la majeure partie des efforts fut donc concentrée sur la mise en oeuvre des outils et instruments nécessaires à la réalisation la plus automatisée possible des tests (dispositif et support d'irradiation, de tests électriques, four de recuit, frigo de stockage…).

2.1.1.1. Mise en œuvre du dispositif d'irradiation

Si l'étude de l'évolution des caractéristiques d'un senseur au silicium implique surtout des tests avant et après irradiation, les conditions dans lesquelles se déroule cette dernière n'en revêtent pas moins une grande importance.

Ainsi, nous voulons que l'exposition des senseurs au flux de neutrons se déroule dans des conditions les plus proches possibles de celles rencontrées au LHC, dans CMS. De plus, l'irradiation à des tempéretures inférieures à –10 °C a pour avantage de bloquer le recuit prématuré des défauts induits dans la structure cristalline. La zone d'irradiation doit donc être équipée d'un dispositif de refroidissement. La boîte dans laquelle seront placés les senseurs doit contenir de l'air sec pour éviter toute condensation sur les senseurs, et ces derniers doivent être polarisés tout au long de l'irradiation.

Nouvelle boîte froide en zone d'irradiation

La boîte froide existant en T2, et associée au dispositif de régulation de température mis au point en 2001 (cf. rapport cyclone 2001) a été changée au profit d'une nouvelle. Cette dernière présente de bien meilleures caractéristiques d'étanchéité, de sorte que l'humidité relative résiduelle est tombée de 40% à 2-3%. Cette nouvelle boite froide améliore aussi l'autonomie du système. Cette dernière peut désormais atteindre 3 à 4 jours.

Polarisation de structures lors des irradiations

Les essais de polarisation de structures en cours d'irradiation menés fin de l'an passé et début de cette année ont montré que l'utilisation d'aiguilles et de « probe cards » n'est pas fiable.

En effet, si ces méthodes s'avèrent utiles et flexibles lors des tests réalisés avec probe station, la sensibilité des aiguilles aux mouvements est un grand handicap lors de l'utilisation en zone d'irradiation.

Nous avons donc réalisé des supports en plexiglas (Figure 1) pour les « demi-lunes » et les senseurs, sur lesquels nous réalisons les connections électriques avec notre appareil de « bonding » (Figure 2).

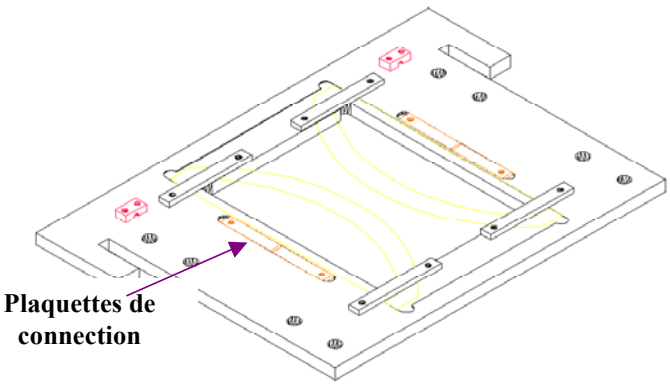

Figure 1 : Support d'irradiation.

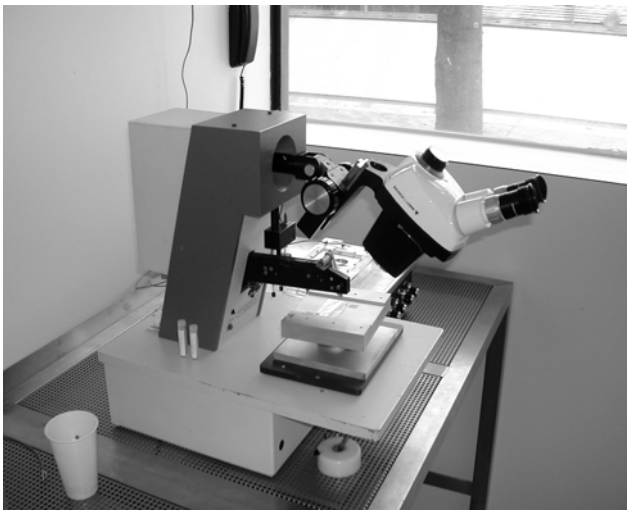

Figure 2 : Machine de bonding.

Si la polarisation de structures de test (« baby detectors ») se fait de manière appropriée avec des alimentations standard de type N470 de chez CAEN (1000 V, 3 mA), ce n'est pas le cas lors de l'irradiation de senseurs de grande taille. En effet, ces derniers ont un courant de fuite plus considérable (s'ils sont issus du même wafer, un senseur a un courant de 20 à 25 fois plus élevé[1]). Pour ces derniers, nous avons mis en œuvre des alimentations de grosse puissance (2 kV, 30 mA).

Le programme d'acquisition utilisé lors des irradiations a été modifié pour intégrer ces nouvelles alimentations.

Dosimétrie

L'évaluation de la fluence neutrons à laquelle sont soumis les senseurs lors des irradiations est évaluée grâce à l'intensité du faisceau primaire de deutons. Cependant, nous réalisons des mesures systématiques de doses au moyen de films alanine, et une évaluation du flux de neutrons a aussi été réalisée au moyen de plaquettes d'activation.

La lecture des films alanine est réalisée au moyen d'un lecteur à résonance paramagnétique électronique Bruker E-scan, acquis cette année par le laboratoire (Figure 3).

Figure 3 : Lecteur de films alanine.

[1] Une structure de test présente une surface de 3,75 cm^2, et un senseur a une surface allant de 76 à 91 cm^2.

L'appareil est calibré (NIST) pour des doses allant de 0.5 à 32 kGy (calibration valable pour une irradiation aux gammas du ^{60}Co). Les films utilisés permettant la lecture de doses dépassant 300 kGy, une future extension de la gamme de calibration à l'aide de la bombe à Cobalt disponible à Louvain-la-Neuve est envisagée.

Les neutrons produits en T2 n'ayant pas le même dépôt de dose que les gammas produits par une source au Cobalt, la réponse des films au spectre neutrons a dû être étudiée.

Selon les mesures réalisées par M. Tavlet (Figure 4) et le spectre énergétique des neutrons produits en T2, les films alanine doivent donner une réponse valant à peu près 4.10^{-11} Gy.cm^2.

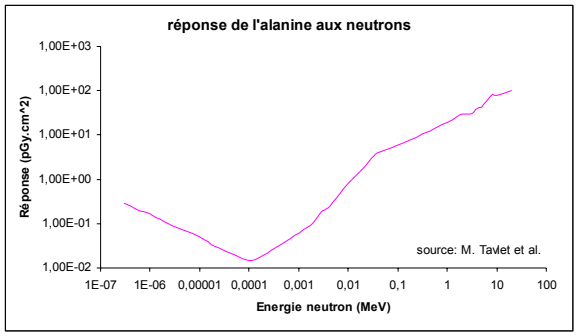

Figure 4 : Réponse des films alanine aux neutrons.

Nous avons obtenu jusqu'à présent une réponse expérimentale un peu inférieure, de l'ordre de 3.10^{-11} Gy.cm^2. Cette valeur n'est pas incompatible avec les valeurs données par Tavlet si l'on considère que cette réponse dépend beaucoup du rapport de concentration alanine/solvant dans le film. Bruker et Kodak n'ont pas donné de renseignements complémentaires concernant la composition des films.

2.1.1.2. Mise en œuvre des tests systématiques autour de la station à micropointes

Connections et matrice de commutation

L'exécution rapide des tests n'est réalisable que si, outre les mouvements de la station à micropointes et le contrôle de la température du chuck, le programme est en mesure de changer automatiquement les connections électriques entre les pointes et les instruments de mesure.

La Figure 5 illustre les connections réalisées au moyen de la matrice de commutation associée au module d'acquisition de données HP34970A.

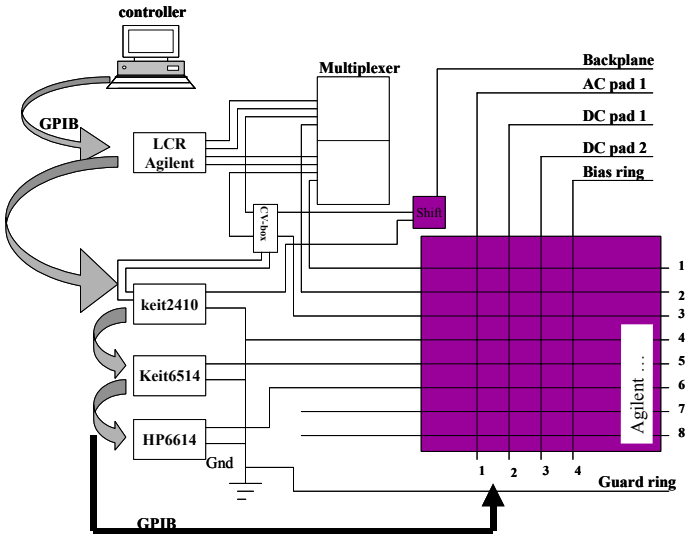

Figure 5 : Matrice de commutation et connections électriques autour de la station à micropointes.

Programme global

Les tests systématiques des senseurs avant et après irradiation, ainsi que l'insertion des résultats dans la base de données de CMS requiert l'écriture d'un programme global, capable de gérer toutes les mesures à réaliser.

Le language de programmation choisi est LabView, de par sa facilité d'utilisation, la portabilité du code et sa compatibilité avec les programmes et routines écrits par les autres instituts en charge des tests sur les senseurs micropiste silicium pour CMS.

Les différentes fonctionnalités nécessaires (CV, IV, R_{poly}, C_{ac}, C_{int}, R_{int}, I_{diel}, I_{strip}, tests sur diodes et MOS) ont été implémentées, l'utilisateur peut à loisir choisir les mesures à réaliser sur la structure en test, et modifier le schéma de polarisation. Les mouvements de la station à micropointes sont implémentés automatiquement selon le type de senseur, et le programme écrit des fichiers de sortie différents selon que les tests sont réalisés avant ou après irradiation. Les résultats pré-irradiation sont automatiquement rechargés pour l'écriture du fichier (xml) à insérer dans la base de données après irradiation.

Par ailleurs, le programme tient compte des corrections à apporter aux mesures (capacités parasites, courants additionnels, lecture de températures…).

Problèmes rencontrés

Outre la réalisation de la boîte de découplage en tension pour les mesures CV (capacité-tension), l'un des problèmes rencontrés est la création de « pinholes » par le système de mesure.

Il est important de pouvoir détecter les pinholes produits lors des irradiations parce qu'un taux de production trop important peut mener à la saturation de l'électronique de lecture lors du fonctionnement réel du détecteur. Une production artificielle de pinholes (Figure 6 et Figure 7) est donc nuisible à une bonne évaluation de la qualité des senseurs livrés par les fabricants.

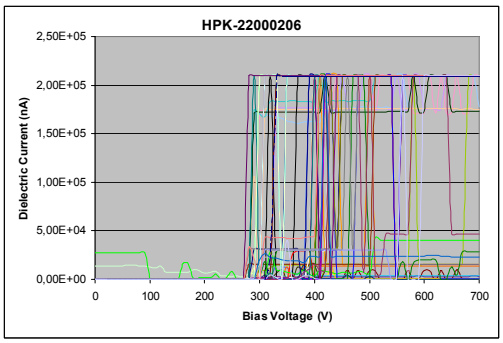

Figure 6 : Production de pinholes sur les structures Hamamatsu (le diélectrique a une tension de claquage de 160 V).

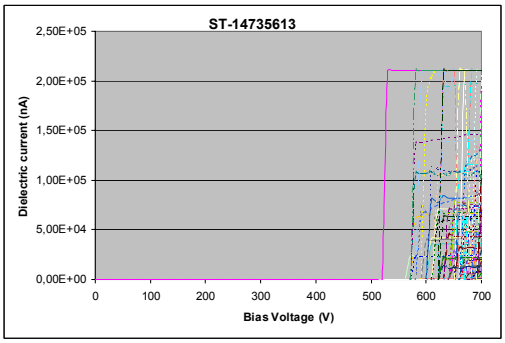

Figure 7 : Production de pinholes sur les structures ST (tension de claquage supérieure à 200 V).

Le schéma de mesure n'étant pas en cause (les connections électriques du senseur étant correctes, les aiguilles en bon ordre d'usage), nous pensons avoir trouvé la source de la création de pinholes dans la manière dont nous utilisions la matrice de commutation pour passer d'une mesure à l'autre (cf. Figure 8 où l'on voit apparaître des pics de tension à chaque utilisation de la matrice). La création d'un court-circuit nécessite que l'amplitude de ces pics soit plus grande que la tension de claquage du diélectrique.

Un regroupement plus judicieux des tests entre eux, ainsi qu'une dépolarisation complète du senseur lors de certaines commutations ont permis d'éliminer ces pics de tension (cf. Figure 9).

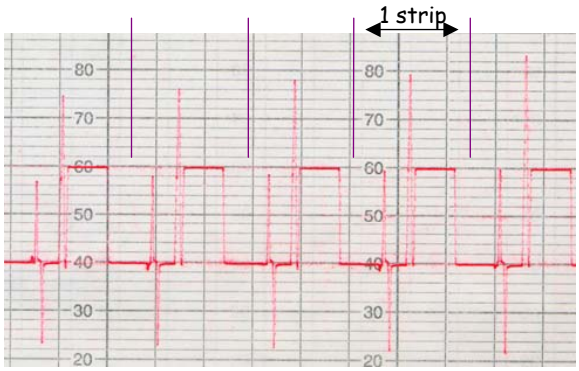

Figure 8 : Tension sur le diélectrique avant modification du programme de commutation.

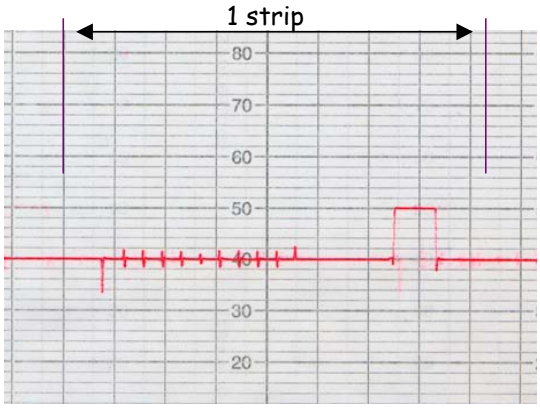

Figure 9 : Tension appliquée sur le diélectrique après modifications du programme.

Le phénomène de création de pinholes ayant principalement été observé avec des structures provenant de Hamamatsu (tension de claquage plus petite), nous attendons les prochains arrivages de senseurs de ce fabricant pour avoir confirmation de la résolution du problème. Les structures présentant le problème et remesurées après les modifications du programme n'ont pas présenté de nouveaux cas de pinholes.

2.1.1.3. Matériel divers

Four de recuit

Si, par exemple, les résistances de polarisation et capacités de couplage ne subissent que peu de dégradation lors des irradiations, il n'en est pas de même pour les mesures de courant de fuite ou de tension de déplétion.

Par ailleurs, comme l'indiquent les résultats présentés à la section précédente, l'état de recuit d'un senseur, d'une structure ou d'une diode influence fortement les résultats obtenus.

Il était donc nécessaire d'équiper le laboratoire d'un four pour effectuer un recuit contrôlé des structures après irradiation. Les caractéristiques de taille, stabilité en température et d'inertie thermique de ce dernier nous

ont fait préferrer la mise au point de notre propre appareil à l'achat d'un four commercial. Ce dernier est illustré à la Figure 10.

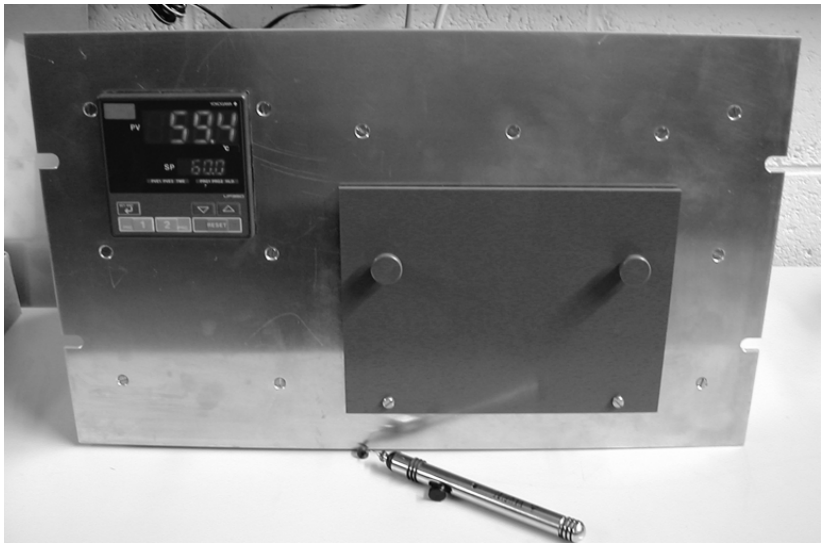

Figure 10 : Four de recuit.

Les caractéristique de ce dernier sont reprises à la Table 1.

Nombre max. de structures	12
Nombre max. de senseurs	3
Gamme de températures	jusque 200 °C
Vitesse de chauffe	4 °C/min.
Uniformité de la température	< 0,7°C
Stabilité de la température	< 0,3°C

Table 1 : Caractéristiques du four de recuit.

2.1.1.4. Résultats

Comparaison des résultats avec Karlsruhe

Des tests comparatifs des résultats obtenus avec notre dispositif et le dispositif allemand de Karlsruhe, également responsable des tests de résistance aux radiations, ont montré que les mesures de résistances de polarisation, de capacités de couplage (Figure 11), de tension de déplétion et de résistance inter-pistes sont compatibles entre les instituts.

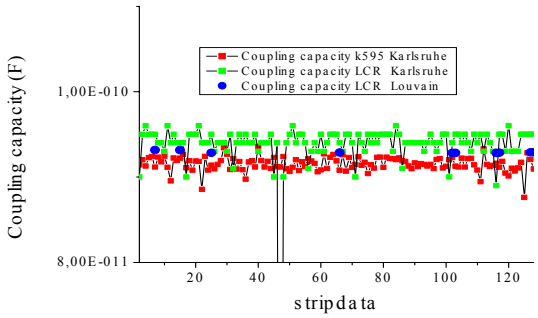

Figure 11: Comparaison des résultats obtenus à Karlsruhe et Louvain pour les capacités de couplage.

Des tests plus approfondis concernant les courants de fuite et les capacités inter-pistes sont à réaliser et nécessitent l'échange de structures, pour avoir des conditions d'irradiation similaires (proton-neutron).

Irradiation de diodes standard (ROSE)

A la suite des irradiations de diodes menées l'an passé, et en parallèle aux mesures réalisées sur les structures CMS, nous avons mené des mesures de recuit sur des diodes standard, pour comparer l'évolution de la tension de déplétion avec les données existantes dans la littérature (modèle de Hambourg). La Figure 12 illustre ces résultats.

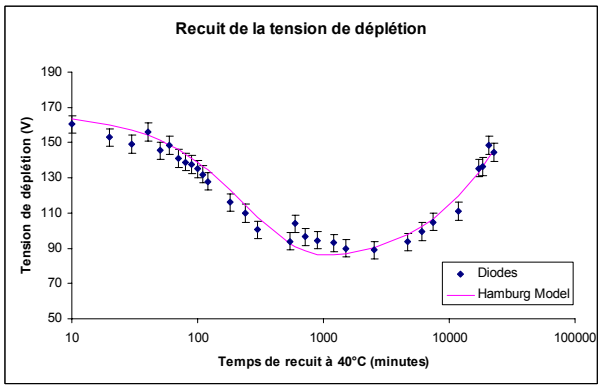

Figure 12 : Comparaison de l'évolution de la tension de déplétion d'une diode en fonction du temps de recuit à 40°C avec le modèle de Hambourg.

Les mesures concernant le courant de fuite sont actuellement en cours d'analyse.

2.1.1.5. Perspectives

Parallèlement aux tests de qualification pour le trajectographe de CMS, nous projetons de réaliser d'autres types de mesures.

Ainsi, nous avons entamé un travail de mesure de la résolution en énergie des structures CMS, en utilisant une source Alpha. Actuellement, nous en sommes à la mise en œuvre d'un dispositif de mesure dans la voie R du cyclotron.

Dans un contexte beaucoup plus général, et dans le cadre d'une collaboration née récemment au CERN (RD50, dont les travaux ont commencé cette année), nous projetons d'irradier aux neutrons et tester électriquement des échantillons semi-conducteurs conçus de différentes manières et avec différents matériaux.

2.1.2. Conception des circuits de refroidissement des pétales

Un premier prototype de pétales a été construit et les essais mécaniques et thermiques sont terminés. Dans l'état actuel, les résultats de ces essais sont satisfaisants: d'une part, les déformations mécaniques lors de la mise en froid sont faibles; les caractéristiques thermodynamiques (débits, pertes de charge) sont meilleures que prévues; les performances thermiques (gradient de température, échanges ...) atteintes satisfont les exigences de dissipation de l'électronique des pétales. Ils visent à déterminer les paramètres mécaniques (déformations, contraintes à basse température ...) et thermiques de l'installation (débits, gradients de température, échanges de chaleur ...).

Il faut toutefois réaliser que les conditions de ces essais ne représentent qu'imparfaitement la situation réelle de CMS avec des détecteurs opérationnels qui ne sont pas encore à notre disposition. Cela concerne en particulier les gradients thermiques au niveau des senseurs en silicium et des circuits hybrides de l'électronique de lecture.

Les essais proprement dits ont été effectués dans une enceinte refroidie qui simule les conditions réelles de fonctionnement dans le détecteur CMS final. Tous les paramètres d'environnement (température, débits, humidité ...) de cette enceinte sont enregistrés en continu pendant les essais.

Une prochaine campagne de mesures avec des circuits thermiques plus réalistes est en préparation.

2.1.3. Construction de groupes froids

La mise en oeuvre des essais thermiques nous a conduit à concevoir un groupe de refroidissement performant, spécialement adapté aux éléments du trajectographe de CMS. Ce groupe est devenu le modèle reconnu par CMS pour toutes les installations similaires de la collaboration.

Ces groupes sont entièrement programmables par ordinateur pour être insérés dans les dispositifs d'acquisition des données de Lyon-CMS.

Notre groupe a ainsi construit cinq unités de refroidissement pour les centres chargés de l'assemblage des pétales: Aachen 1 et Aachen 3, Bruxelles, Lyon, Strasbourg.

2.1.4. Tests de circuits hybrides

Le laboratoire est responsable de la réalisation d'un dispositif de contrôle de qualité des circuits électroniques hybrides à construire dans l'industrie. Cette activité commencée en 2001 s'est poursuivie en 2002 en collaboration avec Aachen (Allemagne), Strasbourg (France) et le CERN. Plusieurs dispositifs ont été réalisés et distribués dans ces laboratoires afin de valider le dispositif avant sa distribution dans l'industrie. Les développements réalisés à Louvain se situent au niveau des cartes électroniques et du progiciel associé, du logiciel de contrôle et des aspects mécaniques du dispositif.

2.1.5. Tests ("burn-in") des modules et des pétales

L'UCL est responsable des essais de quelques 800 modules des pétales du trajectographe de CMS. Ces tests dits de « longue durée » visent à vérifier la fiabilité des sous-détecteurs tout en s'assurant de leur uniformité et en enregistrant les différents paramètres de calibration. Ils nécessitent l'acquisition des données du détecteur proprement dit, ainsi que des paramètres extérieurs (température, humidité, …). L'acquisition se fait à l'aide d'un logiciel développé pour la collaboration à l'Université d'Anvers. Il a cependant fallu l'adapter à la configuration propre à Louvain-la-Neuve. Ceci à nécessité d'intégrer le code « LabView », gérant le contrôle lent de l'environnement, et le code natif C++ (fournit par Anvers) pour le reste de l'acquisition et la synthèse des informations. Une première version, basée sur une connexion TCP/IP entre les deux systèmes est opérationnelle (voir 2.1.5.1.).

En outre un important dispositif à atmosphère contrôlée, permettant de refroidir jusqu'à cinq pétales en parallèle, a été réalisé avec son système de contrôle et de régulation. C'est aussi dans ce contexte qu'un générateur de liquide froid de puissance suffisante a été réalisé.

Une enceinte de grand volume (480 litres) est en cours d'installation, en ce compris tous les dispositifs de mesure (mesure des flux de liquide de refroidissement, pressions différentielles, température ...) et de commande à distance par ordinateur.

Ces résultats ont fait l'objet de plusieurs présentations dans le cadre des réunions de la collaboration CMS au CERN.

2.1.5.1. Data Acquisition developments for the CMS tracker modules tests

C. Delaere, O. Militaru, T. Keutgen, O. van der Aa (Institut de Physique Nucléaire, Université catholique de Louvain, Louvain-la-Neuve)

The Nuclear Physics Institute is one of the few qualification centers for the CMS tracker end-caps assembly. In that context, we are involved into the deployment of software and hardware necessary to achieve the whole schedule of conditions. The hardware system shown in Figure 1 has been setup, tested and is being evolved in order to match the local specificities and external developments.

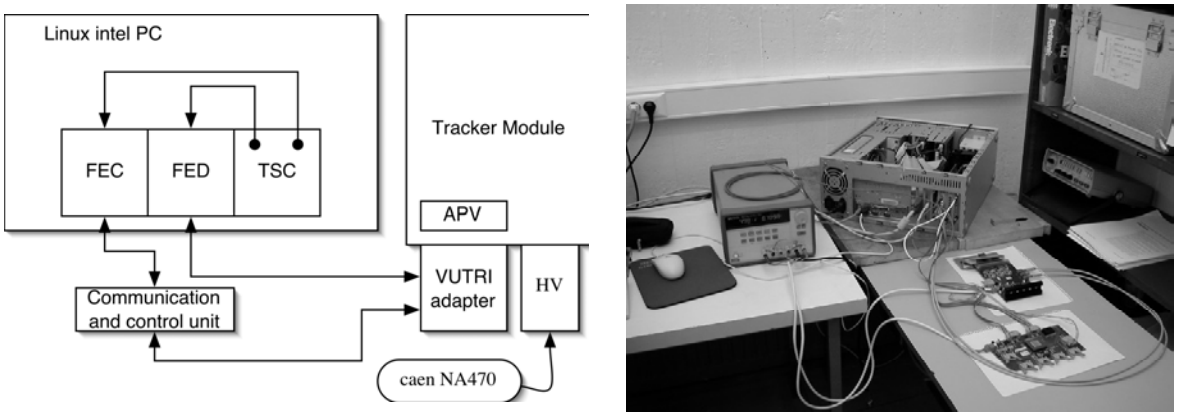

Figure 1 : Schematic and photograph of the CMS-like DAQ system for module testing.

From the software point of view, the acquisition system can be logically divided in two parts: the slow control and the APV readout system. The slow control system handles the high voltage settings of the detector, reads the temperature and humidity probes and measures the leakage current. It has been chosen to manage all the slow control hardware via LabView[1] under windows, whereas the "fast" DAQ system is running on a Linux machine [2]. This has the big advantage of factorizing the two subsystems on different PCs, so that the slow control cannot be affected by a random failure of the DAQ system. In order to interface the main DAQ software with the LabView system, a proxy has been implemented that is connected on one side to the LabView software via tcp/ip. On the other side, the proxy is a service that is plugged in the standard dim [3] framework used by the main DAQ system. The whole concept is schematized on Figure 2.

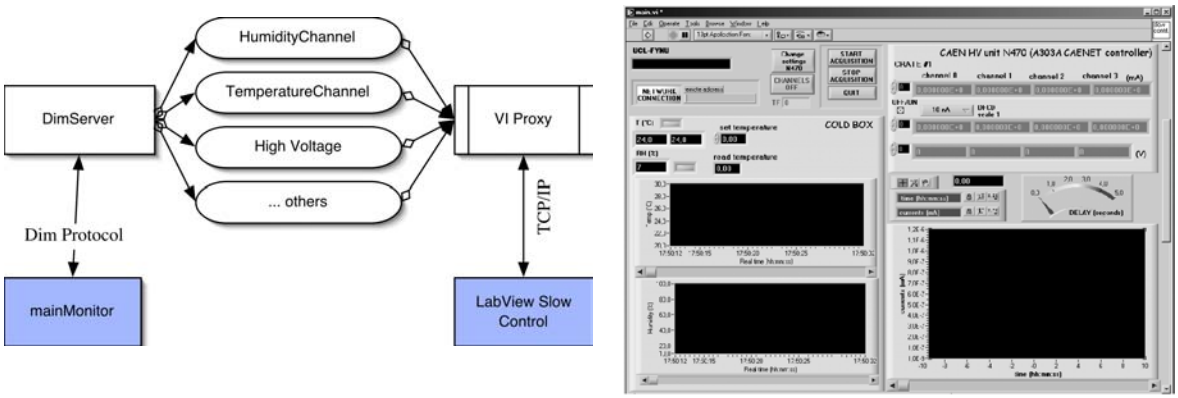

Figure 2 : Integration of the slow control. (Left) Logical description of the link implemented between the main DAQ software (mainMonitor) and the LabView slow control. (Right) Screenshot of the labview interface to the slow control.

Only preliminary results have been obtained up to now (Figure 3). A module has been tested at room temperature with a depletion voltage of 100 V. Pedestal measurements, noise, common mode, and other tests performed seems to agree with results obtained by the module assembly center[4]. A more detailled analysis is being carried on.

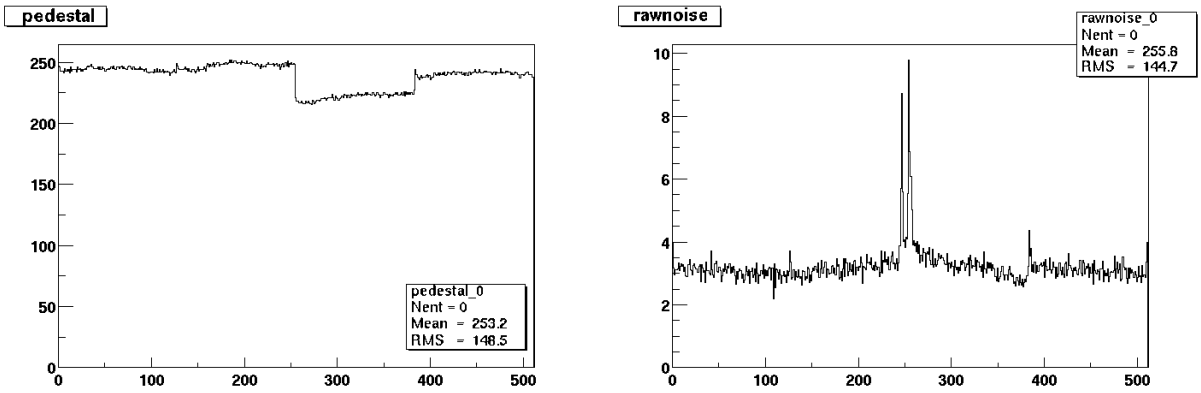

Figure 3 : Pedestal (Left) and raw noise (Right) four our first module, tested with a depletion voltage of 100 V at room temperature. Two noisy channels are present in the center. That region is geographically close to the edges of the sensor.

[1] http://sine.ni.com/apps/we/nioc.vp?cid=1381&lang=US.

[2] http://hep.uia.ac.be/cms/testing.

[3] C. Gaspar, M. Donszelmann, DIM – A Distributed Information Management System for the DELPHI Experiment at CERN , Proceedings of the 8th Conference on Real-Time Computer applications in Nuclear, Particle and Plasma Physics, Vancouver, Canada, June 1993.

[4] http://www.physik.rwth-aachen.de/group/IIIphys/CMS/tracker/en/archome.html.

2.2. Activités relatives à l'acquisition des données

Une étude détaillée des protocoles rapides de communication (Gigabit et Fast Ethernet) qui pourraient être utilisés dans le futur système d'acquisition de CMS a été réalisée. Elle a permis de démontrer que l'utilisation de cartes standards doubles Gb/Ethernet permet d'atteindre des performances comparables à la technologie plus onéreuse Myrinet (et propriété d'une seule firme). Ce résultat aura des conséquences sur le choix de la technologie qui sera finalement utilisée pour le switch du système d'acquisition de CMS. Ces développements ont fait l'objet d'un chapitre important dans le Technical Design Report pour la partie "acquisition des données" (DAQ/TDR Chap 6.3.1). Voir aussi Logistique Informatique § V.3.6.

2.3. Activités liées à la sélection et à la reconstruction des événements

Le laboratoire continue de se spécialiser dans les développements d'algorithmes de sélection en ligne qui utilisent le trigger électron-jet et le trigger électron-tau_jet. Les algorithmes de « haut niveau » (HLT) développés ont fait l'objet d'une section dans le rapport technique "TDR" de l'event filter et du DAQ de CMS. Ces résultats sont publiés dans le Technical Design Report pour la partie "acquisition des données" (DAQ/TDR, Chap. 15.5.8) (voir 2.3.1.).

2.3.1. High level trigger activities

V. Lemaître, O. van der Aa (Institut de Physique Nucléaire, Université catholique de Louvain, Louvain-la-Neuve)

The triggering scheme for $gg \rightarrow bbA^0/H^0$, $A^0/H^0 \rightarrow 2\tau \rightarrow$ e+τ-jet has been studied for M_H = 200 GeV/c^2. The trigger accepts events with either a single electron trigger or a combined electron-tau ("eTau") trigger. In what follows, it will therefore be known as the "e+eTau" trigger. The eTau trigger requires the presence of both an electron and a τ-jet, but with lower threshold than used in the single electron or single tau triggers. This allows one to recover low P_T events that would be rejected by the single electron trigger alone. The τ-jet

candidate at Level-1 is defined as the most energetic τ-jet that is not collinear with the electron candidate. This condition avoids misidentification in signal events (the τ purity in signal events increases from 61 % to 99 %) with little influence on the overall efficiency.

2.3.1.1. High Luminosity

Figure 1 shows the Level-1 "e+eTau" trigger rate at a luminotiy of $10^{34}cm^{-2}s^{-1}$, as a function of the electron and τ-jet thresholds used in the eTau trigger. The dots with numbers on the "e+eTau" trigger iso-rate curves indicate the Level-1 selection efficiency for the signal. For a given Level-1 trigger rate, the efficiency increases when the electron threshold is reduced and the τ-jet threshold is raised. This results from the steeply falling PT spectrum of the electron in the signal channel. Figure 2 shows the increase in Level-1 efficiency obtained by using the "e+eTau" trigger, as opposed to just the single electron trigger, as a function of the extra bandwidth which one devotes to the eTau trigger. The curves are each obtained by fixing the threshold for the electron in eTau trigger and varying the threshold on τ-jet.

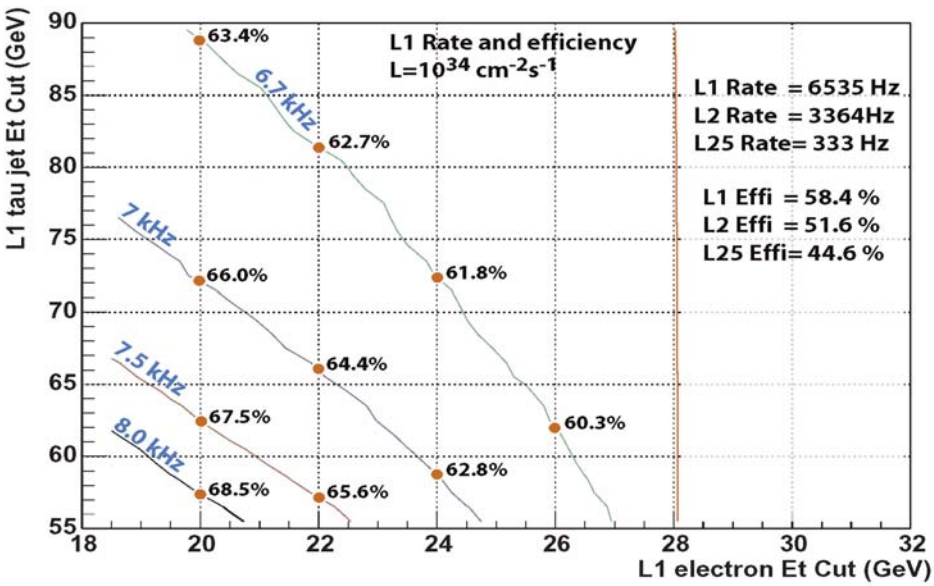

Figure1 : Level-1 "e+eTau" trigger rate at a luminosity of $10^{34}cm^{-2}s^{-1}$ as a function of the *e* and τ-jet thresholds, for a fixed single-*e* trigger threshold. The four curves correspond to additional bandwidths of 0.14 kHz, 0.39 kHz, 0.85 kHz and 1.28 kHz, respectively, being devoted to the eTau trigger, on top of the constant 6.54 kHz devoted to the single-*e* trigger. The vertical line at 28 GeV corresponds to the single-*e* trigger. The values listed in the upper right corner are the rates and efficiencies for the single-*e* trigger at Level-1, Level-2.0 and Level-2.5.

The HLT selection is applied independently on the electron stream and the eTau stream at Level 2.0 and Level-2.5. At Level-2.0, a threshold is applied only on the electron candidate. At Level-2.5, pixel/super-cluster matching is used for the electron candidate [1] and the τ-jet identification is applied as described in [2].

Table 1 shows the details of the full selection for four scenarios. In both cases, the eTau trigger uses an electron threshold corresponding to 25.5 GeV on the Level-1 95 % efficiency scale, while the τ threshold is varied in such a way that the rate added by the eTau trigger to the single-electron trigger rate is 0.14 kHz, 0.39 kHz, 0.85 kHz and 1.28 kHz respectively. Accepting an additional rate of 0.85 kHz atLevel-1 leads to a relative improvement in efficiency, at Level-2.5, of about 10 % at a price of a 7 Hz rate increase. This is illustrated in Figure 3 which shows the PT spectrum of the electron that is recovered at Level-2.5 when the eTau trigger is added to the single electron trigger at Level-1.

2.3.1.2. Low Luminosity ($2x10^{33}$ $cm^{-2}s^{-1}$)

Since the single electron thresholds are lower in the low luminosity scenario, less is gained by adding the combined eTau Trigger. The HLT selection scheme is the same as at high luminosity but the Level-1 thresholds are different. For a scenario where 0.82 kHz for the eTau trigger is added at Level-1, the relative gain in efficiency at Level-2.5 is ~ 4 %.

		e + eTau	trigger		e trigger
L1 eTau thresh (GeV)	**(20, 57)**	**(20, 62)**	**(20, 72)**	**(20, 89)**	**(28)**
L1 Rate (Hz)	7819	7389	6933	6677	6535
L1 Additional Rate (Hz)	1284	854	398	142	
L1 Efficiency	0.685	0.675	0.661	0.634	0.584
L1 Additional Efficiency	0.101	0.091	0.077	0.050	
L2.0 Rate (Hz)	4219	3945	3631	3452	3364
L2.0 Additional Rate (Hz)	855	581	267	88	
L2.0 Efficiency	0.614	0.605	0.590	0.562	0.5165
L2.0 Additional Efficiency	0.098	0.089	0.074	0.046	
L2.5 Rate (Hz)	343	339	338	333	332
L2.5 Additional Rate (Hz)	11	7	6	1	
L2.5 Efficiency	0.492	0.489	0.483	0.469	0.446
L2.5 Additional Efficiency	0.046	0.043	0.037	0.023	

Table 1 : Evolution of the rate and the efficiency of the different trigger levels at highh luminosity. Results for four different tau thresholds in the eTau trigger are shown, as are results obtained with no eTau trigger (only the single electron trigger).

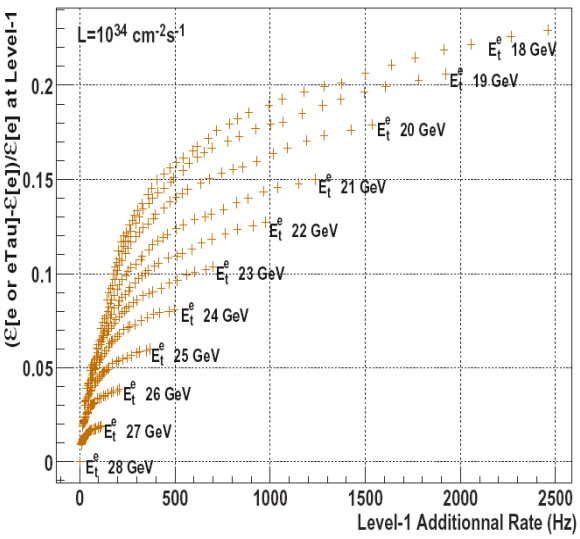

Figure 2 : The increase in Level-1 efficiency, at $10^{34}cm^{-2}s^{-1}$, obtained using the "e+eTau" trigger, as opposed to just the single electron trigger, as a function of the extra band-width devoted to the eTau trigger. Each curve is obtained by fixing the e threshold (E_{Te} in the plot) and varying the threshold for the τ-jet.

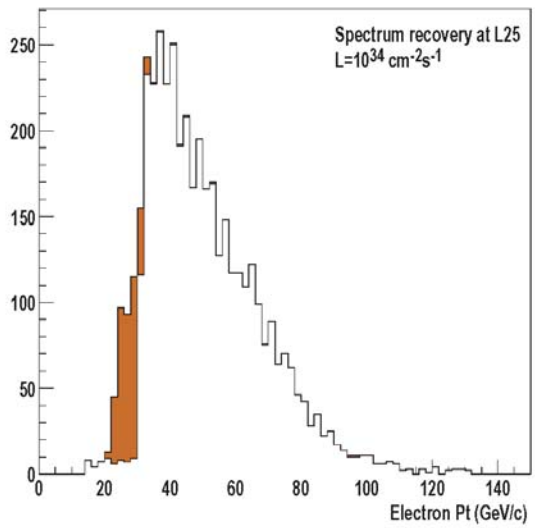

Figure 3 : Electron P_T in $A^0/H^0 \rightarrow 2\tau \rightarrow e+\tau$-jet events, at $10^{34}cm^{-2}s^{-1}$. The filled portion of the histogramme corresponds to the gain observed at Level-2.5 by adding the Level-1 e+τ trigger, the remaining unfilled part corresponds to electrons passing the single electron trigger.

[1] E. Meschi et al., "Electron Reconstruction in the CMS Electromagnetic Calorimeter", CMS Note 2001/034.

[2] D. Kotlinski, A. Nikitenko and R. Kinnunen, "Study of a Level-3 Tau Trigger with the Pixel Detector", CMS Note 2001/017.

Plus récemment, une ferme de PC ainsi qu'une station de stockage capable de faire fonctionner les programmes de reconstruction et de simulation de CMS a été installée. Elle permettra au laboratoire d'être complètement indépendant et d'être activement impliqué au niveau du réseau GRID puisque les logiciels CONDOR et GLOBUS sont également opérationnels (voir 2.3.2.).

2.3.2. Development of a computing/filtering farm

C. Delaere, T. Keutgen, G. Leibenguth, V. Lemaître, A. Ninane, O. van der Aa (Institut de Physique Nucléaire, Université catholique de Louvain, Louvain-la-Neuve)

In the context of the High Level Trigger, studies that are being carried out at the Institute[1]. The first steps to the development of a local computing farm has been achieved. The objectives of these developments are twofold: to be able to generate and process simulated events for High level trigger Studies and, in a further step, to start the tests of a small filter farm.

Deployment of the farm means both hardware and software activities. From the hardware point of view, we have chosen to develop the system in three steps. In a first action, we have brought a mass storage of 1.2 TB that uses raid5 technology for data protection as well as a dual 2Ghz XEON machine that will act as a manager and software repository for the whole system (Figs. 1 and 2). These two components are connected through a non blocking switch that has 24 Fast Ethernet ports and 2 Gigabit Ethernet links. In a second stage (short term) SuSE will be installed on 8 existing Celeron machines to make a small test bench of the CONDOR[1] job submission system. The last step will then consist in buying a set of additional PCs in order to fill the 24 Fast Ethernet ports of the switch.

Figure 1 : Photograph of the CMS production farm (27 November 2002). One sees the workstation (left) and the mass storage (right).

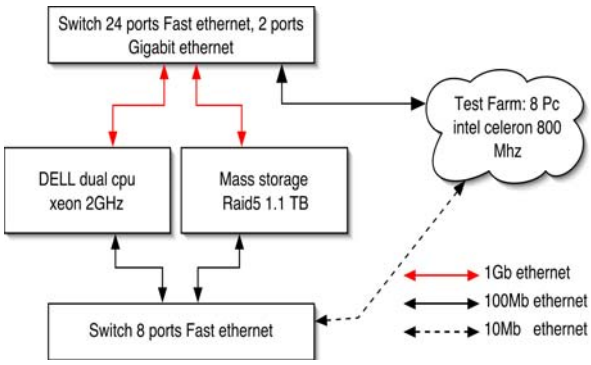

Figure 2 : Architecture of the CMS production environment in Louvain-la-Neuve. The PC farm will be extended in order to match the needs.

This staged scenario has the advantage of keeping us in synchronization with the CMS software certification process for RedHat 7.3 at CERN. This will allow us to install that operating system on the farm. The production setup will then be as similar as possible to the official CERN environment.

The CMS software involves several modules to pursue event generation, simulation, reconstruction and persistent storage[3]. The main modules are shown in Figure 3 and have been installed and tested on the XEON workstation. The test consisted in producing chargino on neutralino events that have been processed through the full simulation and reconstruction chain of CMSKIN, CMSIM, and ORCA. We are currently installing the necessary software on the 8 Celeron machines to make a test bench of the CONDOR job submission system.

The SCRAM[4] utility has been used for the installation and configuration of the CMS software packages. This allows an automated evolution of the software in synchronization with developments and releases at CERN.

Finally, it may be noticed that much care has been taken in the choice of localization of the installation paths in order to facilitate the exportation of the software to the farm machines.

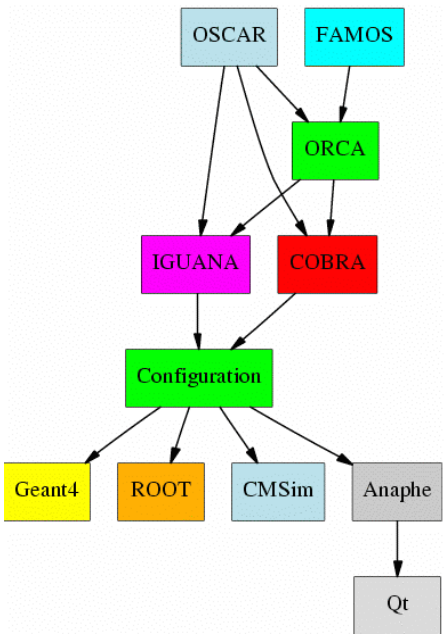

Figure 3 : Dependency graph of the main CMS software components.

[1] Section II.6 of this Annual Report.

[2] Jim Basney and Miron Livny, "Deploying a High Throughput Computing Cluster", High Performance Cluster Computing, Rajkumar Buyya, Editor, Vol. 1, Chapter 5, Prentice Hall PTR, May 1999.

[3] CMS DAQ TDR, to be published.

[4] http://www.ddj.com/articles/2001/0104/0104toc.htm.

2.4. Phénoménologie au LHC

Les chercheurs de l'UCL sont activement impliqués dans la préparation des futures analyses physiques qui pourraient être réalisées au LHC. Les sujets abordés par le groupe de Louvain se situent dans le cadre de l'étude du secteur scalaire de la supersymétrie, du Modèle Standard ou autres modèles exotiques tels que ceux basés sur l'hypothèse de l'existence de dimensions spatiales macroscopiques supplémentaires. Plus précisément, les études portent sur les thèmes suivants.

Les possibilités d'observation d'un Higgs léger dans des canaux de désintégration et production différents de ceux habituellement proposés (gluon + gluon → H → gamma + gamma, et production associée de t-tbar suivie de la désintégration du Higgs en b-bbar).

L'intérêt d'observation d'éventuelles représentations exotiques du secteur de Higgs.

La possibilité d'observer des tours excitées de Kaluza-Klein prédites par les théories possédant des dimensions spatiales macroscopiques supplémentaires (voir 2.4.1.).

La possibilité d'étudier les collisions entre photons (provenant de la radiation des protons incidents) en vue d'observer des processus comme la production de Higgs, de charginos, de paires de W et peut-être aussi de quarks top.

2.4.1. Taux de production d'une paire de bosons Z_0 au LHC dans le modèle A.D.D.

E. Burton (Institut de Physique Nucléaire, Université catholique de Louvain, Louvain-la-Neuve)

Abstract : *Differential cross sections for the production of a pair of Z_0 bosons produced in proton collisions are computed in the context of the « Large extra dimensions » model proposed by Arkani et al. in 1998 (ADD model).*

L'objectif du travail est le calcul de sections efficaces dans le cadre de théories au-delà du Modèle Standard. Les théories considérées ici sont celles à « Larges dimensions supplémentaires » proposées par Arkani-Ahmed, Dimopoulos et Dvali en 1998[1]. Face au problème des hiérarchies d'échelles de masses (disparité entre les échelles fondamentales électrofaible et gravitationnelle), et au vu de l'évidence expérimentale de l'échelle électrofaible, ce nouveau modèle propose un espace temps à 4+δ dimensions dont les δ dimensions supplémentaires sont chacune compactifiées à un cercle dont le rayon, inversement proportionnel à δ, peut atteindre jusqu'à une fraction du millimètre. La gravitation, dont l'échelle fondamentale est ramenée à l'échelle électrofaible, est libre de se propager dans tout l'espace-temps à 4+δ dimensions tandis que les champs du Modèle Standard restent, eux, confinés aux 4 dimensions habituelles. Ils ne ressentent donc que la projection de la gravitation de 4+δ à 4 dimensions. Cela conduit à un propagateur de la gravitation sous forme d'une somme infinie (ou tour) d'états excités de Kaluza-Klein (KK). Puisqu'il n'existe plus qu'une seule échelle d'énergie, m_{ew}~1TeV, les effets de la gravitation doivent être comparables à ceux du Modèle Standard lors d'expériences de même ordre d'énergie et donc a fortiori celles qui seront réalisées au LHC.

Afin de connaître plus précisément les implications expérimentales de telles théories, besoin est de calculer les sections efficaces de processus qui auront lieu dans les accélérateurs. Le travail consiste donc ici à calculer les sections efficaces différentielles de production d'une paire de Z_0 à partir de la collision de deux protons. Ce choix est motivé par la trace quadri-fermionique très claire que peut produire la désintégration d'une paire de Z_0

	Quark-antiquark	Gluon-gluon
Bruit de fond Modèle Standard	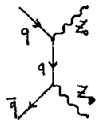	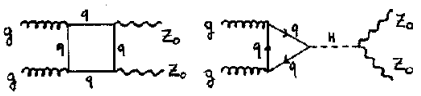
Contribution Modèle ADD		

Tableau 1 : Diagrammes de Feynman partoniques pour pp → Z_0Z_0.

Les processus partoniques considérés sont représentés dans le tableau. Ils constituent la contribution la plus importante compte tenu de la convolution avec les fonctions de structure du proton. Le calcul des amplitudes d'hélicité a été effectué avec FeynCalc dans Mathematica. Celles-ci sont ensuite importées dans un code C++ qui effectue l'intégration sur l'espace de phase de la somme des amplitudes au carré ainsi que la convolution avec les pdf's CTEQ6 (routine traduite en C++). Le programme donne déjà des résultats pour la partie « quark-antiquark ». L'utilisation de LoopTools pour l'évaluation des coefficients de Passarino-Veltman qui apparaissent dans les boucles de quarks donne des instabilités numériques dues à la masse nulle des gluons, d'où la nécessité de produire des amplitudes d'hélicité avec d'autres techniques de factorisation. Rappelons que calcul de l'interférence entre le Modèle Standard et le modèle ADD nécessite l'expression analytique de chacune des amplitudes d'hélicité.

Outre la maîtrise de la contribution des gluons au bruit de fond du Modèle Standard, l'utilisation de librairies numériques et algébriques (CLN, Ginac) devra permettre d'améliorer les temps de calcul pour produire des résultats en fonction des différents paramètres du modèle ADD – nombre de dimensions supplémentaires, échelle d'unification et cut-off imposé sur les tours d'états excités de Kaluza-Klein. Tout cela, afin de déterminer dans quelle mesure l'influence du modèle ADD sur la production de Z_0 est significative ou non, et d'établir ainsi des limites inférieures sur l'échelle de compactification sur base des données expérimentales qui seront récoltées dans l'avenir au LHC.

[1] N. Arkani-Hamed, S. Dimopoulos and G. Dvali, Phys. Lett. B429 (1998) 263-272.

3. HARP : production de hadrons dans les collisions proton-noyau vers 15 GeV/c

J.S. Graulich, Gh. Grégoire (Institut de Physique Nucléaire, Université catholique de Louvain, Louvain-la-Neuve) et collaboration HARP

L'expérience HARP au CERN a poursuivi l'acquisition des données d'avril 2002 jusqu'a la mi-octobre 2002. L'ensemble du programme scientifique prévu par la proposition d'expérience a été accompli. La calibration absolue de la réponse du grand détecteur Cerenkov construit par l'équipe de Louvain a été effectuée à l'aide d'électrons de basse énergie.

L'analyse des résultats recueillis est entamée.

4. MICE : Muon Ionization Cooling Experiment

Gh. Grégoire (Institut de Physique Nucléaire, Université catholique de Louvain, Louvain-la-Neuve) et collaboration MICE

La conception d'une futur accélérateur de muons exige au préalable de résoudre deux problèmes physiques: d'une part il faut une connaissance approfondie des sections efficaces de production de hadrons et d'autre part il faut pouvoir obtenir des faisceaux de muons de très faible émittance avant l'injection dans l'accélérateur. Si l'expérience HARP a pour but de déterminer la production de hadrons, la collaboration MICE tente de répondre au deuxième problème.

Comme les faisceaux de muons sont toujours contaminés par des électrons, il importe de pouvoir discerner ces deux types de particules. Les Universités de Louvain et de Mississipi ont chacune étudié séparément en 2002 une conception particulière d'identificateur électron-muon. Les deux propositions ont été soumises à la collaboration MICE dans son ensemble qui a finalement retenu la solution présentée par Louvain.

L'identificateur sera constitué d'un grand détecteur Cerenkov basé sur un radiateur en aérogel. L'optique de collection de la lumière Cerenkov a été optimisée pour atteindre une efficacité de l'ordre de 80%.

La conception détaillée du dispositif sera entamée en 2003 de façon à disposer de l'ensemble en fin 2004 pour les premiers essais en faisceau au Rutherford Appleton Laboratory (UK).

5. ALEPH

G. de Hemptinne (FRIA), C. Delaere (FNRS), V. Lemaître (FNRS-UCL), O. van der Aa (FRIA) (Institut de Physique Nucléaire, Université catholique de Louvain, Louvain-la-Neuve)

Différentes études ont été réalisées dans le cadre de l'analyse des données de la collaboration ALEPH. L'analyse de la production de bosons W se poursuit. Certains résultats sont encore préliminaires. Les efforts ont principalement porté sur les tests d'un nouveau générateur d'événements qui devrait nous permettre de finaliser l'analyse.

Notre groupe est également impliqué dans l'analyse de la recherche de bosons de Higgs produits dans les collisions e^+e^- et se désintégrant en une paire de bosons W. Le rapport d'embranchement de ce canal de désintégration pour un Higgs de 115 GeV est approximativement de 10% (dépendant fortement de la masse du Higgs). Au vu du récent excès observé à cette masse dans le cas où le Higgs se désintègre en une paire de quarks b, l'objectif est ici de vérifier si un tel excès est également observé dans ce canal de désintégration. L'analyse est en cours.

L'étude de la production d'un Higgs se désintégrant de façon invisible (par exemple en deux neutralinos dans le cas des théories supersymétriques) a été finalisée et une sensibilité (limite attendue) comparable à l'analyse officielle de la collaboration a pu être obtenue. Ce résultat a fait l'objet d'une note interne de la collaboration ALEPH (CERN-ALEPH-2002-034) (voir 5.1.).

Suite à un excès d'événements observés par la collaboration L3 dans la recherche de Higgs chargés, nous avons réalisé une analyse très proche de celle de la collaboration L3 mais avec les données d'ALEPH. Cette recherche n'a pas permis de confirmer l'excès observé et une limite inférieure sur la masse des Higgs chargés de 75.1 GeV a pu être obtenue.

Signalons que les recherches précédemment présentées ont également donné lieu à divers développements techniques au niveau du logiciel d'analyse ALEPH et de ROOT. Ils ont fait l'objet d'une note interne de la collaboration (CERN-ALEPH-2002-033) (voir 5.2.).

5.1. Invisible Higgs decay analysis

C. Delaere, V. Lemaître (Inst. Physique Nucleaire, Universite catholique de Louvain, Louvain-la-Neuve, Belgium)

Abstract : *The possibility to observe a non-minimal CP-even Higgs boson h produced in the reaction* $e^+e^- \rightarrow$ hZ *with the ALEPH detector has been studied. The decay channels considered involve invisible final states for the Higgs and both hadronic and leptonic final states for the Z. An expected limit of 111.74 GeV/c², with 100 % branching ratio. Using data collected from 1998 to 2000, a limit of 111.36 GeV/c² is obtained.*

The reaction $e^+e^- \rightarrow$ hZ leads to topologies involving acoplanar lepton pairs or pairs of jets, depending on whether the Z decays in leptonic or hadronic final states. A selection routine has been implemented using the ALPHA++ package. The topology of interest consists of a pair of jets or leptons with mass close to the Z mass and large missing energy. Monte Carlo samples describing the background from the standard model processes WW, Wen, ZZ and qq and the signal have been used to calculate the relevant efficiencies.

Previous studies of this process at lower energies[1] excluded at 95% CL a mass m_h less than 80 GeV/c², for a value of $\xi^2 = 1$. The main goal of this study is to improve the parameters used by those previous analyses for a LEP energy of 207 GeV, and then to test the Higgs hypothesis.

The analysis method consists in the selection of the signal using a set of ~ 20 cuts followed by a further separation of the background using an artificial neural network. The cuts are optimised in order to minimise the expected confidence level $<CL_s>$ by an iterative process on all the variables. The typical efficiency is 50 %. The neural network is then trained for each mass hypothesis. The resulting distributions are used in the form of a bidimensional plot involving the neural network output and the missing mass to compute the Likelihood ratio.

First, the analysis has been optimised for data obtained at a centre of mass energy of 189 GeV. It has been shown that we were able to reproduce previously published results, with a sensitivity sometimes better that the official results. In addition, the analysis has been shown to be stable with respect to the Higgs mass, and to the estimation of the systematics, as long as no excess is present. This is related to the use of the Likelihood ratio method.

Energy	Luminosity	Hadronic	Leptonic
189 GeV	174.2 pb^{-1}	✓	
192 – 202 GeV	237.0 pb^{-1}	✓	
204 – 209 GeV	216.8 pb^{-1}	✓	✓

Table 1 : Energy and channels used to compute the presented results.

After combination of various optimised analysis for the different energies and for hadronic/leptonic topologies shown in Table 1, it is shown on Figure 1 that the limit on the invisible Higgs boson mass is 111.8 GeV/c^2, with 100 % branching ratio, using data collected in 1999 and 2000,. The expected limit was 112.64 GeV/c^2.

The results are presented in the form of an excluded region in the plane ξ^2/higgs mass. The parameter ξ^2 is the branching ratio of the invisible mode, considering the standard model cross section. The dotted curve correspond to the expected limit obtained considering the background only hypothesis. The other curve correspond to the actual limit obtained considering the data.

Another way to present those results is to look at the evolution of –2lnQ, where Q is the statistic used in order to distinguish signal and background. As shown on Figure , the behaviour of that quantity favours the standard model.

This work resulted in an internal ALEPH note[2].

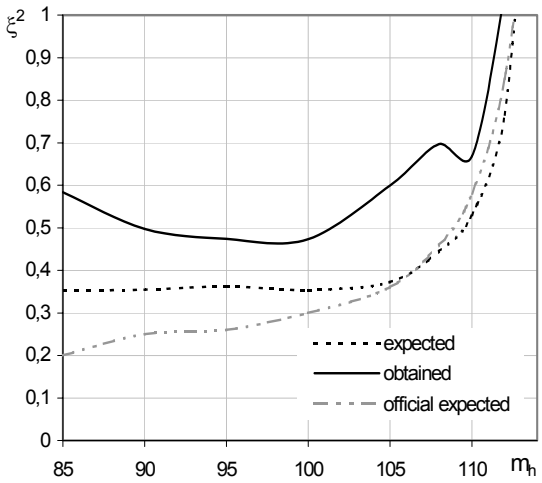

Figure 1 : Excluded region in the plane (ξ^2,m_h). ξ^2 is a factor representing the branching ratio of the invisible mode assuming the standard model cross section, and m_h is the Higgs boson mass. The third curve is from publication[3].

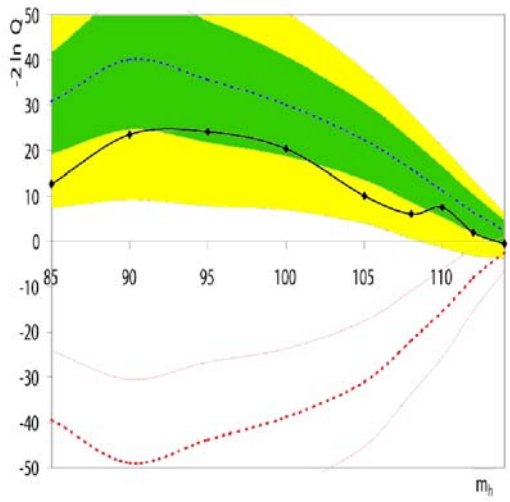

Figure 2 : –2lnQ as a function of the Higgs boson mass. Q is the statistics used in order to distinguish signal and background. Red and blue lines represent respectively the expected value with and without signal. The black line is the observed behaviour. Bands at 1 and 2 sigmas are also shown.

5.2. Further development of a new analysis framework in ALEPH (ALPHA++)

C. Delaere, V. Lemaître (Institut de Physique Nucléaire, Universite catholique de Louvain, Louvain-la-Neuve, Belgium)

Abstract : The project ALPHA++ of the ALEPH collaboration is presented. The Objectivity package has been removed and replaced by ROOT. Some timing issues are shown.

The ALEPH Physics Analysis package ALPHA is intended to simplify FORTRAN programs for physics analysis. ALPHA also provides easy access to physical variables (e.g., momentum, energy), thus the user can write physics analysis programs without detailed knowledge of the ALEPH data structure (tabular BOS banks). An extensive set of utility routines (e.g., kinematics, event shape, secondary vertex finding, b-tagging, etc.) is available as part of the ALPHA package. Motivations for the ALPHA++ object-oriented framework were presented in the 2000 annual report.

We are responsible of the ALPHA++ development. In this context, some administration and outreach developments have been performed. The procedure for standard users has been slightly simplified by the

introduction of a “Workspace”. That development area has to be downloaded and provides, in addition to examples and default makefiles, precompiled libraries, improving greatly the compilation time.

In order to conform to the new CERN licences, the deprecated Objectivity package has been removed from the distribution, and replaced by a ROOT database. That new system allows us to convert data into a new ROOT file, and to access this later in the same way as for original data. In that context, some timing studies have been carried out and show promising results.

	EPIO		ROOT	
	Total time	Time per event	Total time	Time per event
Copy of 11659 events	-	-	606.81 sec	52 msec
Reading of 22 “class 16” (hadronic) events.	1.57 sec	71.36 msec	1.25 sec	56.81 msec
Reading of 256 events	2.56 sec	10 msec	4.16 sec	16 msec

Table 1 : Results of time studies comparing EPIO and ROOT data access.

On the other hand, the resulting ROOT database is far too big and more work is needed to select information to put into in order to have a similar size at the end. As an example, 21.1 MB of EPIO data from 1999 have been converted into a 355 MB ROOT file. This represent 11659 events.

[1] ALEPH Collaboration, "Search for Invisible decays of the Higgs boson in e+e- collisions", ALEPH 98-054.

[2] An alternative invisible Higgs search performed with ALPHA++ / Delaere, C ; Lemaître, V ; CERN-ALEPH-2002-035 ; CERN-ALEPH-SOFTWRE-2002-003. - Geneva : CERN , 16 Sep 2002. - 32 p.

[3] Final results of the searches for neutral Higgs bosons in e^+e^- collisions at $\sqrt{s}$ up to 209 GeV, Heister, A. et al. - ALEPH Collaboration, Phys. Lett. B526 (2002).

6. Interactions photon-photon au LHC

J. de Favereau (FRIA), O. Militaru, K. Piotrzkowski, X. Rouby (Institut de Physique Nucléaire, Université catholique de Louvain, Louvain-la-Neuve)

Nous étudions les collisions entre photons (provenant de la radiation des protons incidents) en vue d’observer des processus comme la production de boson Higgs, de charginos, de paires de boson W et peut-être aussi de quarks top. Ce groupe étudie également la mise en évidence pratique de ces interactions de photons de haute énergie auprès de l'accélérateur LHC à l'aide des "pots romains" de TOTEM. Ces recherches se font sous l'égide du groupe conjoint CMS-TOTEM établi en janvier 2002. Un rapport écrit est attendu pour la fin 2003 et devrait indiquer les avantages physiques d'une opération combinée. Krzysztof Piotrzkowski a participé activement aux trois réunions du groupe organisées par le CERN et Jérôme de Favereau a exposé récemment les premiers résultats préliminaires sur base d'événements générés par le Monte Carlo PYTHIA. Nous avons initié une collaboration avec les théoriciens S. Jadach et F. Krauss pour la génération d'événements spécifiques non disponibles avec les générateurs actuels. Il est aussi envisagé d'étudier les collisions photon-proton. Ces interactions explorent des domaines énergétique et de luminosité encore plus larges. L'identification efficiente de tels événements convertirait le LHC en une sorte d'accélérateur "super-HERA". Nous espérons ouvrir ainsi une nouvelle direction de physique en complément au programme nominal de recherche de CMS.

La possibilité d'étudier les interactions $\gamma\gamma$ lors de collisions d'ions lourds au LHC a été envisagée dans le cadre des collisions ultrapériphériques. En mars 2002, le CERN a organisé une réunion à ce sujet qui a mis en évidence un grand intérêt pour ce domaine: elle a pris la décision de préparer un rapport "jaune" à ce sujet en 2003. K. Piotrzkowski est le rapporteur du chapitre sur les interactions $\gamma\gamma$.

7. RD39 collaboration

O. Militaru, K. Piotrzkowski, X. Rouby (Institut de Physique Nucléaire, Université catholique de Louvain, Louvain-la-Neuve)

Enfin nous considérons le développement de détecteurs au silicium refroidis développés par la collaboration RD-39 comme intéressant pour les "pots romains" à utiliser lorsque le LHC fonctionnera à grande luminosité. Il est prouvé que ces détecteurs sont très résistants aux radiations et qu'ils peuvent être efficaces jusqu'aux bords physiques extrêmes du senseur (détecteurs "sans bords"): c'est une caractéristique essentielle pour la détection de protons aux très petits angles. Nous avons donc décidé d'apporter notre contribution à cette collaboration RD-39 et de participer aux essais de prototypes en faisceau en 2003. Nous envisageons de participer aux irradiations de détecteurs et à l'évaluation de leur résistance aux dégâts radiatifs. L'électronique de lecture sera celle utilisée par le traceur CMS et nous pouvons bénéficier de l'expérience de O. Militaru et X. Rouby.

8. Precision measurement of singlet μp capture in Hydrogen - PSI Experiment R-97-05

V.A. Andreev, D.V. Balin, A.A. Fetisov, V.A. Ganzha, V.I. Jatsoura, A.G. Krivshich, E.M. Maev, O.E. Maev, G.E. Petrov, S.M. Sadetsky, G.N. Schapkin, G.G. Semenchuk, M. Soroka, A.A. Vorobyov, N.I. Voropaev (Gatchina); T. Banks, T.A. Case, K.M. Crowe, S.J. Freedman, B. Gartner, B. Lauss (Berkeley); L. Bonnet, J. Deutsch, J. Govaerts, D. Michotte, R. Prieels (Institut de Physique Nucléaire, Université catholique de Louvain, Louvain-la-Neuve, Belgium); R.M. Carey (Boston); D. Chitwood, S.M. Clayton, P.T. Debevec, D.W. Hertzog, P. Kammel (Urbana); P.U. Dick, A. Dijksman, J. Egger, D. Fahrni, A. Hofer, V.E. Markushin, L. Meier, C. Petitjean, R. Schmidt (PSI, Villigen, Suisse); F.J. Hartmann (Munich); T. Gorringe, P. Zolnierczuk (Lexington)

Résumé : *Description des différents composants intervenant dans le dispositif de mesure du taux de capture de muon par le proton dans l'état 1s [1]. Le détecteur consiste en une chambre à projection temporelle (TPC) contenant un gaz ultra pur d'hydrogène à 10 bars dans lequel s'arrêtent les muons. La chambre TPC permet de tracer le point d'arrêt des muons et deux chambres cylindriques extérieures complémentées par une ceinture de scintillateurs permettent la reconstruction du trajet de l'électron issu de la désintégration du muon.*

In 2002 main parts of the final μCap detector were constructed according to the technical proposal[2,3].The detector consists of an inner part - muon wire chambers (μPC1,2) and a time projection chamber (TPC) operating in ultra pure hydrogen gas at 10 bar as the muon tracking and active stop target - and of an outer part - two cylindrical SINDRUM chambers (ePC1,2) and a two layer scintillator hodoscope (eSC) acting as the tracking electron detector.

8.1. Subsystem details

8.1.1. Hydrogen muon chamber (μPC2)

The hydrogen muon chamber μPC2 is located inside the pressure vessel immediately in front of the TPC. It is a completely new design, since extremely stringent experimental conditions have to be met. Namely, the vessel and its chambers must be operated in 10 bar hydrogen, which has to be ultra clean to a level 0.01 ppm and deuterium-depleted to a level <1 ppm, thus avoiding muon transfers to any other isotopes or impurity elements. To meet these conditions, only UHV-proof materials, bake-able to 130 C, were chosen, e.g. special glass frames with metallic coatings onto which the wires are soldered. The principal function of the μPC2 is the detection of each incoming muon to define the entrance coordinate in the TPC. The anode signals and the induced ones from

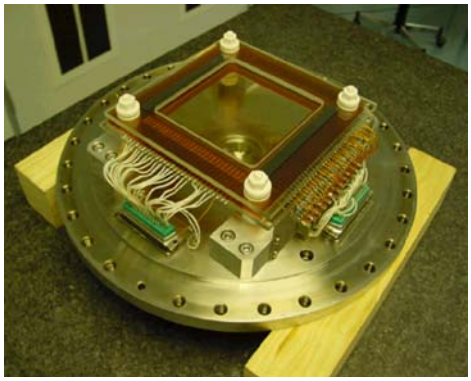

Figure 1 : μPC2 mounted on the entrance flange of the pressure vessel.

perpendicular cathode strips are read out giving the two-dimensional coordinates of the particles in a sensitive area of 88x110 mm^2 (anode wires: pitch 4 mm, $\phi = 25\ \mu$, cathode strips: four 1 mm spaced wires, $\phi = 50\mu$, anode to cathode half gap 3.5 mm).

In May 2002, μPC2 was tested successfully in the μE4 beam. A detailed description and performance report can be found in Ref.[3]. We have demonstrated that μPC2 can detect heavily ionizing slow muons as well as minimum ionizing electrons, depending on the cathode voltage setting (-6.0 kV to -6.5 kV [4]).

8.1.2. Time projection chamber (TPC)

Figure 2 shows the TPC in October 2002 during first assembly in the hydrogen pressure vessel. On the top side, there is a drift volume of height 120 mm, area 300x150 mm^2. The drift voltage of ~30 kV produces a homogeneous electrical field of 2 kV/cm. In 10 bar hydrogen this leads to drift velocities of ~5 mm/μs (total drift times 0 - 24 μs). On the bottom part, the electron charges arrive at a MWPC which is built exactly like μPC2, except for the larger sensitive area (75 anode wires versus 36 cathode strips). All signals are wired via 50 pin feedthroughs to preamplifiers outside the vessel and from there to amplifiers and special customs built TDC boards in 9U VME crates which provide dead-time free data recording at 5 MHz sampling rate.

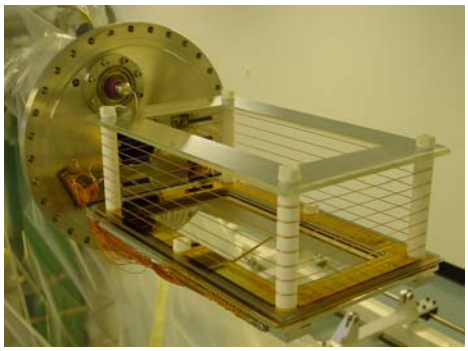

Figure 2 : TPC during assembly.

Figure 3 shows the first setup of the whole μPC2/TPC system for tests in the muon beam, just before installation of the electron detector. Unfortunately the tune-up of the TPC suffered from some delays caused by dust-like impurities, which had to be carefully removed. We expect to get the TPC operational early in 2003 and plan to perform a new test and commissioning run in May 2003 when the PSI accelerators have resumed beam production.

The chambers operating in the ultra-clean hydrogen environment are critical parts of the experiment, as any repair involves significant pumping and conditioning times. The PNPI group has constructed a back-up set of the μPC2 and TPC MWPCs with identical geometry, but different glass-metal technology compared to the PSI development. The collaboration plans to build a complete second target vessel, so that two operating and exchangeable hydrogen chamber systems will become available in 2003.

8.2. Electron detector

The electron detector is an independent detector block that should be moveable relative to the beam quadrupole (to allow easy access to its upstream detectors) as well as relative to the TPC. This latter motion has to be performed within high accuracy due to the small radial distance between the detector elements. Figure 3 displays the engineering model of the overall detector assembly and the electron detector set-up as currently installed in the μE4 area.

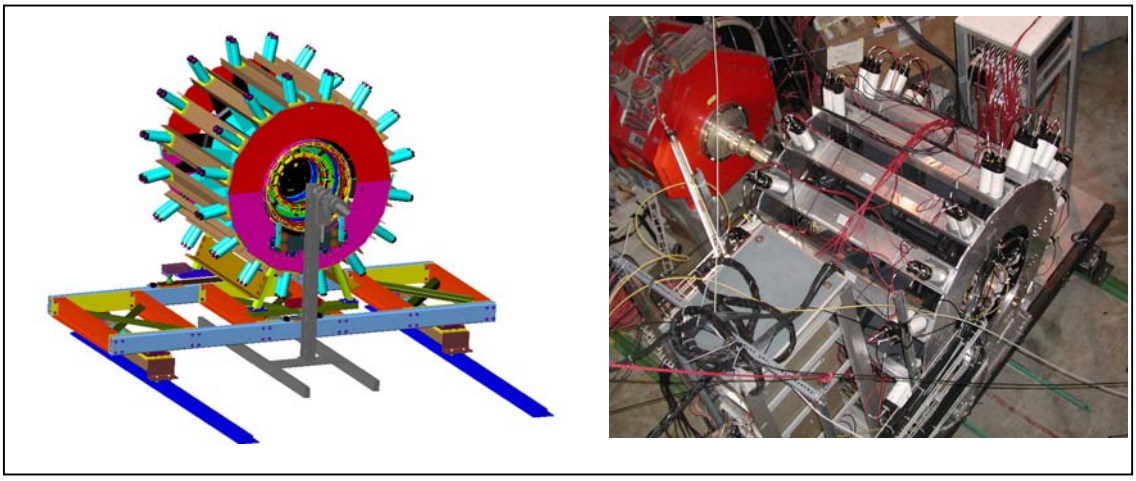

Figure 4.

8.2.1. Electron wire chambers (ePC1/2)

The wire chamber ePC1 was instrumented with new state-of-the-art front-end electronics, optimized for low noise and dead-time free readout. The complete electronics for ~ 2560 channels including also ePC2 (to be built in 2003) has been manufactured. The new preamplifier/discriminator cards are mounted directly on the chamber end-rings. Digital signals using the LVDS standard are processed by custom built data compressors located in the experimental area on the detector frame. Together with careful shielding and grounding this greatly suppresses rf pickup dangerous for this precision lifetime measurement.

The discriminator outputs of the ePC front-end are continuously scanned by 20 compressor modules each handling 128 wires in two FPGAs. These modules collect only the hit wires in order to reduce the data flow. A controller module continuously empties the content of all FIFOs and sends the data to a VME SIS3600 multi-event FIFO input register. Each compressor also provides DAC controlled DC levels to set the front-end discriminator thresholds and exponential test pulses of variable height and polarity for the preamplifiers.

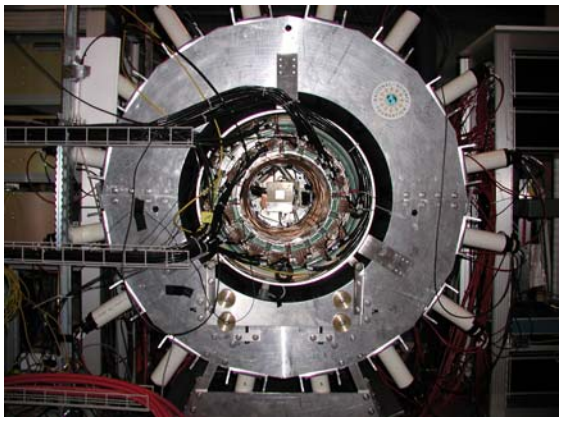

Figure 5 : Downstream side of ePC1 and hodoscope. Shielded LVDS cables connect front-end to data compressors.

8.2.2. Electron scintillation hodoscope (eSC)

The scintillator hodoscope defines the time of the electron decay. It is a barrel of 16 double layered coincidence bars of 5 mm thick scintillators (cf. fig. 4). The detector design had to be carefully optimized to fit the tight μCap geometrical constraints, e.g. different light-guides were constructed for the inner and outer layers. Each scintillator bar is read out by two photomultipliers placed on opposite sides, so that the z position of the electron trajectory can be derived from the light propagation in addition to the ϕ position given by the cylindrical segmentation. The electron hits are highly over-constrained as they correspond to a coincidence of 2 detectors and 4 photomultipliers, which suppresses potential systematic effects due to after-pulsing of the phototubes. The scintillator signals are read out in two complementary ways: a) with discriminators and multihit TDCs, b) with fast wave form digitizers, which are developed for the μLan experiment. Method a) is simple and the detector is already fully instrumented with these TDCs, method b) was applied to 48 multipliers and allows for detailed pulse shape analyses leading to better time resolution, pulse pair rejection and evaluation of systematic effects.

8.3. Data acquisition system

Most of this year's DAQ work was directed towards establishing a fundamental infrastructure. All essential components to operate the four VME crate system with high speed data transfer via the PVIC bus are now in place including hardware control logic, data modules, data transfer connections and control software. During the commissioning run the DAQ system was successfully used to write more than 1 TByte of data to the PSI archive. In 2003, we will begin refining and streamlining the DAQ operation. It is our intention to have a robust and nearly dead-time free DAQ ready in time for the anticipated Fall 2003 run.

8.4. μSR magnet

The remnant polarization for positive muons introduces a position dependent intensity variation of the decay positrons as they are preferentially emitted parallel to the muon spin which precesses in a magnetic field. The weakness of the earth's magnetic field together with unavoidable differences in the local efficiency of the detector would give a very hard to handle contribution in the decay time spectra. Our experiment uses a constant magnetic field in the target region to precess the muons under controlled conditions, with ~ 70 Gauss field resulting in a precession time about half the muon lifetime. Two water-cooled saddle coils in cosθ configuration were extensively tested during the run in fall 2002. They provided an 80 Gauss field with homogeneity of better than 10 % at 200 A current. A pumping system cools the coils to a working temperature of 25°C. Operation safety is provided by temperature switches which block the current supply if the coils heats up to more than 35°C.

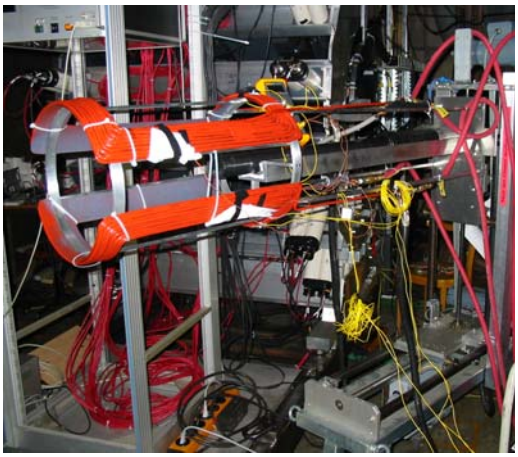

[1] UCL-IISN Rapport d'activité 2001, p. 44.

[2] D.V. Balin et al., High precision measurement of the singlet μp capture rate in H_2 gas, PSI proposal R-97-05 (1996) and documentation on http://www.npl.uiuc.edu/exp/mucapture.

[3] V.A. Andreev et al., Precision Measurement of Singlet Capture in a Hydrogen TPC, Technical Proposal, PSI Proposal R-97-05, February 2001.

[4] J. Egger, D. Fahrni, L. Meier, C. Petitjean, Test of the hydrogen wire chamber PC2 developed for the MUCAP experiment, μCap note 25, see http://www.npl.uiuc.edu/exp/mucapture/documents.

9. A precision measurement of the Michel parameter ξ'' in polarised muon decay

X. Morelle, J. Egger, F. Foroughi, L. Simons (PSI); J. Deutsch, J. Govaerts, P. Knowles, R. Medve, A. Ninane, R. Prieels, P. Van Hove (Institut de Physique Nucléaire, Université catholique de Louvain, Louvain-la-Neuve, Belgium); N. Danneberg, W. Fetscher, M. Hadri, C. Hilbes, K. Kirch, K. Koehler, A. Kozela, J. Lang, M. Markiewicz, O. Naviliat, J. Sromicki (ETHZ)

Résumé : *L'expérience ayant pour objectif la mesure de la polarisation longitudinale des positrons émis par des muons polarisés à l'arrêt a été réalisée en décembre 2000. Deux thèses ont été présentées: l'une portant sur la qualification des performances de l'instrument et la seconde sur une première analyse des données. Ce rapport présente les grandes lignes de la méthode utilisée et donne un résultat provisoire. Des travaux sont en cours pour continuer l'analyse, améliorer la précision et étudier les erreurs systématiques éventuelles.*

Purely leptonic electroweak processes, free of the theoretical difficulties inherent to their hadronic counterparts, are well suited to test the Standard Model (SM) of the electroweak interactions. Muon decay, described by the so-called "Michel parameters" provides the most sensitive of such tests. Most of the Michel

parameters are known to have values close to those predicted by the SM with precisions better than a few percent [1]. One notable exception is the parameter ξ", or the combination (ξ" /ξξ' -1) which vanishes in the SM. Its present published experimental value is (ξ" /ξξ' -1 = -0.35 ± 0.39) [1]. The aim of experiment R-97-06 was to improve the precision of this SM-test by at least one order of magnitude. This combination governs the angular and energy dependence of the positron longitudinal polarization P_l in polarized P_μ decay

$$P_l(x,z) = \xi' + \frac{P_\mu z \xi\xi'(2x-1)}{(3-2x) + P_\mu z \xi(2x-1)} \left(\frac{\xi''}{\xi\xi'} - 1\right), \qquad (1)$$

where $0 \le x \le 1$ is the normalized energy and $z = \cos\theta$, θ being the angle between the muon spin and the positron momentum. The parameters ξ, ξ', ξ" are all equal to 1 in the SM. As can be seen in the previous formula, values of x close to 1 and z close to -1, strongly enhance the impact of a non-vanishing (ξ"/ξξ'-1) on P_l for highly polarized muons.

Moreover, the decay asymmetry of positrons is given by:

$$A(x,z) = \frac{P_\mu z \xi(2x-1)}{(3-2x)} ,$$

which allows to write the longitudinal polarization in term of the observed positron asymmetry A,

$$P_l(x,z) = \xi' \left(1 + \frac{A}{1+A}\left(\frac{\xi''}{\xi\xi'} - 1\right)\right). \qquad (2)$$

The polarization of near end-point positrons ($x \approx 1$) was compared for practically fully polarized and unpolarized muons, stopped in Al and S targets respectively. After selection by an collimator assembly placed in a magnetic field, the momentum of the positrons was determined by three double faced Si detectors located in a homogeneous magnetic field [2]. Their polarization was measured by annihilation-in-flight (ANI) and Bhabha-scattering (BB) on polarized electrons in a layer of oppositely magnetized vacoflux foils. The corresponding events were identified [3] by multiwire proportional chambers interleaved with the foils, a segmented hodoscope and a BGO calorimeter.

Since no satisfactory stable normalization method could be found, we chose to compare the rates of ANI resp. BB events from adjacent vacoflux foils of opposite polarizations.

For eight different conditions j (two tilted positions of the polarimeter, two targets, two event types), the yield ratio of events originating from both foils and their asymmetry r_{j+} and r_{j-} was evaluated for two opposite induction currents '+' and '-'. This yields the experimental longitudinal polarization P_l as shown in the following expressions. Defining $y_{jk\pm}$ as the yield of a given type of events originating from foil k observed in condition j with magnetization ±,

we get :

$$y_{j1+} \sim N_1\, \omega_{j1}\, (1 + P_l.A_{Pj1}),\ y_{j2+} \sim N_2\omega_{j2}\, (1 - P_l.A_{Pj2}),$$

$$y_{j1-} \sim N_1\, \omega_{j1}\, (1 - P_l.A_{Pj1}),\ y_{j2-} \sim N_2\omega_{j2}\, (1 + P_l.A_{Pj2}),$$

$$r_{j+} = \frac{y_{j1+}}{y_{j2+}} \cong \frac{N_1\omega_{j1}}{N_2\omega_{j2}}\, (1 + P_l.(A_{Pj1} + AP_{j2})),$$

$$r_{j-} = \frac{y_{j1-}}{y_{j2-}} \cong \frac{N_1\omega_{j1}}{N_2\omega_{j2}}\, (1 - P_l.(A_{Pj1} + A_{Pj2})),$$

$$A_{e+} = \frac{r_{j+} - r_{j-}}{r_{j+} + r_{j-}} \cong P_l\, (A_{Pj1} + A_{Pj2}), \qquad (3)$$

where N_1, N_2 and ω_{j1}, ω_{j2} are the incoming positrons and the acceptance angle of the polarimeter for each foil, P_l is the longitudinal polarization to be extracted, A_{Pj1} and A_{Pj2} are the analysing powers for condition j for events appearing in foil 1 and in foil 2 respectively. The analyzing power of the events differs from foil to foil: it can be determined from the angle and energy data assuming theoretical cross sections for BB and ANI events.

Since this quantity varies with the positron energy, it was decided to construct from (3) energy dependent experimental functions $P_l(x)$, and by a fit to (2) to extract the quantity $f = (\frac{\xi''}{\xi\xi'} - 1)$ common to each j condition. Hence we write:

$$P_l(x) = \frac{A_{e+}(x)}{A_{Pj1}(x) + A_{Pj2}(x)} = C\_j\,(1 + \frac{A(x)}{1+A(x)} f\,), \qquad (4)$$

where A(x) is the experimental positron asymmetry, and the C_j are the constant free parameters of the fit.

In late Fall 2000 a production run was performed during 6 weeks. About 30 % of the running period was useful and yielded data which passed through various rejection criteria. A preliminary analysis yielded a value of $(\frac{\xi''}{\xi\xi'} - 1) = 0.019 \pm 0.034$ in agreement with the SM-prediction. The error, if inflated by external consistency, becomes 0.042, i.e. an order of magnitude smaller than that of the existing result. The contribution of possible systematic errors is under investigation and a paper is in preparation.

[1] H. Burkard, Phys. Lett. 150B (1985) 242.

[2] P. Van Hove, "L'expérience MELPOMENE, une nouvelle approche à la polarimétrie des positrons dans la désintégration des muons", PhD thesis, Louvain-la-Neuve, 2000.

[3] X. Morelle, "A precision measurement of the Michel parameter ξ" in polarized muon decay", PhD thesis, Zürich, 2002.

III. INSTRUMENTATION ET DÉVELOPPEMENTS TECHNIQUES

1. COMET: COMpressor for Electron Tracks : a data compressor for the 2560 wires of the electron MWPCs used in the singlet μ capture in hydrogen TPC : (experiment undertaken at PSI, Switzerland: R-97-05.20)

L. Bonnet, B. de Callataÿ, D. Michotte, Th. Quériat, R. Prieels (Institut de Physique Nucléaire, Université catholique de Louvain, Louvain-la-Neuve)

Résumé : *Description sommaire d'un compresseur de données basé sur l'emploi de puces électroniques programmables. Lectures permanentes de 2560 fils sans temps mort et sélection des groupes de fils actifs. Le principe de détection est explicité.*

The aim of this note is to present the system COMET developed in Louvain-la-Neuve to compress the data produced by the 2560 wires of the electron MWPCs surrounding the muon TPC. The localization of the crossing points of the e^- (e^+) with the chambers may help in the vertex reconstruction of the decaying muon and in the discrimination of the signal over the background. The cathode and anode wires, 2560 in total, are arranged in 2 times 3 planes located in six nested cylinders.

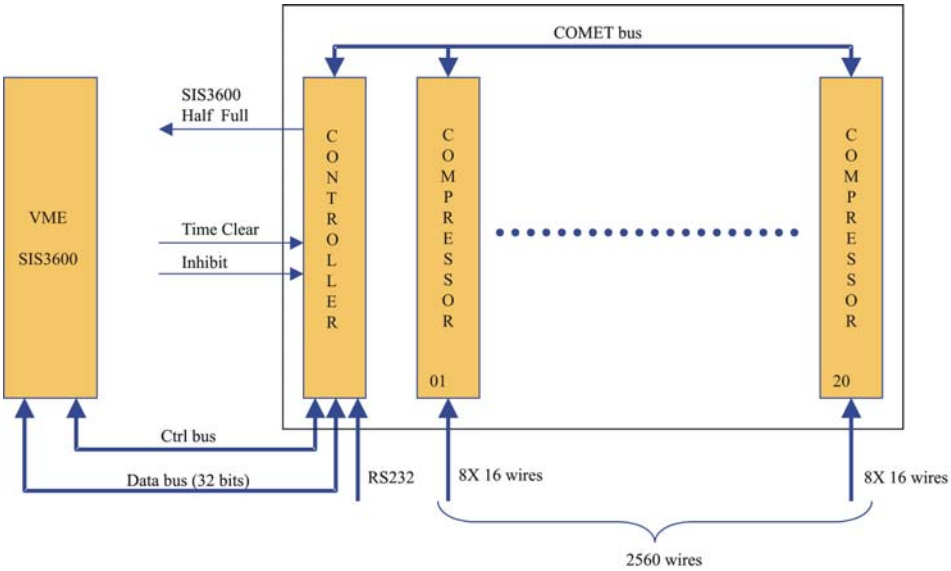

Figure 1 : General concept of the COMET system.

All the wires are be continuously scanned by 20 compressor modules each handling 128 wires. The action of these modules is to collect only the wires hit in order to reduce the data flow in the acquisition process. The 128 wires feeding one compressor are physically grouped in 8 times 16 wires, then logically in 4 times 2, half of them being treated by one FPGA chip. One compressor module consequently contains 2 such FPGAs. We call A and B the two groups of 32 bits analyzed within one FPGA. When at least one wires is hit in the A or B group, the 32 bits belonging to the group(s), is (are) written in the internal FIFO of the FPGA and is preceded by a 32 bits label containing the A or/and B code, the FPGA address and the detection time.

A controller module continuously empties the content of all FIFOs (40 since there are 20*2 FPGAs) and sends the corresponding data to the VME SIS3600 multi-event FIFO input register as shown in Fig. 1. At half-full a signal from the SIS3600 is sent to the compressor controller which inhibits any compressor's action. This half-full signal is dispatched externally to the DAQ which in turn takes over the inhibit signal during the readout of the SIS3600 FIFO. A time clear signal sent to the compressor controller resets the time for all the compressors and a new acquisition cycle may start as soon as the inhibit is relaxed by the DAQ.

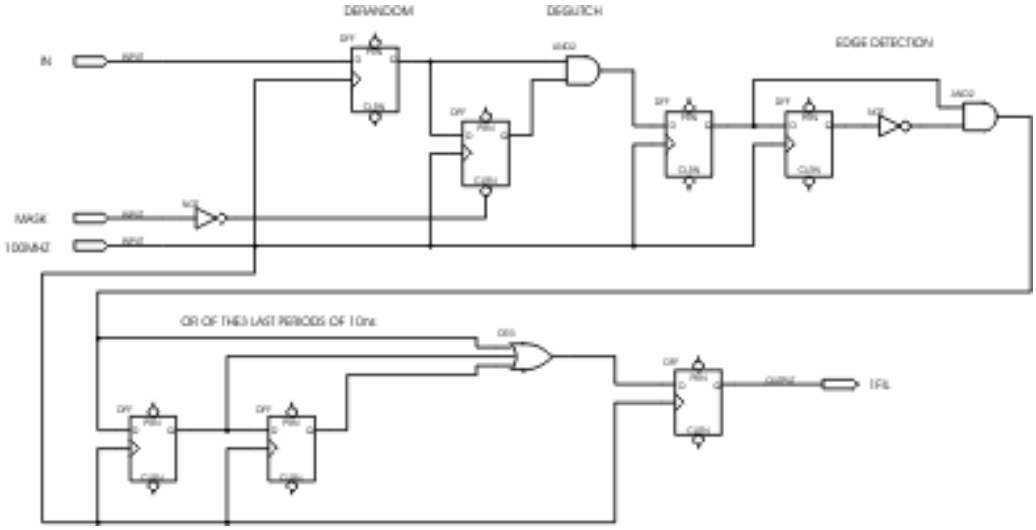

Figure 2 : Detection of a single wire hit.

The heart of the system, displayed in Fig. 2, is the detection of an edge present on the IN signal arising from a single wire hit. Events occur de-synchronized relatively to the 100 MHz clock running the system. Accepting a 10 ns jitter with respect to the real time, the events are forced to synchronize by a de-randomizer DFF. To detect eventual glitches that could induce fake events, we impose a minimum length to the IN signal. This selection is performed by the DEGLITCH part of the circuit where it can be seen that a signal needs to have at least 10 ns duration to start being detected and to last for 20 ns to reach a full 100 % detection efficiency. If the signal extends for longer than 20 ns it will be shaped to 10 ns by the edge detection part of the circuit which feels only the leading edge through the AND of the signal with its complemented version delayed by 10 ns. An extension to a standard signal of 30 ns is then generated by the OR of the three sequential status. The non zero OR of 32 such wires is then required for a data word (A or B) of 32 bits to be written in the FIFO. The 30 ns length of each signal is needed for the 3 steps FIFO storage. The time bits of the event will be stored in synchronization with the first 10 ns period, the A bits in the second one and the B bits in the third one. Except for the dead time due to charge integration in the preamplifier and the associated discriminator shaping time, this system is dead time free. And this statement is strong since the probability to have the same wire hit consecutively by two particle is 2560^2 weaker than for the system taken as a whole.

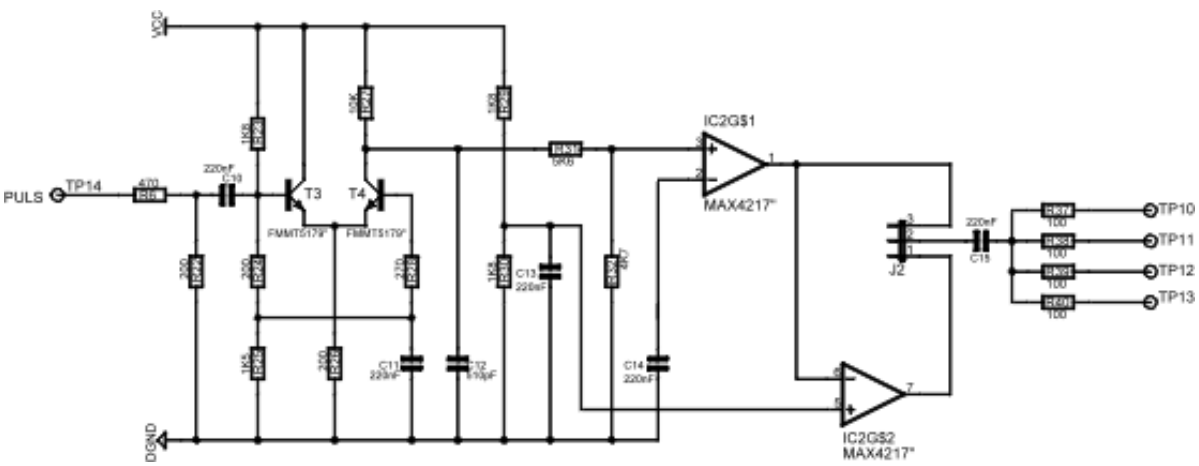

Figure 3 : Positive and negative pulse generator with a fast rising rate and a fixed exponential decay.

Each module contains also a DC level generated from a DAC in order to drive the threshold of the 16 discriminators built in each preamplifier card. Moreover a test pulse of variable height and polarity with a rising slew rate of 10 mV/ns and a slow exponential decay (τ = 5 μs) can also be generated from each compressor module sent towards a test entry in four preamplifier cards. Fig.3 shows the layout of this pulse generator. The height of the generated pulse is controlled through the duration length of the 'PULS' signal. Besides this pulse mode, each FPGA is able to run in a test mode where it generates bit patterns suitable for self test and DAQ acquisition test.

The controller module houses a processor which can receive slow control commands in ASCII format, to set the level of thresholds and pulses, to select the running mode of each FPGA (normal, pulse, test) and to mask single wires.

Such a full system was provided by the end of October 2002 and was functioning during the commissioning run at the end of 2002. The full logics behaved without errors. Unfortunately oscillations occurred between the preamplifiers and the compressor's inputs due to unadapted grounding. Indeed analogue and digital grounds where common since the threshold, DC powers to the preamplifiers and pulse generation were not foreseen at an early stage and are now driven in common with the signals through 40 pin twisted pair flat cables connecting the compressors to the preamplifier cards. Several ground links at various well suited places could remove most of these oscillations and enabled to run with all the wires except for some cathode wires bearing too strong a positive feedback. More work is required to find a more stable solution to this problem.

IV. EXPLOITATION ET DÉVELOPPEMENTS DES CYCLOTRONS

Résumé : Parmi les travaux réalisés en 2002, on notera particulièrement :

- *de longues périodes de faisceaux radioactifs : ^{18}Ne sur cible H, ^{13}N sur cible ^{9}Be et ^{6}He sur cible ^{208}Pb, conduisant respectivement à la première observation du deuxième état excité de ^{19}Na, à la mesure de section efficace de fusion de deux partenaires peu liés (comparée à ^{10}B + ^{12}C), et à l'obtention d'un potentiel optique précis pour ^{6}He ;*

- *la première utilisation du détecteur DEMON en faisceau de protons, qui a nécessité la rénovation de cette voie de faisceau et l'optimisation d'un nouveau transport. La mesure réalisée était la section efficace de fission induite par protons sur ^{238}U et ^{239}Pu ;*

- *les premiers essais concluants de diminution du bruit de fond ^{39}K sortant d'une source ECR. Ce bruit de fond masque le signal de ^{39}Ar qui sera utilisé pour la datation de la circulation océanique ;*

- *l'installation de la sonde de phase et le développement de nouveaux faisceaux sur CYCLONE44 et la première expérience en ^{19}Ne avec prise de données utilisant le séparateur ARES ;*

- *le développement des faisceaux radioactifs : ^{15}O, ^{11}C et ^{10}C ;*

- *les développements sur la source ECR (SCAMPI) donnant de meilleures performances du point de vue de la stabilité pour les ions métalliques et de l'intensité à la fois pour les gaz et pour les métalliques.*

1. INTRODUCTION

In 2002, radioactive ion beams (RIB) have been intensively used during several long runs. We can mention ^{18}Ne on hydrogen, ^{13}N on ^{9}Be and ^{6}He on ^{208}Pb targets leading respectively to the observation, for the first time, of the 2nd excited state of ^{19}Na, to the measurement of the fusion cross section of two weakly bound nuclei (compared to ^{10}B + ^{12}C), and to the obtention of a precise optical potential for ^{6}He. DEMON has been used for the first time with proton beams. The beam line has been modified and the beam transport has been improved to reduce background. Proton induced fission cross section measurements of ^{238}U and ^{239}Pu have been carried out. First successful tests have been carried out on our ECR source to reduce the ^{39}K output. This "background" masks the ^{39}Ar signal in its isotopic ratio measurement, used for tracing and dating measurements of the oceanic currents. CYCLONE44 has been equipped with a new phase probe, new beams have been developed (including in the new 8th harmonic mode) and the first data with the ^{19}Ne ($T_{1/2}$ = 17 s) beam, using ARES, have been taken. New RIB have been developed: ^{15}O, ^{11}C and ^{10}C. Further developments of the ECR source SCAMPI have resulted in improved stability for the metal ion beams and increased intensities for both metallic and gaseous elements.

2. OPERATION

Statistics on the allocation of beam time in 2002 from CYCLONE110, CYCLONE30, CYCLONE44 and the ECR-source « SCAMPI » are given in Tables 1 to 4.

		Hours	%
Physics :		2437	51.5
using light ions	1148		
heavy ions	470		
radioactive ions	819		
Technological applications		1352	28.6
Radiobiology		43	0.9
Accelerator development		147	3.1
Maintenance		680	14.4
Unscheduled shutdown		72	1.5
		4731	100.0

Table 1 : Beam time delivered by CYCLONE110 in 2002.

	Hours
Isotope production for PET	1041
Isotope production for RIB	1012
Beam developments	33
Maintenance	147
	2233

Table 2 : Beam time delivered by CYCLONE30 in 2002.

	Hours
Physics	524
Beam developments	339
Maintenance	82
Unscheduled shutdown	63
	1008

Table 3 : Beam time delivered by CYCLONE44 in 2002.

	Hours
As Injector into CYCLONE110 :	
- Physics	1442
- Technological applications	1133
Stand alone :	
- Test-runs and conditioning after exchange of plasma chambers	466
- Source developments	205
	3246

Table 4 : Operating time distribution of the ECR-source « SCAMPI » in 2002 including source tuning and beam optimisation.

The lists of ions accelerated by CYCLONE110 and by CYCLONE44 during the year 2002 are given in Tables 5 and 6.

Particle	Hours	%
Protons	962	24.2
Deuterons	298	7.5
^{4}Helium^{+1}	41	1.0
^{4}Helium^{+2}	412	10.4
*^{6}Helium^{+1}	122	3.1
*^{6}Helium^{+2}	96	2.4
^{6}Lithium^{+1}	21	0.5
*^{7}Beryllium^{+1}	35	0.9
*^{10}Carbon^{+1}	12	0.3
*^{10}Carbon^{+2}	19	0.5
*^{11}Carbon^{+1}	160	4.0
*^{11}Carbon^{+2}	9	0.2
*^{11}Carbon^{+3}	27	0.7
*^{13}Nitrogen^{+2}	95	2.4
*^{13}Nitrogen^{+3}	116	3.0
^{14}Nitrogen^{+2}	12	0.3
^{16}Oxygen^{+4}	10	0.2
^{18}Oxygen^{+3}	15	0.4
^{18}Oxygen^{+4}	4	0.1
*^{18}Neon^{+3}	170	4.3
*^{18}Neon^{+4}	12	0.3
^{20}Neon^{+4}	16	0.4
^{20}Neon^{+5}	105	2.6
^{36}Argon^{+10}	120	3.0
^{36}Argon^{+11}	17	0.4
^{40}Argon^{+8}	13	0.3
^{40}Argon^{+9}	298	7.5
^{40}Argon^{+11}	65	1.7
^{39}Potassium^{+8}	24	0.6
^{58}Nickel^{+10}	86	2.2
^{132}Xenon^{+26}	11	0.3
**A/Q = 5	568	14.3
	3971	100.0

Table 5 : List of ions accelerated by CYCLONE110 in 2002.

* = radioactive ion
** = "ion cocktail" : $^{10}B^{2+}$, $^{15}N^{3+}$, $^{20}Ne^{4+}$, $^{40}Ar^{+8}$, $^{84}Kr^{+17}$, $^{132}Xe^{+26}$

Particle	Energy (MeV/A)	W_{TOT} (MeV)
^{15}Nitrogen^{+2}	0.42	6.4
	0.43	6.5
	0.55	8.18
^{15}Oxygen^{+2}	0.55	8.18
^{19}Fluor^{+2}	0.28	5.3
^{19}Fluor^{+3}	0.52 0.69	9.8 13.2
*^{19}Neon^{+3}	0.52	9.8
^{20}Neon^{+3}	0.60	12.7

Table 6 : List of ions accelerated by CYCLONE44 in 2002.

The list of physics experiments which received beam time in 2002 is given in Table 7.

		Hours	%
PH-157	The lifetime of the 4.033 MeV state of ^{19}Ne (Univ. Edinburgh – Univ. Notre Dame – UCL)	97	3.98
PH-172	Formation and decay of ^{22}Na fusion reactions induced by stable and weakly bound radioactive beams (INFN Catania - UCL)	236	9.68
PH-174	Deformation in quasi-spherical Po and Pb isotopes approaching the neutron mid-shell (KULeuven - Univ. Bonn)	39	1.60
PH-177	Beta-decay of neutron deficient nuclei below ^{100}Sn (KULeuven – GSI Darmstadt – Univ. Edinburgh)	72	2.95
PH-179	Characterisation of a detector designed to measure the flux of high energy magnetospheric charged particles with high mass, angular and spectral resolution (UCL - IASB Brussels)	32	1.31
PH-181	Production of neutral and charged particles in the alpha induced reactions on Si between 20 and 65 MeV (UCL - LPC Caen)	410	16.82
PH-182	Study of neutron-induced fission of nuclei in the vicinity of ^{208}Pb (PTB Braunschweig - Khoplin Radium Inst. Russia - UCL)	168	6.89
PH-185	Spectroscopy of ^{19}Na via the ^{18}Ne(p,p)^{18}Ne resonant elastic scattering (UCL - ULB - GANIL Caen - KULeuven - Univ. Edinburgh)	185	7.59
PH-186	Study of ^{11}C + p reactions (Univ. Edinburgh – UCL – ULB – LNS Catania)	138	5.66
PH-189	Exploring the dynamics of low energy ^{6}He elastic scattering on heavy targets (IEM Madrid – Univ. Sevilla – Univ. Huelva – UCL – KULeuven – Univ. Birmingham – LNS Catania – Ruhr Univ. Bochum)	245	10.05
PH-192	Study of proton-induced fission of actinide nuclei between 20 and 80 MeV bombarding energies (UCL – Texas A&M Univ.)	298	12.23
PH-193	Study of the lattice location by MNRON on implanted ^{56}Mn in $MnCl_2$ - $4H_2O$ – Determination of the atomic magnetization of giant spin Mn12-ac using implanted ^{56}Mn (KULeuven – Univ. British Columbia – TRIUMF)	114	4.68
PH-194	Tests for the realization of a quasi-uniform energy spectrum of neutron secondary beam induced by protons on a thick ^{nat}Li target (UCL)	55	2.26
PH-195	(n,xn) cross section measurements by in-beam gamma-ray spectroscopy (IreS Strasbourg – Techn. Univ. Wien – Vinca Inst. Belgrade – UCL)	40	1.64

PH-196	Measurement of the $^{6}He \rightarrow \alpha + d + e^{-} + \nu$ branching ratio (KULeuven – CEA Saclay – UCL)	27	1.11
PH-199	Investigation of resonances in ^{7}He using the $^{9}Be(^{6}He,^{8}Be)^{7}He$ reaction (UCL – CEA Saclay – FLNR Dubna – INFN Catania – ULB)	30	1.23
PH-200	A systematic study of the ^{39}K background from ECR sources – a crucial step in developing an AMS detection method for natural ^{39}Ar (Univ. Wien – Columbia Univ. – Argonne Nat. Lab. – UCL – Hebrew Univ. Jerusalem)	35	1.44
DT-	Laser	216	8.86
		---	---
		2437	100.0

Table 7 : Beam time allocation to physics experiments in 2002.

3. RESEARCH AND DEVELOPMENT

3.1. Development of radioactive ion beams: ^{15}O, ^{11}C and ^{10}C

The value of the $^{15}O(\alpha,\gamma)^{19}Ne$ reaction cross section is one of the crucial data for nuclear astrophysics. Given its low expected value, very intense ^{15}O ($T_{1/2}$ = 2 min) beams and novel techniques for its measurement will be needed. During a test of CYCLONE 44, the dedicated post-accelerator cyclotron, both ^{19}Ne and ^{15}O beams were produced, using the LiF target, and post-accelerated. The ^{15}O is produced through the $^{19}F(p,\alpha - n)$ reaction. This test run was also used to confirm the production target's capability to accept very high primary beam currents (> 220 μA). With a sustained primary proton beam current of 270 μA at 30 MeV (8.1 kW of beam power dissipated in this target!), we have obtained 10^{8} pps of $^{15}O^{1+}$ at the exit of CYCLONE44. This result sets a new intensity record for this beam and allows to plan experiments to validate nuclear models used to calculate this cross section.

The development of a post-accelerated ^{11}C (T1/2 = 20.4 min) beam has been resumed to answer the request for an experiment (PH-186). The production target consists of a 3 mm thick boronnitride pellet. The production yield for ^{11}C through the $^{11}B(p,n)^{11}C$ and $^{14}N(p,\alpha)^{11}C$ reactions is several 10^{-3} /incident proton. However, the maximum primary beam current is, unlike for most other targets in use, only 100 μA due to the decomposition of the material at higher temperatures.

We were able to produce with CYCLONE110 an intensity of 10^{7} pps in the 1+ charge state, at the user's target, with a primary beam current of 75 μA. This proved to be the optimal current for production and ionization.

Using the same target we tried also to produce a ^{10}C ($T_{1/2}$ = 19.3 seconds) beam through the $^{10}B(p,n)^{10}C$ reaction. Since carbon is only extracted from the target in CO or CO_2 form, its extraction out of the target depends on chemical reactions. Compared to ^{11}C, a strongly reduced ^{10}C intensity is expected due to its short half-life and to a much lower production rate because of the 20% ^{10}B abundance in natural BN. During this first experiment, we obtained $2 \cdot 10^{5}$ pps of $^{10}C^{1+}$ and 10^{4} pps of $^{10}C^{2+}$ out of CYCLONE110. A proposal for an experiment (PH-198) using this beam has been accepted.

The available Radioactive Ion Beams are given in table 8.

Element	$T_{1/2}$	q	Intensity [pps]*	Energy range [MeV]
^{6}Helium	0.8 s	1+	$9\cdot10^{6}$	5.3-18
		2+	$3\cdot10^{5}$	30-73
^{7}Beryllium	53 days	1+	$2\cdot10^{7}$	5.3-12.9
		2+	$4\cdot10^{6}$	25-62
^{10}Carbon	19.3 s	1+	$2\cdot10^{5}$	5.6-11
		2+	1.10^{4}	24-44
^{11}Carbon	20 min	1+	1.10^{7}	6.2-10
^{13}Nitrogen	10 min	1+	$4\cdot10^{8}$	7.3-8.5
		2+	$3\cdot10^{8}$	11-34
		3+	$1\cdot10^{8}$	45-70
^{15}Oxygen	2 min	2+	$6\cdot10^{7}$	10-29
			1.10^{8}	6-10.5 †
^{18}Fluorine	110 min	2+	$5\cdot10^{6}$	11-24
^{18}Neon	1.7 s	2+	$6\cdot10^{6}$	11-24
		3+	$4\cdot10^{6}$	24-33,45-55
^{19}Neon	17 s	2+	$2\cdot10^{9}$	11-23
		2+	$5\cdot10^{9}$	4 -9.5†
		3+	$1.5\cdot10^{9}$	23-35,45-50
		4+	$8\cdot10^{8}$	60-93
^{35}Argon	1.8 s	3+	$2\cdot10^{6}$	20-28
		5+	$1\cdot10^{5}$	50-79

- *Typical intensity at the experiment location (after acceleration and separation)*

† ***With CYCLONE44***

Table 8 : List of available Radioactive Ion Beams at Louvain-la-Neuve.

3.2. An improved configuration for SCAMPI

The high charge-state ECR ion source SCAMPI has previously been used to produce nickel beams using both the sputtering method and a micro-oven. The micro-oven was introduced instead of the polarisation electrode. While the micro-oven produced higher beam intensities, the extracted beam was very unstable and difficult to control. Careful investigation of this problem showed that the presence of a polarised electrode as an electron source is mandatory for the plasma stability. This problem was found to be related to the injection configuration of the source. In its normal configuration, the source has an on-axis gas injection with a biased electrode in the same location. This biased disk is crucial to achieve high performance with the source. When using the micro-oven, this disk is replaced with the oven. This means that the biased disk cannot be used, implying a lower efficiency for high charge states, but also that the on-axis plasma leak touches the oven. The oven, which is heated resistively, is now also heated by the plasma. This makes it difficult to control the oven temperature. Moreover, since the vapor pressure of nickel is very sensitive to the temperature, minor plasma changes result in very important fluctuations in the amount of nickel injected in the source and hence the extracted beam intensity. To circumvent this problem, the injection side of the source has been redesigned to allow an off-axis oven placement while maintaining the on-axis polarisation electrode.

This would solve the temperature controllability problem of the oven and would at the same time allow simultaneous oven and biased disk operation, enhancing high charge-state performance. To go a step further, the on-axis tube would now only have to support the biased disk so that its diameter could be reduced. This in turn allowed more iron to be placed at the injection side, increasing the magnetic field and thus also enhancing performance.

The results were very satisfactory. The nickel beam was very stable, approaching the stability of beams from gaseous elements. The experiment using this beam ran for several days with an intensity at the source of 8 μA of Ni^{10+} (intensity after collimating with slits).

The increase in performance from the enhanced magnetic field were also notable. The reference beam of Ar^{9+} (see annual report 2001) using a calibrated leak and standard field and microwave power settings was

about 40 eμA in the standard configuration. Using a larger biased disk in this configuration, this intensity was increased to 50 eμA. The new configuration (with small disk) increased this to 70 eμA. This means an efficiency increase for this charge state from 4.5 % to 7.5 %. In this tuning (optimized for 9+, standard conditions), the total efficiency for the 6+ to 12+ states increases from about 23 % to 32 % with a mean charge state (equal currents at higher and lower charge states) shifting from 7.53 to 7.85.

This new configuration could also be applied to the standard gas configuration. In this case the oven inlet would not be needed and could be replaced with iron, increasing the injection magnetic field a little further. This modification would especially benefit experiments needing higher charge states.

3.3. Measurement of the cosmogenic ^{39}Ar isotopic ratio for oceanography

The objective of this project consists in developing a viable method for the measurement of cosmogenic ^{39}Ar (abundance of $2 \cdot 10^{-16}$ of ^{39}Ar/^{40}Ar for a "modern" sample) using the Accelerator Mass Spectrometry (AMS) method. A half-life of 269 years and its conservative geochemical behavior makes ^{39}Ar one of the interesting dating and tracing tools for oceanography. The goal to be reached is the measurement of an "ancient" (3 half lives) sample in a few hours with an accuracy of about 10 to 20 %.

One of the main difficulties to be solved results from the ^{39}K isobaric background coming from the ECR ion source. Since the relative mass difference between ^{39}Ar and ^{39}K is only 1.55×10^{-5}, these isobars cannot be separated with an accelerator/mass separator system. A set of experiments aiming at the measurement of the ionisation and acceleration efficiencies and the ^{39}K contamination, obtained with the SCAMPI ECR-source and with CYCLONE110, have been carried out.

The first test measured the contamination from a source chamber which had been in use for several hundred hours without being opened, and which had thus been extensively cleaned by the plasma. The test used a series of argon and krypton calibrated gas leaks to tune the source and the cyclotron, first to several pilot beams with masses very close to ^{39}K ($^{40}Ar^{8+}$, $^{83}Kr^{17+}$ and $^{78}Kr^{16+}$) and finally to $^{39}K^{8+}$.

By measuring in a particle detector the number of ^{39}K atoms accelerated, we calculated that the amount of $^{39}K^{8+}$ coming from the source was 1.72×10^6 particles per second under operational conditions (i.e. with Argon, simulating a sample to be measured, injected in the source). This corresponds to a ^{39}K/^{39}Ar ratio for a modern sample of 4.3×10^7.

This first measurement shows that the level of potassium impurities from a chamber cleaned with plasma for several hundred hours turns out to be still very high. Therefore, since the embedded impurities proper to the metal seemed not to be completely removed, a test using a "burying" method was set up.

The chamber walls were covered with a layer of SiO_2. SiO_2 was chosen because the source needs wall materials with very good secondary electron emission properties for good performance. The walls itself are made from aluminum, which is oxidized by running the source on oxygen gas, to Al_2O_3 which is a very good secondary electron emitter. SiO_2 is almost as good. This layer was deposited by running the source for a few days on silane (SiH_4) and oxygen. After this conditioning, it was found that the performance for the relevant charge state (Ar^{8+}) was reduced by about 30 %.

The exact same experiment as that before the conditioning was performed again. This time we found that the $^{39}K^{8+}$ current coming from the source was 1.57×10^4 particles per second, a reduction of a factor 110, resulting in a ^{39}K/^{39}Ar ratio for a modern sample of 6×10^5.

Although these results are very promising, more investigations are necessary and will be carried out: the ^{39}K suppression has to be further improved, the extracted Ar^{8+} beam from the source has to be increased and its memory effect for ^{78}Kr (one of the pilot and calibration beams) has to be reduced.

3.4. Development of CYCLONE44

3.4.1 Control System

The hardware (PC's), and input/output, analog and communication network boards) as well as the SIEMENS WinCC software required for the new control system, have been installed. The control systems (PLC's and PC's) of CYCLONE30, the RIB facility and CYCLONE44 have been interconnected into a local network. The new control concept has been tested succesfully with the main coil power supply of CYCLONE44. Work is now underway to realize, in a first step, the controls of the still manually controlled part of CYCLONE44, and, in a second step, to convert the existing COROS part to WinnCC.

3.4.2 Beam Diagnostics

A new main probe head has been built and installed, allowing the simultaneous measurement of the accelerated beam intensity and the beam bunch phase w.r.t. the RF. We have developed a measurement system, which allows to extract the weak beam signal from the leaking RF-noise. Although the numerical simulations allow to predict quite precisely the ideal trimcoil settings, the phase history measurements have proven to be very useful for the development and tuning of new beams.

3.4.3 New Beams

For beam tests with ARES, we have developed successfully the first beam in 8th harmonic mode ($^{19}F^{2+}$ at 5.3 MeV or 0.28 MeV/A). This mode, together with harmonic modes 5 and 6 used up to now, allows to cover the entire energy range foreseen for the nuclear astrophysics experiments. Besides the stable beams of $^{20}Ne^{3+}$, $^{19}F^{2}$ and $^{3+}$, and $^{15}N^{2+}$, routinely used for ARES development, two radioactive beams have been accelerated: $^{15}O^{2+}$ during an RIB development run and $^{19}Ne^{3+}$ for the first experiment using ARES.

3.5. Technological Applications

3.5.1. Wear measurements using an accelerated ^{7}Be beam

During the last three years an intense, isobarically pure, post-accelerated beam of ^{7}Be has been developed for experiments in nuclear physics. In parallel, some tests have been performed to use this beam in wear measurements. Its half-life of 53 days and its light mass make ^{7}Be a very good candidate to be used in wear measurements of materials which can not readily be activated (ceramics, polymers etc.)

Its half-life is long enough to allow time for systematic measurements, yet not too long that it becomes a major problem for waste management. Its light mass ensures that it does not damage the material structure too much.

After two test implantations the previous years, to explore the feasibility of the method, this year we have implanted an artificial hip joint made from aluminumoxide. The requirements were to implant from a depth of 2 µm up to the surface with a flat density distribution. The total number of implanted atoms was to be above 10^{11} particles, to allow wear measurements down to a few nm.

Using a new tilted foil technique as energy modulator, we achieved implanting 1.4×10^{11} ^{7}Be atoms to a depth of 2.5µm. The distribution from the surface up to 1.8 µm was constant within 15 %. The sample is currently under test at the CERAVER company.

3.5.2. Heavy ion Irradiation Facility

During 2002, 535 hours in heavy ions have been scheduled for electronic device testing and characterization.

The following table presents the different experiments, classified by user, using the "Heavy Ion Irradiation Facility" (HIF).

Institute / Company	Purpose
UCL/FSA/ELEC/DICE	TILT study.
TRAD, France	SEE on linear devices. Process testing.
Alcatel ETCA, Belgium	SEE in memories.
Nuclétudes, France	SEE in logic devices.
SAAB, Sweden	FPGA testing. Transient in Optocouplers. SET in operational amplifiers. SEE in line drivers.
TIMA, France	FPGA testing.
HIREX, France	SEB – SEGR in Power MOS. SEE in EEPROM. FPGA testing.
Astrium, United Kingdom	High Frequency RX/TX modules. Bipolar circuit testing.
Astrium, Germany	Dual Port RAM testing. ADC testing.
Surrey, United Kingdom	SEE in GPS circuits.
ONERA, France	SEE in logic devices.
SOREQ, Israel	SEE in processors. SET in logic devices.
CEA, Bruyères-le-Châtel, France	Investigation of SOI and bulk sensitivity with device integration.
SIRA, United Kingdom	DAC tseting.

3.5.3. Light ion Irradiation Facility (LIF)

During 2002, 144 hours in protons have been scheduled for electronic device testing and characterization.

The following table presents the different experiments, classified by user, using the "Light Ion Irradiation Facility" (LIF).

Institute / Company	Components
CERN / ATLAS – INFN Roma	ATLAS level1 muon trigger electronics: CMOS driver, NAND, I2C register, Switch, ADC, phase detector, temperature sensor, flash memory, CMOS – ECL converter.
CERN / ATLAS - LAPP	Liquid Argon Calorimeter dedicated devices in DMILL technology.
CERN / ATLAS – Max Planck Institut	FPGA Quick Logic SEE testing.
ETCA	SEE memory testing.
CNES - ONERA	SEE memory testing.
CERN / CMS - CIEMAT	Read out electronics of the Drift Tube chamber of CMS muon barrel detector: FPGA – Altera, ASIC Clear Logic.
IMEC	SEE testing in cryogenic conditions.
CERN / EP / ED	SEU/SEL testing of several commercial and custom IC SEL mechanism and the protection circuits: FPGA, Linear Voltage Regulators, Eprom, Clock Buffers, ADC, Reference voltage regulators, Linear Buffers, Bipolar Transistots.
CERN / ATLAS – CEA Saclay	SEL in operational amplifiers used in the Larg Calorimeter

Glossary : ADC = Analog to Digital Converter
ASIC = Application Specific IC
CCD = Charge Couple Device
COTS = Components Off The Shelf

DAC = Digital to Analog Converter
DRAM = Dynamic RAM
EEPROM = Electrically Erasable Programmable Memory
FPGA = Field Programmable Gate Arrays
GPS = Global Positioning System
LU / SEL = Single Event Latchup
PLL = Phase locked loop
SEB = Single Event Burnout
SEE = Single Event Effect
SEGR = Single Event Gate Rupture
SET = Single Event Transient
SEU = Single Event Upset
SOI = Silicon On Insulator
SRAM = Static RAM

3.5.4. TILT Project (in collaboration with UCL - FSA/ELEC/DICE)

A complete set of simulations using ATLAS has been made for the 8 µm wide test structure (diode). We have chosen to strike the diode in the middle, on the edge and at three different angles (30°, 50° and 60°).

Simulations were done using a Xe beam with the same energy as for the experiment (459 MeV), and a 3V reverse bias. It is clearly shown that the current peak is much higher for an ion strike in the middle of the diode than on the edge. Furthermore, for tilted irradiation conditions, the cathode current peak value decreases for increasing angle as can be seen on figure 1.

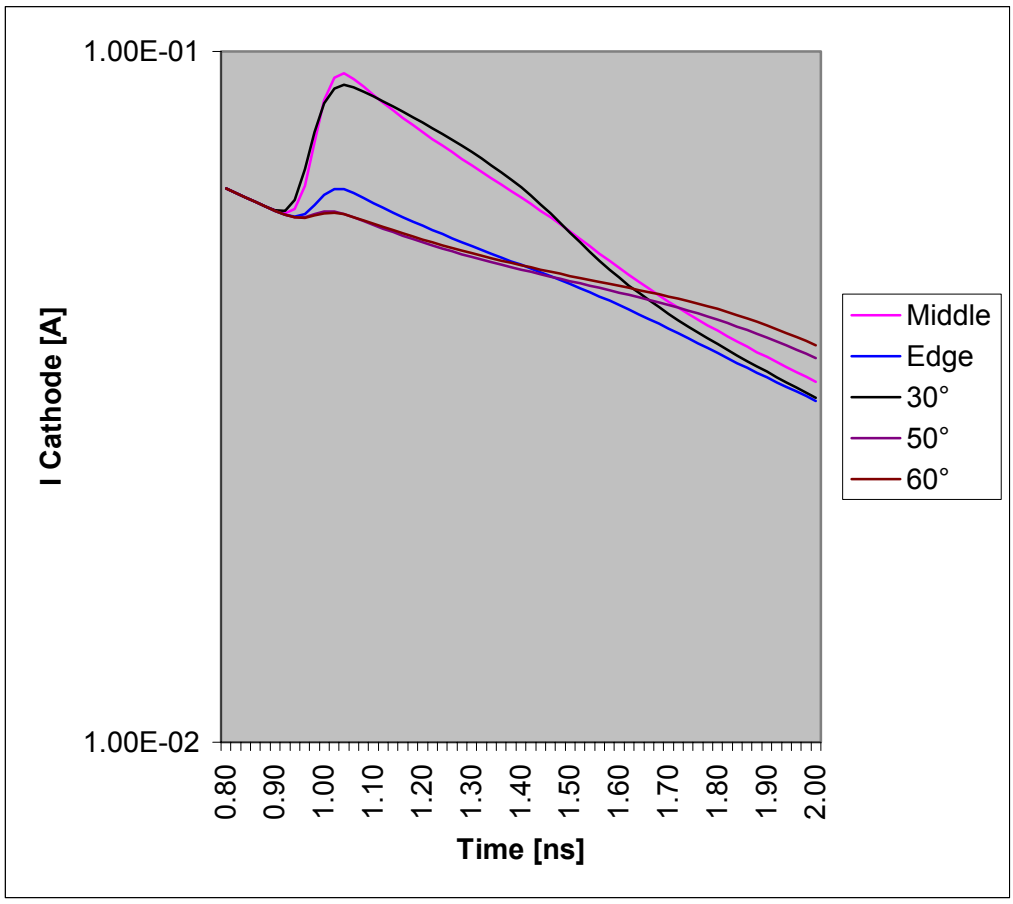

Figure 1 : Angular effect on the cathode current.

Experimental data were taken using a Xenon beam at 459 MeV, different test structures of different sizes were irradiated. Diodes were reverse biased at 3 V and the deposited charge was recorded. It was observed that signal of consecutive strikes presents a large distribution of amplitudes.

At normal incidence, most of the events occur for a collected charge of about 1 pC, which is in fair correlation with the charge computed using a 1D model and for an ion strike in the central part of the device. The number of occurrence for charges below half of the peak value accounts for less than 10 % of the total number of events, also in qualitative agreement with the area ratio, for a 100 µm x 100 µm device, between the central device zone and its peripheral zone starting at about 3 µm of the device edge, as observed in our simulations.

Furthermore, the collected charge amplitude also lowers with increasing angle while its distribution widens. It is also in fair agreement with simulations.

V. LOGISTIQUE

1. MECANIQUE

W. Binon, Th. De Buck, J.-M. Delforge, D. Duysens, D. Hougardy, P. Nemegeer

Le tableau ci-dessous indique la ventilation des heures de travail prestées par l'atelier de mécanique en 2002.

Domaine	Sujet	Heures	Total heures
Accélérateurs	Cyclone 110	904	
	Cyclone 44	1008	
	Cyclone 30	1736	
			3648
CMS	Groupes froids	678	
	Usinage titane	132	
	Irradiations	118	
	Matériaux composites et gabarits	446	
	Divers	446	
			1820
	Grand total		**5468**

Dans l'état actuel, la majorité des travaux pour l'expérience CMS au CERN est liée à la construction des pétales en matériaux composites pour le support des détecteurs au silicium de type microstrip. Dans le courant 2003, les développements relatifs à l'usinage de titane et à la soudure laser prendront plus d'importance.

2. ELECTRONIQUE

2.1. Simulation thermique d'un pétale du détecteur CMS

Un pétale de CMS est constitué de plusieurs détecteurs assemblés en modules, ainsi que des modules accessoires tels que alimentations, contrôles, etc..

Ces modules sont fixés sur un support qui assure également le refroidissement. Pour cela, le support constitué d'un panneau léger est parcouru par un tube dans lequel circule un fluide de refroidissement. Chaque point de fixation des différents modules est en contact thermique avec le tube.

Afin de pouvoir tester les performances thermiques et mécanique de ce système, un simulateur a été développé. Il est constitué de 40 sondes équipées d'un générateur de chaleur et d'un thermomètre. En connaissant la chaleur produite par les différent modules, il est possible de reproduire les conditions réelles de l'expérience, sans disposer des modules réels dont la plupart n'existent pas encore sous leur forme finale.

2.2. Description détaillée

Chaque sonde est munie d'un support en laiton en contact thermique avec un transistor alimenté par une tension fixe (20V) et parcouru par un courant réglable au moyen d'un DAC (convertisseur digital vers analogique). Cet ensemble constitue un générateur de chaleur réglable entre 0 et 5 Watt. Sur l'autre face du support, la température est mesurée par un circuit intégré effectuant une conversion directe de la température vers une valeur digitale ; la précision, après réglages est de 1/16°C. La sonde est munie d'un connecteur

contenant les alimentations (de puissance, digitale et analogique) et un bus I2C. Chaque sonde a sa propre adresse entre 0 et 7, ce qui permet de contrôler 8 sondes distinctes sur un même bus I2C.

L'ensemble comporte 5 guirlandes auxquelles 8 sondes sont connectées tous les 25 cm, ce qui permet de répartie les 40 sondes sur les deux faces du pétale ; les guirlandes aboutissent à un circuit de contrôle local, connecté à un PC au moyen d'une ligne RS232. L'alimentation doit pouvoir fournir 200W, soit 20V, 10A.

Logiciel de commande :

- les deux circuits de refroidissement sont représentés, l'un en rouge, l'autre en vert.
- Les sondes, numérotées de 0 à 39 selon leur adresse sur le bus I2C, sont fixées sur la face supérieure (en rouge) ou sur la face inférieure (en vert).
- La puissance (en mW) appliquée à chaque sonde est réglable par l'opérateur
- L'élévation de température par rapport à un piédestal est affichée pour chaque sonde
- D'autre commandes et mesures sont prévues : mesure de pression, débit, etc..

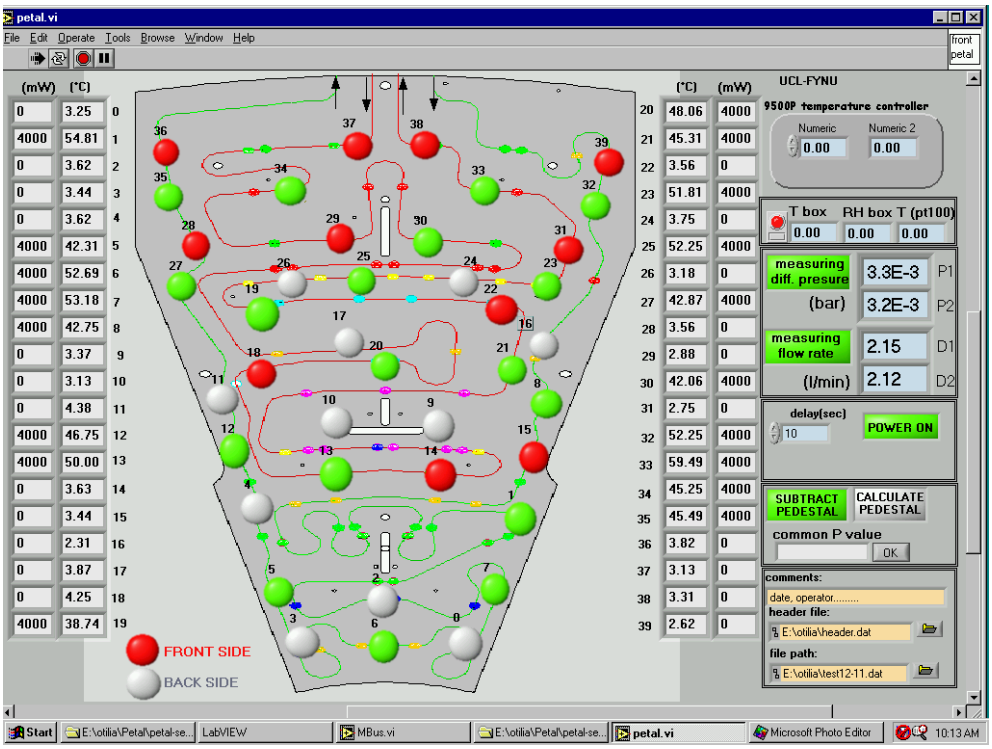

2.3. COMET

Les développements et tests ont été poursuivis (voir développements techniques).

Les 25 modules (au format VME) composant le système ont été fabriqués.

2.4. FHIT (Front-end Hybrid Industrial Tester)

FHIT est un système compact et autonome destiné à tester les Front-end hybrides (FEH) de CMS lors de leur première mise sous tension. Le test s'effectue en trois étapes :

- test des connections

- test électrique

- test fonctionnel

Le test fonctionnel utilise le système ARC développé au RWTH à Aachen.

FHIT peut fonctionner de manière autonome pour des tests simplifiés ou sous le contrôle d'un PC (Labview) pour des tests approfondis.

Ce développement commencé en 2001, a été achevé et mis en service chez le fabricant des FEH en 2002. Plusieurs modifications ont été apportées, en fonction des nouvelles spécifications des FEH et des fonctionnalités et versions de FHIT.

Huit modules FHIT ont été fabriqués et mis en service.

3. LOGISTIQUE INFORMATIQUE

3.1. Gestion journalière des systèmes

Outre les tâches de gestion journalière des systèmes, comme la création de nouveaux comptes utilisateurs, la gestion des espaces disques, l'ajout ou la mise à jour de systèmes, ... l'équipe informatique s'est focalisée sur les points suivant :

3.2. Sécurité informatique

Un nouveau firewall a été installé. La nouvelle configuration basée sur un logiciel dit *stateful* permet de mieux filtrer le trafic entrant à l'Institut tout en autorisant le trafic sortant. Depuis la mise en place de ce système, plus aucune intrusion dans nos systèmes n'a été détectée et aucun système n'a du être réinstallé suite à une dégradation ou compromission.

3.3. Messagerie électronique

L'ancien système de messagerie basé sur *sendmail* a été remplacé par le système *qmail* qui a l'avantage d'être plus sécurisé, plus aisé du point de vue de la configuration, plus performant et efficace. Par ailleurs, le nouveau système de messagerie inclut maintenant un mécanisme de réjection des virus et courriers non-sollicités (spams) dès leur arrivée sur le serveur.

3.4. Nouvel environnement Unix

Un nouvel environnement Unix/Linux a été déployé. Il s'articule autour de trois serveurs DELL:

- 1 serveur DELL Poweredge 1550 équipé de deux processeurs Intel Pentium III à 1.26 GHz, 512 MB de mémoire RAM et de deux disques SCSI de 36 GB.

- 2 serveurs DELL Poweredge 2650 chacun équipé de deux processeurs Intel Xeon à 2 GHz, 2 GB de mémoire RAM et de 4 disques SCSI de 18 GB configurés en RAID 5.

Le premier serveur est destiné à la gestion des utilisateurs et des services réseaux (web, mails, logging, ...). Ce système contient également les répertoires principaux des utilisateurs. Les deux autres serveurs sont eux destinés à accueillir les applications des utilisateurs.

Le nouvel environnement se caractérise par une gestion plus aisée, une meilleure mise à jour des logiciels installés, une uniformisation des accès aux disques des différentes stations de travail et serveurs sous Unix ou Linux. Ces espaces disques sont répartis en trois catégories: home, users et scratch. L'espace home est

situé sur le serveur principal tandis que les espaces users sont situés sur les serveurs de calcul ainsi que les stations de travail individuelles. Ces deux espaces sont sauvegardés sur base journalière. Les espaces scratch sont aussi installés sur les stations de travail mais aucune sauvegarde n'est effectuée.

Des procédures d'installation automatique de Linux et d'intégration de nouveaux systèmes dans l'environnement ont été développées de telle sorte que le processus ne dure que 20 à 30 minutes.

3.5. Nouvel environnement Windows

Un nouvel environnement de gestion des postes de travail de bureautique essentiellement basé sur Windows est en cours de déploiement. Sa caractéristique principale est qu'il sera basé sur le nouvel environnement Windows 2000 et que les contrôleurs de domaines ne seront plus des machines Windows dédicacées mais bien les serveurs Unix décrits plus haut. Ce mode de fonctionnement permettant de rapprocher les deux mondes Unix et Windows est possible grâce au logiciel libre Samba.

3.6. Développements pour CMS

Dans le cadre de l'étude du démonstrateur de l'event builder CMS, nous avons poursuivi le développement de drivers Linux de façon à exploiter au maximum les perfornances des cartes réseaux Gigabit. Les drivers développés en 2000 ont été adaptés aux nouvelles versions du noyau Linux (2.4.x). Par la même occasion les drivers ont été modifiés de façon à pouvoir gérer un nombre N de cartes réseaux dans un système. Les performances de transfert en point-à-point entre des PCs 1GHz équipés d'un bus PCI 66 MHz x 64 bit sont présentées aux figures suivantes:

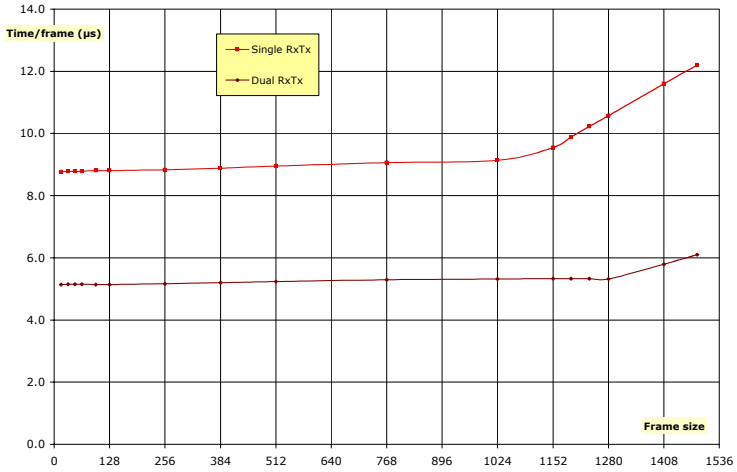

Figure 1 : Time to send a frame vs frame size.

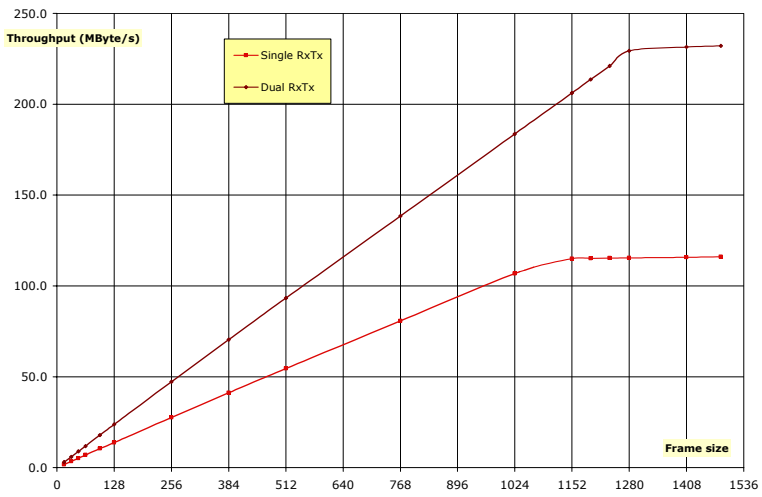

Figure 2 : Data throughput vs frame size.

Les performances atteintes dans la configuration dual controllers (230 MByte/s) font du Gigabit Ethernet un candidat valable comme technologie réseau pouvant être utilisée dans l'event builder CMS.

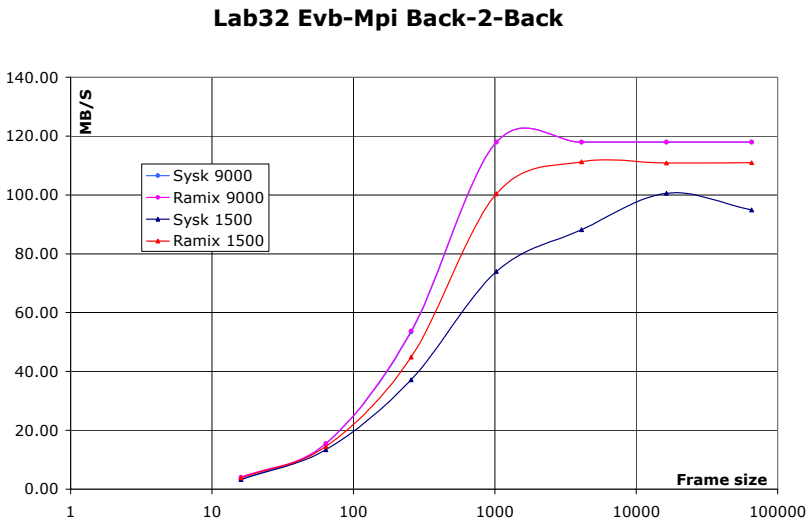

Figure 3.

Par ailleurs les performances du protocole TCP/IP ont été évaluées dans différentes configurations de PCs, de cartes Gigabit Ethernet, de logiciels. La figure suivante représente les performances obtenues avec les PCs décrits précédemment. Différentes cartes réseaux sont utilisées aussi bien avec des frames standards (1500 bytes) que jumbo (9000 bytes) et ce à travers un switch ou bien en connection directe back-to-back. Les grandes variations de performances observées font de TCP/IP un protocole encore fragile pour être intégré de manière fiable dans l'event builder.

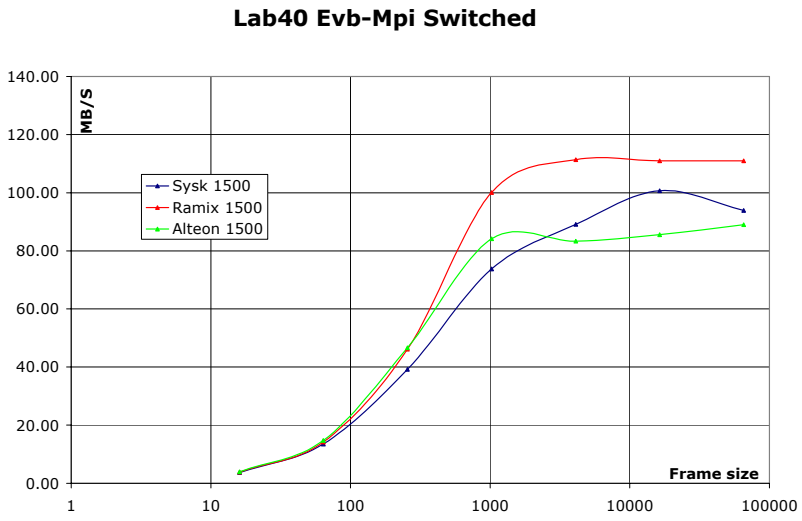
Lab40 Evb-Mpi Switched
MB/S
140.00
120.00
100.00
80.00
60.00
40.00
20.00
0.00
Sysk 1500
Ramix 1500
Alteon 1500
Frame size
1
10
100
1000
10000
100000

Figure 4.

VI. ANNEXES

1. Publications dans des revues

ALEPH Collaboration (A. Heister et al.), Search for scalar leptons in $e^+ e^-$ collisions at center-of-mass energies up to 209 GeV, Eur. Phys. J. C21 (2001) 423-441.

P. Kammel, V.A. Andreev, D.V. Balin, R.M. Carey, T. Case, D.B. Chitwood, S.M. Clayton, K.M. Crowe, J. Deutsch, P.T. Debevec, P.U. Dick, A. Dijksman, J. Egger, D. Fahrni, A.A. Fetisov, S.J. Freedman, V.A. Ganzha, B. Gartner, J. Govaerts, F.E. Gray, F.J. Hartmann, W.D. Herold, D.W. Hertzog, V.I. Jatsoura, A.G. Krivshich, B. Lauss, E.M. Maev, O.E. Maev, V.E. Markushin, C.J.G. Onderwater, C. Petitjean, G.E. Petrov, C.C. Polly, R. Prieels, S.M. Sadetsky, G.N. Schapkin, R. Schmidt, G.G. Semenchuck, M. Soroka, A.A. Vorobyov, N.I. Voropaev, Precise Measurement of Muon Capture on the Proton, Proceedings of the Muon Catalyzed Fusion and Related Exotic Atoms Conference 2001, μCF01, April 22 – 26, 2001, Shimoda (Japan), Hyperfine Int. 138 (2001) 435 – 443.

V.M. Villanueva, J. Govaerts and J.-L. Lucio, Quantizing Gauge Theories without Gauge Fixing: the Physical Projector, Proceedings of the International Conference dedicated to the memory of Professor E.S. Fradkin, Quantization, Gauge Theories and Strings, June 5 – 10, 2000, Moscow (Russia), Volume II, eds. A. Semikhatov, M. Vasiliev and V. Zaikin (World Scientific Publishing, Singapore, 2001), pp. 270 – 276.

F. Albernhe, V. Borrel, P. Frabel, G. Vedrenne, R. Coszach, J.-M. Denis, P. Leleux, Degradation and recovery of Ge detectors : tests prior to a space mission, Nucl. Instr. Meth. Phys. Res. A492 (2002) 91-96.

S. Assouak, J.L. Bonnet, E. Burton (FNRS), B. de Callatay, J. de Favereau de Generet (FRIA), G. de Hemptinne (FRIA), C. Delaere (FNRS), Th. Delbar, D. Favart, E. Forton, J. Govaerts, Gh. Grégoire, G. Leibenguth, V. Lemaître (FNRS-UCL), Y. Longrée, D. Michotte, O.Militaru, A. Ninane, F. Payen, K. Piotrzkowski, X. Rouby, O. Van Der Aa (FRIA) et collaboration CMS, The TRIDAS Projet: Technical Design Report Volume 2. Data Acquisition and High Level trigger, Rapport CERN/LHCC 02-26, CMS TDR 6.

G. Avossevou and J. Govaerts, The Schwinger Model and the Physical Projector: a Nonperturbative Quantization without Gauge Fixing, Proceedings of the Second International Workshop on Contemporary Problems in Mathematical Physics, October 28th – November 2nd, 2001, Cotonou (Republic of Benin), eds. Jan Govaerts, M. Norbert Hounkonnou and Alfred Z. Msezane (World Scientific, Singapore, 2002), pp. 374 – 394.

I.G. Bearden, D. Beavis, C. Besliu, Y. Blyakhman, B. Budick, H. Boggild, C. Chasman, C.H. Christensen, P. Christiansen, J. Cibor, R. Debbe, E. Enger, J.J. Gaardhoje, K. Hagel, O. Hansen, A. Holm, A.K. Holme, H. Ito, E. Jakobsen, A. Jipa, J.I. Jordre, F. Jundt, C.E. Jorgensen, R. Karabowicz, T. Keutgen, E.J. Kim, T. Kozik, T.M. Larsen, J.H. Lee, Y.K. Lee, G. Lovhoiden, Z. Majka, A. Makeev, B. McBreen, M. Mikelsen, M. Murray, J. Natowitz, B.S. Nielsen, J. Norris, K. Olchanski, J. Olness, D. Ouerdane, R. Planeta, F. Rami, C. Ristea, D. Rohrich, B.H. Samset, D. Sandberg, S.J. Sanders, R.A. Sheetz, P. Staszel, T.F. Thorsteinsen, T.S. Tveter, F. Videbaek, R. Wada, A. Wieloch, I.S. Zgura, Pseudorapidity distributions of charged particles from Au+Au collisions at the maximum RHIC energy, root s(NN)=200 GeV, Physical Review Letters 88 (20) (2002) 202301.

S. Benck, I. Slypen, J.-P. Meulders, V. Corcalciuc and M. B. Chadwick, Fast neutron-induced emission of light charged particles on aluminium (E_n=25 to 55 MeV), Nucl. Sc. and Eng. 140 (2002) 86-95.

S. Benck, I. Slypen, J.-P. Meulders and V. Corcalciuc, Secondary light charged particle emission from the interaction of 25- to 65-MeV neutrons on silicon, Nucl. Sc. and Eng. 141 (2002) 55-65.

S. Benck, E. Raeymackers, I. Slypen, J.-P. Meulders and V. Corcalciuc, Secondary light charged particle emission from the interaction of 25-65-MeV neutrons on uranium, Journal of Nuclear Science and Technology, Supplement 2, (August 2002) 335-338.

L. Benussi, N. Bruski, N. D'Ambrosio, Y. Declais, J. Dupraz, J.P. Fabre, V. Fanti, E. Forton, D. Frekers, A. Frenkel, C. Girerd, S.V. Golovkin, G. Grégoire, K. Harrison, G. Jonkmans, P. Jonsson, S. Katsanevas, I. Kreslo, J. Marteau, G. Martellotti, S. Martinez, A.M. Medvedkov, G. Moret, K. Niwa, V. Novikov, G. Van Beek, G. Penso, V.G. Vasilchenko, J.L. Vuilleumier, G. Wilquet, P. Zucchelli, Large liquid-scintillator trackers for neutrino experiments. CERN-EP-2002-006, Jan 2002, 20 pp, Nucl. Instrum. Meth. A488 (2002) 503-516.

D. Bertrand, J. Govaerts and G. Stenuit, Nanoscopic Superconducting Slab in Static Electric and Magnetic Fields, Proceedings of the Second European Conference "Vortex Matter in Superconductors", September 15 – 25, 2001, Agia Pelagia (Crete, Greece), Physica C369 (2002) 339 – 342.

A. Bulte, K. Winter, M. Litmaath, Y. Gernitzky, J. Goldberg, G. Grégoire, K. Niwa, T. Nakano, M. Komatsu, K. Itoh, D. Frekers, N. Bruski, J. Kuckmann, The CHARON detector: an emulsion/counter hybrid set-up to measure the mean free path of near-elastic pion scattering in nuclear emulsion (white kink) at 2-GeV/c, 3-GeV/c and 5-GeV/c, Nucl.Instrum. Meth. A485 (2002) 426-438.

S. Cherubini, C. Angulo, M. Couder, W. Galster, J.S. Graulich, P. Leleux, P. Lipnik, M. Loiselet, A. Musumarra, A. Ninane, G. Ryckewaert, J. Vervier, M. Aliotta, P. Figuera, M. Lattuada, M.G. Pellegriti, C. Spitaleri, T. Davinson, A. Di Pietro, A.M. Laird, A.N. Ostrowski, A.C. Shotter, P.J. Woods, J. Hinnefeld, S. Typel, H. Wolter, New Developments and Recent Results in Nuclear Astrophysics at Louvain-la-Neuve, Nucl.Phys. A701 (2002) 632c.

C. Delaere, V. Lemaitre, An alternative Invisible Higgs search performed with ALPHA++, CERN-ALEPH-2002-034.

C. Delaere et al., ALPHA++ User's Manual-ALEPH OO Physics Analysis Package Version 3.4, CERN-ALEPH-2002-033.

Th. Delbar, D. Favart, G. Grégoire, S. Kalinin, I. Makhlioueva et collaboration CHORUS, Determination of the semi-leptonic branching fraction of charm hadrons produced in neutrino charged-current interactions. CERN-EP-2002-075, Oct 2002, 12 pp, Phys. Lett. B549 (2002) 48-57.

Th. Delbar, D.Favart, Gh. Grégoire, S. Kalinin, I. Makliouevа and the CHORUS collaboration, Measurement of D^0 production in neutrino charged current interactions, Publ. Ref.: CERN-EP/2002-005, Phys. Lett. B527 (2002) 173-181.

Th. Delbar, D.Favart, Gh. Grégoire, S. Kalinin, I. Makliouevа and the CHORUS collaboration, Observation of one event with the characteristics of associated CHARM production in neutrino charged-current interactions, Publ. Ref.: CERN-EP/2002-036, Phys. Lett. B539 (2002) 188-196.

N. de Séréville, A. Coc, C. Angulo, M. Assuncao, D. Beaumel, B. Bouzid, S. Cherubini, M. Couder, P. Demaret, F. de Oliveira Santos, P. Figuera, S. Fortier, M. Gaelens, F. Hammache, J. Kiener, D. Labar, A. Lefebvre, P. Leleux, A. Ninane, M. Loiselet, S. Ouichaoui, G. Ryckewaert, N. Smirnova, V. Tatischeff, J.P. Thibaud, A New Experiment for the Determination of the $^{18}F(p,\alpha)$ Reaction Rate at Nova Temperatures, nucl-ex/0206014, 6/21/2002 (2002).

N. de Séréville, A. Coc, C. Angulo, M. Assuncao, D. Beaumel, B. Bouzid, S. Cherubini, M. Couder, P. Demaret, F. de Oliveira Santos, P. Figuera, S. Fortier, M. Gaelens, F. Hammache, J. Kiener, D. Labar, A. Lefebvre, P. Leleux, M. Loiselet, A. Ninane, S. Ouichaoui, G. Ryckewaert, N. Smirnova, V. Tatischeff, J.-P. Thibaud, Study of the $^{18}F(p,\alpha)^{15}O$ Reaction for Application to Nova γ-Ray Emission, nucl-ex/0209017, 9/24/2002 (2002).

S. Dutta, G. Berger, L. Borrello, A. Buffini, S. Busoni, C. Civinini, R. D'Alessandro, G. Grégoire, R. Dell'Orso, M. Lenzi, M. Meschini, A. Messineo, G. Segneri, A. Starodumov, G. Tonelli, P.G. Verdini, Performance of 500-μm thick silicon microstrip detectors after irradiation. 3rd International Conference on Radiation Effects on Semiconductor Materials, Detectors and Devices, Florence, Italy, 28-30 Jun 2000, Nucl. Instrum. Meth. A476 (2002) 739-743.

J. El Bachir Mendy and J. Govaerts, A General Effective Four-Fermion Lagrangian for Dirac and Majorana Neutrino-Charged Matter Interactions, Proceedings of the Second International Workshop on

Contemporary Problems in Mathematical Physics, October 28th – November 2nd, 2001, Cotonou (Republic of Benin), eds. Jan Govaerts, M. Norbert Hounkonnou and Alfred Z. Msezane (World Scientific, Singapore, 2002), pp. 268 – 289.

Y. El Masri, N. Moroso, V. Zaconte, Ch. Heitz, J. Cabrera, Ch. Dufauquez, V. Roberfroid, J. Van Mol, J. Lehmann, F. Vanderbist P. Leleux and M. Couder, Analysis of ^{4}He implanted in Al foils using the ^{4}He(p,p)^{4}He backscattering interaction, Nuclear Instruments and Methods in Physics Research B197 (2002) 271-277.

E. Eskut, A. Kayis-Topaksu, G. Onengut, R. van Dantzig, M. de Jong, J. Konijn, O.Melzer, R.G.C. Oldeman, E.Pesen, C.A.F.J. van der Poel, J.W.E. Uiterwijk, J.L. Visschers, M. Guler, M. Seyrin-Zeyrek, R. Sever, P. Tolun, M.T. Zeyrek, N. Armenise, F. Cassol, M.G. Catanesi, M. De Serio, M.T. Muciaccia, E. Radicioni, S. Simone, L. Vivolo, A. Bülte, K. Winter, P. Annis, R. El-Aidi, M. Vander Donckt, B. Van de Vyver, P. Vilain, G. Wilquet, P. Righini, B. Saitta, E. di Capua, Y. Yshii, T. Kawamura, M. Kazuno, S. Ogawa, H. Shibuya, J. Brunner, D. Cussans, M. Doucet, J.P. Fabre, W. Flegel, M. Litmaath, H. Meinhard, E. Niu, H. Overas, J. Panman, I.M. Papadopoulos, S. Ricciardi, A. Rozanov, D. Saltzberg, P. Strolin, R. Tsenov, C. Weinheimer, H. Wong, P. Zucchelli, J. Goldberg, M. Chikawa, E. Arik, A.A. Mailov, I.G. Park, J.S. Song, C.S. Yoon, K. Kodama, N. Ushida, S. Aoki, T. Hara, G. Brooijmans, Th. Delbar, D. Favart, G. Gregoire, S. Kalinin, I. Makhlioueva, A. Artamonov, P. Gorbunov, V. Khovansky, V. Shamanov, I. Tsukerman, D. Bonekämper, N. D'Ambrosio, D. Frekers, D. Rondeshagen, T. Wolff, K. Hoshino, M. Komatsu, Y. Kotaka, T. Kozaki, M. Miyanishi, T. Nakano, K. Niu, K. Niwa, Y. Obayashi, O. Sato, T. Toshito, N. Bruski, S. Buontempo, A.G. Cocco, G. De Lellis, F. Di Capua, A. Ereditato, G. Fiorillo, R. Listone, M. Messina, P. Migliozzi, V. Palladino, V. Tioukov, K. Nakamura, T. Okusawa, A. Capone, D. De Pedis, S. Di Liberto, U. Dore, P.F. Loverre, L. Ludovici, A. Maslennikov, G. Piredda, G. Rosa, R. Santacesaria, A. Satta, F.R. Spada, E. Barbuto, C. Bozza, G. Grella, G. Romano, S. Sorrentino, Y. Sato, I. Tezuka, Measurement of D^0 production in neutrino charged-current interactions, CERN-EP-2002-005, Jan 2002, 10 pp, Phys. Lett. B527 (2002) 173-181.

P. Froment, I. Tilquin, M. Cogneau, Th. Delbar, J. Vervier, G. Ryckewaert, The production of radioisotopes for medical applications by the adiabatic resonance crossing (ARC) technique, Nucl. Instr. Meth. Phys. Res. A493 (2002) 165.

M. Gaelens, M. Loiselet, G. Ryckewaert, ECR sources and rare isotopes beams at Louvain-la-Neuve, Review of Scientific Instruments 73, Number 2 (2002) 714-716.

M. Gaelens, M. Loiselet, C. Wagemans, J. Wagemans, G. Goeminne, Realization of Nuclear Targets by Ion Implantation : the ^{17}O case, 20th World Conference of the International Nuclear Targets Development Society, 3-8 October 2000, Antwerp, Belgium, Nuclear Instruments and Methods in Physics Research A480 (2002) 233-236.

M. Gaelens, Experience with dedicated targets for RIB production at Louvain-la-Neuve, Indian. J. Phys. 76S (2002) 113-117.

W. Glasser, R. Michel, S. Neumann, H. Schuhmacher, V. Dangendorf, R. Nolte, U. Herpers, A. N. Smirnov, I. Ryzhov, A. V. Prokofiev, P. Malmborg, D. Kollár, J.-P. Meulders, Radionuclide production from lead by neutron-induced reactions up to 175 MeV, Journal of Nuclear Science and Technology, Supplement 2, (August 2002) 373-376.

J. Govaerts, The Quantum Geometer's Universe: Particles, Interactions and Topology, Proceedings of the Second International Workshop on Contemporary Problems in Mathematical Physics, October 28th – November 2nd, 2001, Cotonou (Republic of Benin), eds. Jan Govaerts, M. Norbert Hounkonnou and Alfred Z. Msezane (World Scientific, Singapore, 2002), pp. 79 – 212.

J. Govaerts, Proceedings of the Second International Workshop on Contemporary Problems in Mathematical Physics, October 28th – November 2nd, 2001, Cotonou (Republic of Benin), eds. Jan Govaerts, M. Norbert Hounkonnou and Alfred Z. Msezane (World Scientific, Singapore, 2002), 501 pages.

J.-S. Graulich, R. Coszach, P. Leleux, Nuclear astrophysics experiments : reactions and elastic scattering, Europ. Phys. Journal A13 (2002) 221-225.

D. Groombridge, A.C. Shotter, W. Bradfield-Smith, S. Cherubini, T. Davinson, A. Di Pietro, J. Görres, J.S. Graulich, A.M. Laird, P. Leleux, A. Musumarra, A. Ninane, A.N. Ostrowski, J. Rahighi, H. Schatz, M. Wiescher, and P.J. Woods, Breakout from the hot CNO cycle via the $^{18}Ne(\alpha,p)^{21}Na$ reaction. II. Extended energy range $E_{c.m.} \sim 1.7 – 2.9$ MeV, Physical Review C66 (2002) 055802.

Gh. Grégoire et al., The compact emulsion spectrometer, Rapport CERN-EP/2000-060 (9 mai 2000).

A. Kayis-Topaksu, G. Onengut, R. van Dantzig, M. de Jong, J. Konijn, O.Melzer, R.G.C. Oldeman, E.Pesen, J.L. Visschers, M. Guler, M. Seyrin-Zeyrek, P. Tolun, M.T. Zeyrek, N. Armenise, M.G. Catanesi, M. De Serio, M. Ieva, M.T. Muciaccia, E. Radicioni, S. Simone, A. Bülte, K. Winter, R. El-Aidi, B. Van de Vyver, P. Vilain, G. Wilquet, B. Saitta, E. di Capua, S. Ogawa, H. Shibuya, A. Artamonov, J. Brunner, M. Chizov, D. Cussans, M. Doucet, D. Kolev, H. Meinhard, J. Panman, I.M. Papadopoulos, S. Ricciardi, R. Tsenov, J.W.E. Uiterwijk, P. Zucchelli, J. Goldberg, M. Chikawa, E. Arik, J.S. Song, C.S. Yoon, K. Kodama, N. Ushida, S. Aoki, T. Hara, Th. Delbar, D. Favart, G. Gregoire, S. Kalinin, I.Makliouevа, P. Gorbunov, V. Khovansky, V. Shamanov, I. Tsukerman, N. Bruski, D. Frekers, K. Hoshino, M. Komatsu, M. Miyanishi, M. Nakamura, T. Nakano, K. Narita, K. Niu, K. Niwa, O. Sato, T. Toshito, S. Buontempo, A.G. Cocco, N. D'Ambrosio, G. De Lellis, G. De Rosa, F. Di Capua, A. Ereditato, G. Fiorillo, T. Kawamura, M. Messina, P. Migliozzi, V. Palladino, P. Strolin, V. Tioukov, K. Nakamura, T. Okusawa, U. Dore, P.F. Loverre, L. Ludovici, A. Maslennikov, P. Righini, G. Rosa, R. Santacesaria, A. Satta, E. Barbuto, C. Bozza, G. Grella, G. Romano, S. Sorrentino, Y. Sato, I. Tezuka, Determination of the semi-leptonic branching fraction of charm hadrons produced in neutrino charged-current interactions, CERN-EP-2002-075, Oct 2002. 12pp. Phys. Lett. B549 (2002) 48-57.

M. Kerveno, F. Haddad, Ph. Eudes, T. Kirchner, C. Lebrun, I. Slypen, J.P. Meulders, C. Le Brun, Fr. Lecolley, J.F. Lecolley, M. Louvel, F. Lefèbvres, S. Hilaire, A.J. Koning, Hydrogen isotope double differential production cross sections induced by 62.7 MeV neutrons on a lead target, Physical Review C66 (2002) 0147601-1 - 0147601-8.

A. Koning, H. Beijers, J. Benlliure, O. Bersillon, J. Blomgren, J. Cugnon, M. Duijvestijn, P. Eudes, D. Filges, F. Haddad, S. Hilaire, C. Lebrun, F.-R. Lecolley, S. Leray, J.-P. Meulders, R. Michel, R. Neef, R. Nolte, N. Olsson, R. Ostendorf, E. Ramstroem, K.-H. Schmidt, H. Schuhmacher, I. Slypen, H.-A. Synal, R. Weinreich, HINDAS: a european nuclear data program for accelerator-driven systems, Journal of Nuclear Science and Technology, Supplement 2, (August 2002) 1161-1166.

A. Laird, S. Cherubini, A.N. Ostrowski, M. Aliotta, T. Davinson, A. Di Pietro, P. Figuera, W. Galster, J.S. Graulich, D. Groombridge, J. Hinnefeld, M. Lattuada, P. Leleux, L. Michel, A. Musumarra, A. Ninane, M.G. Pellegriti A.C. Shotter, C. Spitaleri, A. Tumino, J. Vervier and P. Woods, An indirect study of the astrophysically important $^{15}O(\alpha,\gamma)^{19}Ne$ reaction through $d(^{18}Ne,^{19}Ne)p$, Phys. Rev. C66 (2002) 048801, 1-4.

V. Lemaître (CERN et UCL) et collaboration ALEPH (A. Heister et al.), Search for gamma-gamma decays of a Higgs boson in E^+E^- collisions at S**(1/2) up to 209-GeV, Phys. Lett. B544 (2002)16-24.

V. Lemaître (CERN et UCL) et collaboration ALEPH (A. Heister et al.), Absolute lower limits on the mases of selectrons and sneutrinos in the MSSM, Phys. Lett. B544 (2002) 73-88.

V. Lemaître (CERN et UCL) et collaboration ALEPH (A. Heister et al.), Search for single top production in E^+E^- collisions at S**(1/2) up to 209-GeV, Phys. Lett. B543 (2002) 173-182.

V. Lemaître (CERN et UCL) et collaboration ALEPH (A. Heister et al.), A flavor independent Higgs boson search in E^+E^- collisions at S**(1/2) up to 209-GeV, Phys. Lett. B544 (2002) 25-34.

V. Lemaître (CERN et UCL) et collaboration ALEPH (A. Heister et al.), Search for scalar quarks in E^+E^- collisions at S**(1/2) up to 209-GeV, Phys. Lett. B537 (2002) 5-20.

V. Lemaître (CERN et UCL) et collaboration ALEPH (A. Heister et al.), Search for charginos nearly mass degenerate with the lightest neutralino in E^+E^- collisions at center-of-mass energies up to 209-GeV, Phys. Lett. B533 (2002) 223-236.

V. Lemaître (CERN et UCL) et collaboration ALEPH (A. Heister et al.), Search for $\gamma\gamma \rightarrow \varepsilon(B)$ in E^+E^- collisions at LEP-2, Phys. Lett. B530 (2002) 56-66.

V. Lemaître (CERN et UCL) et collaboration ALEPH (A. Heister et al.), Final results of the searches for neutral Higgs bosons in E^+E^- collisions at S**(1/2) up to 209-GeV, Phys. Lett. B526 (2002) 191-205.

V. Lemaître (CERN et UCL) et collaboration ALEPH (A. Heister et al.), Search for R parity violating production of single neutrinos in E^+E^- collisions at S**(1/2) = 189-GeV to 209-GeV, Eur. Phys. J. C25 (2002) 1-12.

V. Lemaître (CERN et UCL) et collaboration ALEPH (A. Heister et al.), Measurement of triple gauge couplings at LEP energies up to 189-GeV, Phys. Lett. B526 (2002) 206-220.

S. Michotte, L. Piraux, S. Dubois, F. Pailloux, G. Stenuit and J. Govaerts, Superconducting Properties of Lead Nanowires Arrays, Physica C377 (2002) 267 – 276.

J.B. Natowitz, R. Wada, K. Hagel, T. Keutgen, M. Murray, A. Makeev, L. Qin, P. Smith, C. Hamilton, Caloric curves and critical behavior in nuclei, Physical Review C65 (3) (2002) 034618.

N. Nica, S. Benck, E. Raeymackers, I. Slypen, J.-P. Meulders and V. Corcalciuc, Light charged particle emission induced by fast neutrons (25 to 65 MeV) on 59 Co, J. Phys. G: Nucl. Part. Phys. 28 (2002) 2823-2842.

R. Nolte, M. S. Allie, P. J. Binns, F. D. Brooks, A. Buffler, V. Dangendorf, K. Langen, J.-P. Meulders, W. D. Newhauser, F. Roos and H. Schuhmacher, Measurement of ^{235}U, ^{238}U, ^{209}Bi and ^{nat}Pb fission cross sections using quasi-monoenergetic neutrons with energies from 30 MeV to 150 MeV, Journal of Nuclear Science and Technology, Supplement 2, (August 2002) 311-314.

A.N. Ostrowski, A.M. Laird, A.C. Shotter, M. Aliotta, F. Cappuzzello, S. Cherubini, A. Cunsolo, T. Davinson, W. Galster, J.S. Graulich, D. Groombridge, J. Hinnefeld, P. Leleux, L. Michel, S. Morrow, A. Musumarra, A. Ninane, A. Spitaleri, A. Tumino, J. Vervier, Break-out from the hot-CNO cycle studied with radioactive beams, Nuclear Physics A701 (2002) 621c-624c.

K. Piotrzkowski et ZEUS Collaboration, Measurement of proton dissociative diffractive photoproduction of vector mesons at large momentum transfer at HERA, Rapport hep-ex/0205081; Soumis pour publication à Eur. Phys. J.

K. Piotrzkowski, High energy two-photon interactions at the LHC, Rapport hep-ex/0201027, Proceedings of the Workshop on Electromagnetic Probes of Fundamental Physics, Erice, Italy, Oct 2001.

K. Piotrzkowski et ZEUS Collaboration, Measurement of diffractive production of D^{*+-}(2010) mesons in deep inelastic scattering at HERA, Rapport hep-ex/0206020, Phys. Lett. B545 (2002) 244-260.

K. Piotrzkowski et ZEUS Collaboration, Inclusive jet cross-sections in the Breit frame in neutral current deep inelastic scattering at HERA and determination of α_S, Rapport hep-ex/0208037, Phys. Lett. BB547 (2002) 164-180.

K. Piotrzkowski et ZEUS Collaboration, Measurement of high Q^2 *ep* neutral current cross-sections at HERA and the extraction of xF_3, Rapport hep-ex/0208040, Soumis pour publication à Eur. Phys. J.

K. Piotrzkowski et ZEUS Collaboration, A ZEUS next-to-leading-order QCD analysis of data on deep inelastic scattering, Rapport hep-ex/0208023, Accepté pour publication dans Phys. Rev.

R. Raabe, L. Weissman, A. Andreyev, C. Angulo, D. Baye, W. Bradfield-Smith, S. Cherubini, T. Davinson, P. Descouvemont, A. Di Pietro, M. Huyse, A.M. Laird, W.F. Mueller, A. Musumarra, A. Ostrowski, A. Piechaczek, A. Shotter, G. Terwagne, P. Van Duppen, A. Wohr, Measurement of the ^{4}He(^{6}He, ^{6}He)^{4}He Cross Section with a ^{4}He-Implanted Al Target, Nucl.Phys. A701 (2002) 387c.

E. Raeymackers, I. Slypen, S. Benck, J.-P. Meulders, N. Nica and V. Corcalciuc, Light charged particle production induced by fast neutrons (E_n = 25 – 65 MeV) on ^{209}Bi, Journal of Nuclear Science and Technology, Supplement 2 (August 2002) 354-357.

G. Ryckewaert, J.M. Colson, M. Gaelens, M. Loiselet, N. Postiau, Recent results from the Louvain-la-Neuve RIB-facility, 5th International Conference on Radioactive Nuclear Beams, 3-8 April 2000, Divonne, France, Nuclear Physics A701 (2002) 323c-326c.

S.J. Sanders, I.G. Bearden, D. Beavis, C. Besliu, Y. Blyakhman, J. Brzychczyk, B. Budick, H. Boggild, C. Chasman, C.H. Christensen, P. Christiansen, J. Cibor, R. Debbe, J.J.Gaardhoje, K. Grotowski, K. Hagel, O. Hansen, A. Holm, A.K. Holme, H. Ito, E. Jakobsen, A. Jipa, J.I. Jordre, F. Jundt, C.E. Jorgensen, T. Keutgen, E.J. Kim, T. Kozik, T.M. Larsen, J.H. Lee, Y.K. Lee, G. Lovhoiden, Z. Majka, A. Makeev, B. McBreen, M. Murray, J. Natowitz, B.S. Nielsen, K. Olchanski, J. Olness, D. Ouerdane, R. Planeta, F. Rami, D. Rohrich, B.H. Samset, R.A. Sheetz, Z. Sosin, P. Staszel, T.F. Thorsteinsen, T.S. Tveter, F. Videbaek, R. Wada, A. Wieloch, I.S. Zgura, Charged particle multiplicities at BRAHMS, Acta Physica, Hungarica A New Series-Heavy Ion Physics 15 (3-4) (2002) 315-326.

P. Staszel, I.G.Bearden, D. Beavis, C. Besliu, Y. Blyakhman, B. Budick, H. Boggild, C. Chasman, C.H. Christensen, P. Christiansen, J. Cibor, R. Debbe, E. Enger, J.J. Gaardhoje, K. Hagel, O. Hansen, A. Holm, A.K. Holme, H. Ito, E. Jakobsen, A. Jipa, J.I. Jordre, F. Jundt, C.E. Jorgensen, R. Karabowicz, T. Keutgen, E.J. Kim, T. Kozik, T.M. Larsen, J.H. Lee, Y.K. Lee, G. Lovhoiden, Z. Majka, A. Makeev, B. McBreen, M. Mikelsen, M. Murray, J. Natowitz, B.S. Nielsen, J. Norris, K. Olchanski, J.Olness, D. Ouerdane, R. Planeta, F. Rami, C. Ristea, D. Rohrich, B.H. Samset, D. Sandberg, S.J. Sanders, R.A. Sheetz, T.F. Thorsteinsen, T.S. Tveter, F. Videbaek, R. Wada, A. Wieloch, I.S. Zgura, Results from BRAHMS experiment at RHIC, Acta Polonica B33 (6) (2002) 1387-1406.

G. Stenuit, J. Govaerts and D. Bertrand, Half-Integer Number Vortices in the Ginzburg-Landau-Higgs Model, Proceedings of the NATO Advanced Research Workshop "New Trends in Superconductivity", September 16 – 20, 2001, Yalta (Ukraine), eds. J. Annett and S. Kruchinin, NATO Science Series II: Mathematics, Physics and Chemistry, Vol. 67 (Kluwer Academic Publishers, Dordrecht, 2002), pp. 375 – 384.

F. Vanderbist, C. Angulo, M. Couder, Y. El Masri, P. Leleux, M. Loiselet, G. Tabacaru, Realization and analysis of He-implanted foils for the measurement of (α,γ) reaction cross-sections in nuclear astrophysics, Nucl.Instrum.Methods Phys.Res. B197 (2002) 165-171.

F. Videbaek, I.G. Bearden, D. Beavis, C. Besliu, Y. Blyakhman, J. Brzychczyk, B. Budick, H. Boggild, C. Chasman, C.H. Christensen, P. Christensen, J. Cibor, R. Debbe, J.J. Gaardhoje, K. Grotowski, K. Hagel, O. Hansen, A. Holm, A.K. Holme, H. Ito, E. Jakobsen, A. Jipa, J.I. Jordre, F. Jundt, C.E. Jorgensen, E.J. Kim, T. Kozik, T. Keutgen, T.M. Larsen, J.H. Lee, Y.K. Lee, G. Lovhoiden, Z. Majka, A. Makeev, B. McBreen, M. Murray, J. Natowitz, B.S. Nielsen, K. Olchanski, J. Olness, D. Ouerdane, R. Planeta, F. Rami, D. Roehrich, B.H. Samset, S.J. Sanders, R.A. Sheetz, Z. Sosin, P. Staszel, T.F. Thorsteinsen, T.S. Tveter, F. Videbaek, R. Wada, A. Wieloch, I.S. Zgura, Results from the BRAHMS experiment at RHIC, Nuclear Physics A698 (2002) 29C-38C.

J. Wagemans, C. Wagemans, G. Goeminne, O. Serot, M. Loiselet, M. Gaelens, The $^{17}O(n,\alpha)^{14}C$ reaction from subthermal up to approximatively 350 keV neutron energy, Physical Review C65 (2002) 034614.

C. Wagemans, J. Wagemans, G. Goeminne, M. Loiselet, M. Gaelens, Preparation of highly enriched 17O samples for neutron induced reaction studies, 20th World Conference of the International Nuclear Targets Development Society, 3-8 October 2000, Antwerp, Belgium, Nuclear Instruments and Methods in Physics Research A480 (2002) 229-232.

V. Wiaux, R. Prieels, J. Deutsch, J. Govaerts, V. Brudanin, S. Egorov, C. Petitjean and P. Truoel, Muon Capture by ^{11}B and the Hyperfine Effect, Phys. Rev. C65 (2002) 025503 (8 pages).

2. Communications et participations à des Congrès

- *CMS-Week CERN, December 1-8, 2001, Genève, Suisse*
  S. Assouak , E. Forton, G. Grégoire, IQC status of readiness.

- *Tracker-week CERN, January 20-26, 2002, Genève, Suisse*
  S. Assouak , E. Forton, G. Grégoire, Status of IQC.

- *EC-NSF Workshop on "Nanotechnology: Revolutionary Opportunities and Societal Implications, January 31-February 1, 2002, Lecce, Italy*
  R. Legras, Nanopores, nanowires and nanotubes : 2 European projects coordinated by UCL (poster).

-- *Workshop on "String Theory and Quantum Gravity: New Developments and Links to Low-Energy Physics", Stellenbosch Institute for Advanced Study (STIAS), February 4–22, 2002, University of Stellenbosch, Stellenbosch (Republic of South Africa)*
J. Govaerts, Quantization of Constrained Systems (invited lectures).

- *Workshop on Ion Track Technology (EuNITT), February 25-26, 2002, Caen, France*
R. Legras, Nanopores and nanowires : a challenge for new properties and applications (invited talk).

L. Dauginet-De Pra, Characterisation of the optical and vibrational properties of electrochemically synthesised polymer nanostructures.

Participants : E. Ferain, F. Dehaye

- *IQC meetings, March 14-15, 2002, Karsruhe, Allemagne*
S. Assouak , E. Forton, G. Grégoire, IQC Louvain- Irradiations.

S. Assouak, E. Forton, G.Grégoire, IQC Louvain-Measurements.

- *JEFF (Joint Effort for Fission and Fusion) data working group, 23-25 avril 2002, Aix en Provence, France*
J.-P. Meulders, Neutron-induced reaction studies at Louvain-la-Neuve (conférence invitée).

- *14th EMIS Conference, Electro Magnetic Isotope Separators and techniques related to their applications, Victoria, British Columbia, Canada, May 6-10, 2002*
M. Gaelens, A pure accelerated ^{7}Be beam using an ECR ion source cyclotron combination (présentation orale).

- *UCL-CERMIN "Feynman" Workshop, May 22, 2002, Louvain-la-Neuve (Belgium)*
G. Stenuit, S. Michotte and J. Govaerts: oral communication by G. Stenuit, Vortex Configurations in Mesoscopic Superconducting Nanowires.

Participants: D. Bertrand, J. Govaerts, G. Stenuit

- *5th International Symposium on Swift Heavy Ions in Matter (SHIM 2002), May 22-25, 2002, Giardini Naxos, Taormina - Italy*
F. Dehaye, Chemical modifications induced in bisphenol A polycarbonate by swift heavy ions.

E. Ferain, Track etched templates use for nanoscale materials synthesis.

Participant : R. Legras

- *5th International Symposium on Functional p-electron Systems, May 2002,Ulm, Germany*
L. Dauginet-De Pra, S. Demoustier-Champagne, Characterisation of the optical and vibrational properties of electrochemically synthesised polymer nanostructures (talk).

- *International Conference on Classical Nova Explosions, May20-24, 2002, Sitges, Spain*
N. de Séréville et al., A new experiment for the determination of the ^{18}F(p,α) reaction rate at nova temperatures. AIP Conf. Proc. 637 (2002) 420-424.

Société Belge de Physique, General scientific meeting, Liège, 5-6 juin 2002
S. Benck et al., Secondary light charged particle emission from the interaction of 25-65 MeV neutrons on uranium.

Ch. Delaere, Search for an invisibly decaying Higgs boson with the data collected in 2000 by the ALEPH experiment at centre-of-mass energies from 189 GeV up to 209 GeV (talk).

E. Raeymackers et al., Light charged particle production induced by fast neutrons (E_n = 25-65 MeV) on ^{209}Bi (poster).

F. Vanderbist et al., Realization and analysis of He-implanted foils for the measurement of (α,γ) reaction cross-sections in nuclear astrophysics (talk).

Participant : M. Couder

- *2nd Workshop on scientific and technological perspectives at the CNA, Centro Nacional de Aceleradores, June 3-4, 2002, Séville, Espagne*
  C. Angulo, Cross section measurements of reactions relevant for the p-process nucleosynthesis (talk).

- *CMS-Week CERN, June 9-14, 2002, Genève, Suisse*
  S. Assouak, E. Forton, G. Grégoire, IQC status of Louvain

- *15th International Workshop on ECR Ion Sources, ECRIS 02, June 12-14, 2002, University of Jyväskylä, Finland*
  M. Gaelens, Novel techniques for the ionization of radioactive metallic elements (présentation orale).

- *Halo' 02, June 13-15,* 2002*, Göteborg, Suède*
  C. Angulo, Spectroscopy of ^{19}Na via the ^{18}Ne+p resonant elastic scattering at the LLN-RIB facility (talk).

- *5th International Symposium on Polymer Physics (PP'2002), July 2-6, 2002, Qingdao, China*
  R. Legras, Nanopores and nanowires : a challenge for new properties and applications (invited talk).

- *First International Conference on String Phenomenology, Department of Theoretical Physics, July 6-11, 2002, University of Oxford, Oxford (UK)*
  Participant: E. Burton

- *4th International Conference on Radiation Effects on Semiconductor Detectors and Devices, July 10-12, 2002, Florence, Italy*
  S. Assouak, E. Forton, Gh. Grégoire, Irradiation of CMS Silicon sensors with fast neutrons**.**

- *Int. Conf. Nuclei in the Cosmos VII, July 81-12, 200, Fuji-Yoshida, Japan*
  N. de Séréville et al., Study of the ^{18}F(p,α) reaction for application to nova γ-ray emission.

  R.H. France III, L.T. Baby, C. Bordeanau, Th. Delbar, J.A. Dooley, M. Gai, M. Hass, J.E. McDonald, A. Ninane, and C.M. Przybycien, Destruction of 7Li and 7Be in Astrophysical Environments, Poster A27.

- *224th ACS Fall National Meeting, August 2002, Boston, USA*
  S. Demoustier-Champagne, L. Dauginet, M. Delvaux, E. Ferain, R. Legras, P-Y. Stavaux, Nanopores and nanotubes : synthesis and properties (poster).

- *EPSRC-IoP Summer School on Condensed Matter Theory, September 1-13, 2002, Ambleside (Cumbria, UK)*
  Participant: D. Bertrand

- *International Conference on Modern Problems in Superconductivity, September 9–14, 2002, Yalta (Ukraine)*
  G. Stenuit, S. Michotte, J. Govaerts, L. Piraux and D. Bertrand: Invited oral contribution by G. Stenuit, Vortex Configurations in Mesoscopic Superconducting Nanowires, to appear in the Proceedings, Mod. Phys. Lett. B, 10 pages.

- *Ninth International Conference on Accelerator Mass Spectrometry (AMS-9), September 9-13, 2002, Nagoya (Japan)*
  Ph. Collon, I. Ahmand, M. Bichler, W.S. Broecker, J. Caggiano, L. DeWayne Cecil, Y. El Masri, R. Golser, C.L. Jiang, A. Heinz, D. Henderson, W. Kutschera, B.E. Lehmann, P. Leleux, H.H. Loosli, R.C. Pardo, M. Paul, K.E. Rehm, P. Schlosser, R.H. Scott, W.M. Smethie, Jr. and R. Vondrasek, Tracing the oceans with ^{39}Ar (Oral presentation, Conference Abstract p. 107-108).

- *The 14th Annual Graduate School of Particle Physics (Joint Belgian-Dutch-German School), September16-27, 2002, Nijmegen (The Netherlands)*
  J. Govaerts, A Pedestrian Introduction to Quantum Field Theory (invited lectures).

  E. Burton and J. Govaerts, Tutorials on Quantum Field Theory.

  K. Piotrzkowski, Introduction to Accelerators (invited lectures).

  E. Forton, Silicon Radiation Hardness Tests with Neutrons (seminar).

  X. Rouby, Front End Hybrid Industrial Tester (seminar).

  Participants: S. Assouak, J. de Favereau, G. de Hemptinne, Ch. Delaere, E. Forton, F. Payen, X. Rouby

- *XXXIII European Cyclotron Progress Meeting, September 17-21, 2002, Warsaw, Poland*
  M. Loiselet, Cyclotrons in Radioactive Beam Facilities (invited talk).

  Participants : J.M. Colson, N. Postiau, G. Ryckewaert

- *RADECS 2002 Workshop, September 19-20, 2002, Padova, Italy*
  G. Berger, M. Moreno, I. Martinez, A. Akheyar, R. Harboe-Sorensen, G. Ryckewaert, D. Flandre, Edge effects and tilt dependency of heavy ion SEE characterization in PN junctions.

- *5th International Symposium on Ionizing Radiation and Polymers (IRaP 2002), September 21-26, 2002, Sainte-Adèle (Québec) Canada*
  E. Ferain, Micro- and nanofabrication using ion-track membranes (invited talk).

  R. Legras (participant)

- *Nuclear Physics in Astrophysics, 17th International Nuclear Physics Divisonal conference of the European Physical Society, NPDC-17, September 30 – October 4, 2002, Debrecen, Hungary*
  C. Angulo, Spectroscopy of the Proton-Rich Nuclei ^{19}Na by the Elastic scattering ^{1}H(^{18}Ne,p)^{18}Ne at the LLN-RIB Facility (talk).

  C. Angulo, The elastic scattering ^{7}Be+p at low energies: implications to the ^{7}Be(p,γ)^{8}Be reaction (poster).

- *Seventh Information Exchange Meeting on Actinide and Fission Product Partitioning and Transmutation, Jeju, Korea, 14-16 octobre 2002*
  E. Raeymackers, N. Nica, I. Slypen, S. Benck, J-P. Meulders, V. Corcalciuc
  Light charged particle production induced by fast neutrons (E_n = 25 – 65 MeV) on ^{59}Co and ^{nat}Fe.

- *International Nuclear Conference 2002 (INC'2002), October 15-18, 2002, Kuala Lumpur, Malaysia*
  R. Legras, Nanopores and nanowires : a challenge for new properties and applications (invited talk).

- *Tracker-Week CERN, October 21-23, 2002, Genève, Suisse*
  S.Assouak, E. Forton, G. Grégoire, IQC update of Louvain.

- *19th Meeting between Astrophysicists and Nuclear Physicists, December 2-3, 2002, Brussels*
  M. Couder, Performance of the ARES recoil separator for (p,γ) reaction measurements.

  P. Leleux, Gamma-Ray astronomy and the INTEGRAL mission.

  F. Vanderbist, Realization and analysis of He-implanted foils for the measurement of (α,γ) reaction cross-sections in nuclear astrophysics.

- *CMS-Week CERN, December 2-6, 2002, Genève, Suisse*
  S.Assouak, E. Forton, G. Grégoire, IQC status of Louvain.

- *National Science Foundation/European Commission Workshop : from Nanomaterials to Nanotechnology, December 5-8, 2002, Boston, Massachusetts*
  R. Legras, Nanopores and nanowires : a challenge for new properties and applications (invited talk).

- *REX ISOLDE Workshop, December 16-18, 2002*
  C. Angulo, Recent experiments at the Louvain-la-Neuve RIB facility (invited talk).

3. Rapports Internes

J. Govaerts, Self-Adjoint Extensions of the Dirac Hamiltonian in the Presence of a δ-Sphere Scalar Potential, December 2001, 11 pages.

J. Govaerts, Quantized Cosmological Constant in One-Dimensional Matter Coupled Quantum Gravity, Dedicated to John R. Klauder on the occasion of his 70th birthday, January 2002, 19 pages.

J. Govaerts, The Hamiltonian Noether Algebra, December 2002, 8 pages.

4. Séminaires et séjours de recherche

4.1. Séminaires et cours de 3e cycle

J. Gasiot (Univ. Montpellier II, France) : Electronic and Radiations (10/01/02).

F. Vanderbist (UCL, FYNU) : Mise au point de cibles d'^{4}Hélium implanté (07/02/02).

G. Tabacaru (UCL, FYNU) : Multifragmentation de systèmes très lourds étudiés avec le multidétecteur INDRA (21/02/02).

Th. Keutgen (UCL, FYNU) : Modèle de coalescence dans les collisions entre ions lourds aux énergies intermédiaires (28/02/02).

V. Roberfroid (UCL, FYNU) : Eventualité de l'effet de peau de neutrons dans les réactions ^{64}Ni + ^{116}Sn et ^{58}Ni + ^{122}Sn autour de 6 MeV/nucléon (07/03/02).

D. Bertrand (UCL, FYNU) : Phénomènes électromagnétiques dans un plan supraconducteur mésoscopique (14/03/02).

J.S. Graulich (UCL, FYNU) : HARP, a hadron production experiment for future neutrino physics (05/04/02).

N. Nica (UCL, FYNU) : Spectroscopie gamma à l'aide du détecteur EUROGAM 2 (11/04/02).

N. Olsson (Uppsala Univ., Suède) : Neutron-induced cross section measurements at the 20-180 MeV neutron beam facility at the Svedberg Laboratory (26/04/02).

F. Peeters (Univ. Antwerpen) : Superconductivity, the Ginzburg-Landau model and the mesoscopic superconductors (14-15/05/02).

J.B. Natowitz (Texas A&M Univ., USA) : Using caloric curves to explore the nuclear equation of state (16/05/02).

St. Jadach (INP Krakow, Pologne) : Monte Carlo Methods in high energy physics (16,17,21,22/05/02).

G. Lutz (CERN, Genève, Suisse) : Semiconductor radiation detectors (23-24/05/02).

H.-Ch. Schultz-Coulon (Univ. Dortmund, Allemagne) : The H1 upgrade project – status and future perspectives (23/05/02).

S. Chouridou (Ludwig-Maximilians Univ. München, Allemagne) : Wire calibration of the ATLAS muon chambers and studies of neutralino decays at LHC (27/05/02).

J. Cugnon (Univ. Liège) : Les mécanismes des réactions nucléaires. Du noyau composé à la diffusion multiple (3-4/07/02).

F. Metlica (Imperial College London, UK) : Polarization at HERA (12/07/02).

E. Casarejos (Univ. Santiago de Compostela) : Isotopic production cross sections of fragmentation residues in reactions induced by ^{238}U in deuterium (17/10/02).

V. Corcalciuc (Bucarest, Roumanie) : Nuclear reactions mechanisms at low and intermediate energies (21,23,25, 28, 30,31/10/02).

H. Yildiz (Middle East Technical Univ., Ankara, Turquie) : Observing Higgs in weak boson fusion with forward jet tagging at the CERN CMS experiment (28/10/02).

S. Engel (TRIUMF, Canada) : Awakening of the DRAGON (07/11/02).

C. Foudas (Imperial College Londres, UK) : Modern HEP Electronics (12,14,19, 21/11/02).

S. Kruchinin (Bogolyubov Inst., Kiev, Ukraine) : Thermodynamics effects in high-Tc superconductors (28/11/02).

R. Cavanaugh (Univ. Florida, USA) : The emerging grid infrastructure : will it change the way we do physics ? (09/12/02).

Ph. Collon (Columbia Univ., New-York, USA) : First steps in detecting ^{39}Ar in Seawater using accelerator mass spectroscopy (12/12/02).

F. Krauss (CERN, Genève, Suisse) : Event generation in C++ (16/12/02).

4.2. Séminaires et conférences donnés à l'extérieur

J. Govaerts, La cosmologie … ou encore une histoire de pomme, Conférence, Institut Notre-Dame du Bon Accueil, Beaumont (15/01/02).

J. Govaerts, An Introduction to String Theories, Invited Lectures, Institut de Mathématiques et de Sciences Physiques, University of Abomey-Calavi, Porto-Novo (Republic of Benin) (28/04/02 – 5/05/02).

J. Govaerts, In Search of Quantum Geometry, Invited Conference, Department of Physics, University of Abomey-Calavi, Cotonou (Republic of Benin) (3/05/02).

C. Angulo, Nuclear Astrophysics with low-energy radioactive beam: exploding stars in the laboratory, IOP Half Day meeting, Keele University (25/06/02).

J. Govaerts, Gauge Fixing and the Cosmological Constant, The Spinoza Institute, Institute of Theoretical Physics, University of Utrecht (Utrecht, The Netherlands) (14/11/02).

4.3. Séjours de recherche à l'étranger

Th. Delbar, Institut Weizmann, Rehovot, Israël (13-24/01/02).

J. Govaerts, Fellow of the Stellenbosch Institute for Advanced Study (STIAS), Stellenbosch (Republic of South Africa), 4-22/02/02.

M. Loiselet, GANIL, Caen (France), 4-15/03/02.

J. Govaerts, Institut de Mathématiques et de Sciences Physiques (IMSP), Université d'Abomey-Calavi, Porto-Novo (Republic of Benin), 28/04-5/05/02.

Th. Delbar, Yale University, Yale, New Haven, CT, USA (20-29/07/02).

C. Angulo, Collaboration with the group of F. Hannape (ULB) and N. Orr (LPC, Caen). Participation at the experiment E378 at the LISE spectrometer (GANIL) (21-27/11/02).

4.4. Divers

N. Postiau, Formation Opera 3D Modeleur, Vector Services, Maurepas, France (26-27/02/02).

D. Bertrand, G. Stenuit, Organization, supervision and execution with the collaboration of physics students at all levels and J. Govaerts, of demonstrations on superconductivity phenomena aimed at the general public and high school students, on the occasion of the Science Festival of the Faculty of Sciences, "Festival ScienceInfuse" (18-24/03/02).

V. Depauw, L. Dricot, F. Dufour, X. Rouby and J. Govaerts, Organization and execution of a conference with demonstrations and video animation aimed at the general public and high school students on the

EQUIMASS experiment flown on the European Space Agency parabolic flight campaign of July 2001, on the occasion of the Science Festival of the Faculty of Sciences, "Festival ScienceInfuse" (18-24/03/02).

D. Bertrand, O. van der Aa, Organization and supervision of a visit at CERN for third year undergraduate physics students (4-7/04/02).

G. Stenuit, Supervision of a 6th grade pupil of the primary school "Ecole des Bruyères" (Louvain-la-Neuve, Belgium) in the preparation of his school oral presentation on the topic of nuclear physics, together with an experimental demonstration of the measurement of the absorption of radioactive radiation in matter (May - June 2002).

J. Govaerts, Contribution to the Science Awareness Periodical "ScienceInfuse" of the Faculty of Sciences : Mais tout cela est relatif, mon cher Albert ! (December 2002).

5. Diplômes

5.1. Thèses de doctorat

Gabriel AVOSSEVOU
Théories de jauge et états physiques à 0+1 et 1+1 dimensions (défendue le 30 avril 2002) (UCL, J. Govaerts ; Institut de Mathématiques et des Sciences Physiques, Porto-Novo, République du Bénin, M.N. Hounkonnou).

Juan CABRERA JAMOULE
Etude des processus de fusion-fission et de fusion-évaporation dans l'interaction ^{20}Ne + ^{159}Tb entre 8 et 16 MeV/nucléon (défendue le 22 juillet 2002), (UCL, Y. El Masri).

5.2. Diplômes d'Etudes Approfondies ou Spécialisées (DEA, DES)

Martin MORELLE : Analyse stœchiométrique de couches d'altération du plomb et authentification d'icônes russes par diffusion RBS de protons et la technique PIXE (UCL, Y. El Masri)

5.3. Mémoires de Licence

Dominique BELGE: Réalisation d'un faisceau de neutrons à distribution énergétique constante de 10 à 65 MeV (UCL, R. Prieels)

Jérôme de FAVEREAU : Sélection de bosons de Higgs chargés dans l'expérience CMS (UCL, V. Lemaître)

Gwendoline de HEMPTINNE : Recherche de bosons de Higgs chargés dans l'expérience ALEPH (UCL, V. Lemaître)

Florian PAYEN : Propriétés quantiques de compactifications toroïdales de cordes bosoniques (UCL, J. Govaerts)

Xavier ROUBY : Caractérisation des circuits hybrides et des modules de détection pour le trajectographe de CMS (UCL, V. Lemaître)

6. Personnel

6.1. Institut de Physique Nucléaire

Personnel académique et scientifique

S. Assouak, boursière SCO
D. Belge, étudiant libre
S. Benck, chargé de recherche FNRS
D. Bertrand, assistant de recherche UCL
E. Burton, aspirante FNRS
J. Cabrera Jamoulle, assistant UCL (jusqu'au 31/09/02), assistant de recherche PAI (du 1/09/02 au 31/12/02)
M. Couder, collaborateur scientifique FNRS (jusqu'au 31/08/02), assistant de recherche IISN (à partir du 1/09/02)
M. Cyamukungu, chargé de recherche ESA/PRODEX
J. de Favereau, boursier FRIA à partir du 1/9/2002
G. de Hemptinne, boursière UCL-FSR
Ch. Delaere, aspirant FNRS
Th. Delbar, professeur UCL, responsable de l'Institut de Physique Nucléaire
J. Deutsch, professeur émérite UCL
Ch. Dufauquez, assistant de recherche IISN
Y. El Masri, chercheur qualifié FNRS, professeur UCL
D. Favart, professeur UCL
A. Ferrant, étudiant libre
E. Forton, assistant de recherche IISN
J. Govaerts, professeur UCL
J.-S. Graulich, chargé de recherche FNRS (mandat suspendu à partir du 30/09/02)
Gh. Grégoire, professeur UCL
L. Grenacs, professeur émérite UCL
S. Kalinin, assistant de recherche IISN
Th. Keutgen, assistant de recherche IISN
J. Lehmann, chef de travaux UCL (pensionné au 15/09/02)
G. Leibenguth, assistant de recherche PAI (à partir du 15/09/02)
P. Leleux, directeur de recherches FNRS, professeur UCL
V. Lemaître, chargé de recherches FNRS, chargé de cours UCL
P. Lipnik, professeur émérite UCL
P. Macq, professeur émérite UCL
J. Martinez-Martinez, assistant de recherche UCL (à partir du 1/09/02)
J.-P. Meulders, professeur UCL
O. Militaru, boursière post-doctorale UCL (à partir du 1/04/02)
M. Morelle, chercheur libre (jusqu'au 15/09/02)
I. Nanobashvili, assistant de recherche ESA/PRODEX (jusqu'au 31/07/02)
N. Nica, professeur invité, titulaire du Fonds Spécial de Recherche UCL (jusqu'15/07/02)
Fl. Payen, aspirant FNRS (à partir du 1/10/02)
K. Piotrzkowski, professeur UCL
R. Prieels, professeur ordinaire UCL
E. Raeymackers, assistant de recherche UCL
V. Roberfroid, assistant UCL
X. Rouby, assistant de recherche UCL (à partir du 15/09/02)
I. Slypen, assistante de recherche UE
I. Smits, assistante de recherche UCL 50 %
G. Stenuit, collaborateur scientifique FNRS (jusqu'au 31/08/02), assistant de recherche IISN (à partir du 1/09/02)
G. Tabacaru, assistant de recherche PAI (jusqu'au 22/07/02)
O. van der Aa, boursier FRIA
F. Vanderbist, assistant de recherche IISN
J. Vervier, professeur émérite UCL

Personnel administratif et technique

Administration

L. Kruijfhooft
J.P. Page
G. Tabordon
Ch. Thielens-Lengelé

Bureau de dessin

E. Lannoye

Electronique

L. Bonnet
B. de Callataÿ
M. Jacques (50 %)
D. Michotte de Welle
Th. Quériat (50 %)

Informatique

F. Boldrin
Y. Longrée
A. Ninane

Mécanique

W. Binon (responsable)
J.-M. Delforge
D. Hougardy
P. Noël (décédé le 19/02/02)

Techniciens de groupe

P. Demaret
J. Van Mol

6.2. Centre de Recherches du Cyclotron

Staff

J.M. Colson
M. Loiselet
N. Postiau
G. Ryckewaert

Secrétariat

C. Baras

Groupe Exploitation

J.P. Clare
T. Dretar
P. Jonckman
P. Leclercq
F. Mathy
G. Urbain (à partir du 15/03/02)

J. Viatour

Groupe Projets

C. Angulo Perez
G. Berger
Th. Daras
B. Florins
P. Froment (jusqu'au 31/03/02)
M. Gaelens
I. Tilquin (jusqu'au 31/03/02)

Atelier de Mécanique

Th. Debuck
D. Duysens (jusqu'au 09/09/02)
P. Nemegeer